Diplomarbeit

The role of *Nr4a1* in the *c-Myc* driven lymphomagenesis

eingereicht von

Marco Bischof

zur Erlangung des akademischen Grades

Doktor der gesamten Heilkunde

(Dr. med. univ.)

an der

Medizinischen Universität Graz

ausgeführt an der

Klinischen Abteilung für Hämatologie der

Medizinischen Universität Graz

unter der Anleitung von

Priv.-Doz. Mag.rer.nat. Dr.scient.med. Alexander Deutsch

&

Dr.med.univ. Dr.scient.med. Katharina Prochazka

Graz, am 15. November 2016

Eidesstattliche Erklärung

Ich erkläre ehrenwörtlich, dass ich die vorliegende Arbeit selbstständig und ohne fremde Hilfe verfasst habe, andere als die angegebenen Quellen nicht verwendet habe und die den benutzten Quellen wörtlich oder inhaltlich entnommenen Stellen als solche kenntlich gemacht habe.

Graz, am 15. November 2016

Marco Bischof eh.

Declaration

I hereby declare that this diploma thesis is my own original work and that I have fully acknowledged by name all of those individuals and organizations that have contributed to the research for this degree diploma thesis. Due acknowledgement has been made in the text to all other material used. Throughout this thesis and in all related publications I followed the guidelines of "Good Scientific Practice".

Graz, November 15, 2016

Marco Bischof eh.

Acknowledgement

First of all, I would like to thank Dr. Alexander Deutsch, my diploma supervisor, for giving me the opportunity to work with him and his team. He is a great researcher and I appreciate that he shared his knowledge with me.

I need to say thank you especially to Kerstin Wenzl, who taught me lots of new techniques, as we realized at the beginning that even using a pipette was not that easy for me. I wish her all the best for a new period in life that she has started in the United States.

Beata Pursche, Angelika Rosenberger and Olivia Geiger always were there for me whenever I had "another short question". Therefore I want to say a big thank you and a last "Sorry for disturbing you". This is the place where I like to say thank you to the entire team of the haematological department of the University Clinic Graz for their help during my diploma work.

A big thank you goes out to Leijla Sestic, who supported me during my Western blot work in the summer time and who cheered me up when I was down due to another failed Western blot gel, which happened from time to time.

I am also very thankful for having met Karoline Fechter, a specialist in T-cells who showed me that research can be professional and fun at the same time. "Gracías!"

I would like to say thank you to my friends who have not seen me for quite a while. Especially Lisa Posch, who always motivated me to go on, whenever I was demotivated and down.

Talking about people who have not seen me quite often, this Thank you goes out to my family who always showed interest in what I did and who always supported me and never were too tired of listening to my laboratory stories, so thank you "little" sister, mum and dad!

Last but not least, this Thank you goes out to all the people and helping hand names that I missed at this place – unintentionally.

TABLE OF CONTENTS

ABSTRACT 2

ZUSAMMENFASSUNG 4

1 INTRODUCTION/BACKGROUND 6

1.1 LYMPHOMAS 6
1.1.1 LYMPHOMAS – SO MANY DIFFERENT TYPES 6
1.1.2 B-CELL DEVELOPMENT 9
1.1.2.1 Development and differentiation of B-cells 9
1.1.2.2 Important proteins of GC initiation 11
1.1.3 THE CELLULAR ORIGIN OF THE B-CELL LYMPHOMAS 11
1.1.4 MOLECULAR LYMPHOMAGENESIS 13
1.1.4.1 VDJ, SHM and CSR 13
1.1.4.2 Genetic alterations 14
1.1.4.3 Tumour suppressor genes 15
1.1.4.4 Important cell cycle proteins 15
1.1.5 AGGRESSIVE B-CELL LYMPHOMAS 17
1.1.5.1 DLBCL 17
1.1.5.2 Burkitt's Lymphoma – a highly proliferative and aggressive type of lymphoma, mainly in children 17
1.1.6 LYMPHOMA THERAPY APPROACHES 18
1.2 THE NUCLEAR ORPHAN RECEPTOR *NR4A* 20
1.2.1 BACKGROUND OF *NR4A* 20
1.2.2 *NR4A*'S ROLE IN MYELOID NEOPLASMS AND LYMPHOID MALIGNANCIES 21
1.3 THE EμMYC MOUSE 22
1.3.1 EμMYC TRANSGENIC MOUSE MODEL 22
1.3.2 *C-MYC* – THE CELLULAR MYELOCYTOMATOSIS ONCOGENE 23
1.3.3 THE SECOND HIT MODEL OF THE *EμMYC* MOUSE: INACTIVATION OF PRO-APOPTOTIC GENES AND/OR OVEREXPRESSION OF ANTI-APOPTOTIC GENES ARE NEEDED FOR MALIGNANT TRANSFORMATION 24
1.3.4 LOSS OF *NR4A1* ACCELERATED *MYC*-DRIVEN LYMPHOMAGENESIS 25
1.4 AIM 28

2 MATERIALS AND METHODS 29

2.1. THE MICE 29
2.1.1 MOUSE MODELS 29
2.2 DNA-ISOLATION AND GENOTYPING 30
2.2.1 DNEASY MINI KIT (QUIAGEN, HILDEN, GERMANY) 30
2.2.2 GENOTYPING 30
2.3 RNA-ISOLATION AND FURTHER PROCESSING 31
2.3.1 RNA-ISOLATION USING THE RNEASY MINI KIT (QUIAGEN GMBH, HILDEN, GERMANY) 31
2.3.2 CDNA KIT 31
2.3.3 MRNA SEQUENCING 31
2.3.3.1 Use of RIN values 31
2.3.3.2 mRNA sequencing procedure 32
2.4 PROTEIN EXTRACTION 33
2.5 B-CELL ISOLATION 36
2.5.1 B-CELL ISOLATION AND FLOW CYTOMETRY 36
2.6 STATISTICAL METHODS 37

3. RESULTS **38**

3.1 SECOND HIT ANALYSIS **38**
3.1.1 GENOTYPING 38
3.1.2 WESTERN BLOT ANALYSIS OF THE TUMOURS DERIVED FROM THE EμMYC NR4A1+/+ AND EμMYC NR4A1-/- MICE 39
3.2 ANALYSIS OF SPLEENIC B-CELLS OF NON-MALIGNANT NR4A1+/+ AND NR4A1-/- MICE **44**
3.2.1 PURITY OF THE ISOLATED CELLS 44
3.2.2 WESTERN BLOT RESULTS OF THE SPLEENIC B-CELLS 45
3.2.3 PARP ANALYSIS COMPARING EμMYC TUMOURS TO WILDTYPE SPLEENIC B-CELLS 50
3.3 GENE EXPRESSION ANALYSIS **52**
3.3.1 QUALITY CHECK VIA RIN-VALUE 52
3.3.2 MRNA EXPRESSION OF *NR4A1* AND *NR4A3* 53
3.3.3 SEQUENCING 55

4 DISCUSSION **58**

SUPPLEMENTARY **60**

BIBLIOGRAPHY **80**

LIST OF TABLES

TABLE 1 LIST OF HUMAN MATURE B-CELL LYMPHOMAS - ADAPTED FROM KÜPPERS, R., ET. AL. (4) 8
TABLE 2 LIST OF THE BCR-STATUS OF VARIOUS TYPES OF LYMPHOMAS - ADAPTED FROM KÜPPERS, R., ET. AL. (4) 12
TABLE 3 LIST OF MICE SAMPLES USED FOR MRNA SEQUENCING ANALYSIS 33
TABLE 4 KDA SIZE OF THE ANTIBODIES AND MEMBRANE ALLOCATION 34
TABLE 5 PARAMETERS FOR THE USE OF THE FIRST ANTIBODIES 35
TABLE 6 PARAMETERS FOR THE USE OF THE SECOND ANTIBODIES 36
TABLE 7 NUMBER OF GENES THAT SHOWED SIGNIFICANT CHANGES IN GENE EXPRESSION THESE CHANGES ARE ILLUSTRATED AT THE UNCORRECTED AND CORRECTED SIGNIFICANCE THRESHOLD WITH LOG2 FOLD CHANGES OF GREATER THAN 1.50 AND LESS THAN -1.50. 55
TABLE 8 WESTERN BLOT OVERVIEW OF ANTIBODIES, INCUBATION TIME, TEMPERATURE AND BLOCKING SOLUTIONS. 78

LIST OF FIGURES

FIGURE 1 ILLUSTRATION OF THE ORIGIN OF VARIOUS TYPES OF LYMPHOMAS - ADAPTED FROM KÜPPERS, R., ET. AL. (4)..... 7
FIGURE 2 ILLUSTRATION OF THE B-CELL DEVELOPMENT - WHERE IT TAKES PLACE AND THE IMMUNOPHENOTYPIC DIFFERENCES OF THE B-CELLS - ADAPTED FROM HTTPS://WWW.BDBIOSCIENCES.COM/DOCUMENTS/BCELL_BROCHURE.PDF 9
FIGURE 3 ILLUSTRATION OF THE DARK AND THE LIGHT ZONE OF A LYMPH FOLLICLE - ADAPTED FROM BALTHASAR, A., HEESTERS, ET. AL., 2014 10
FIGURE 4 ILLUSTRATION OF THE VDJ, THE SHM AND THE CSR IN THE B-CELL DEVELOPMENT - ADAPTED FROM KÜPPERS, R., ET. AL. (4) 13
FIGURE 5 ILLUSTRATION OF THE NR4A1 GENE LOCUS IN HUMAN DNA ADAPTED FROM THE USCS GENOME BROWSER –..... 20
FIGURE 6 ILLUSTRATION OF THE NR4A-FAMILY AND ITS MEMBERS NR4A1 (NUR77), NR4A2 (NURR1) AND NR4A3 (NOR-1) - ADAPTED FROM JOSÉ MARTINEZ-GONZÁLEZ, LINA BADIMON, ET. AL., 2005..... 21
FIGURE 7 SCHEMATIC REPRESENTATION OF THE NR4A1 AND NR4A3 FUNCTIONS IN HEMATOPOIETIC CELLS - ADAPTED FROM WENZL, K., ET. AL., 2015 22
FIGURE 8 ILLUSTRATION OF THE MYC GENE LOCUS IN HUMAN DNA - ADAPTED FROM THE USCS GENOME BROWSER 23
FIGURE 9 ILLUSTRATION OF EFFECTS FROM C-MYC ON TUMOUR SUPPRESSOR GENES - ADAPTED FROM MENG, X., ET. AL. (38) . 24
FIGURE 10 DEVELOPMENT OF LYMPHOMAS AND SURVIVAL OF EμMYC NR4A1+/+ AND EμMYC NR4A1-/- MICE - ADAPTED FROM WENZL, K., ET. AL., 2015 25
FIGURE 11 COMPARISON OF THE RATION OF GR-1+ CELLS TO B220+ CELLS IN BONE MARROW (BM) AND SPLEEN (SPL) AND THE RATIO OF B220+ CELLS TO TCR+ CELLS IN SPL OF EμMYC NR4A1-/- AND EμMYC NR4A1+/+ MICE. – ADAPTED FROM WENZL, K., ET. AL., 2015 THE TRIANGLE DENOTES P<0.05 COMPARED TO WILDTYPE MICE (WT) AND THE ASTERISK DENOTES P<0.05 COMPARED TO EμMYC NR4A1+/+ MICE. 26
FIGURE 12 IN VITRO GROWTH AND PROLIFERATION BEHAVIOUR OF B220+ TUMOUR CELLS EITHER ISOLATED FROM EμMYC NR4A -/- OR EμMYC NR4A1+/+ MOUSE TUMOURS DETERMINED BY ESTIMATION OF CELL NUMBER, BRDU-ASSAY AND B220/7AAD STAINING. – ADAPTED FROM WENZL, K., ET. AL., 2015 *DENOTES P<0.01 COMPARING B220+ CELLS ISOLATED FROM EμMYC NR4A -/- TUMOURS COMPARED TO EμMYC NR4A1+/+. + DENOTES P<0.01 COMPARING B220+ CELLS ISOLATED FROM EμMYC NR4A1-/- TUMOURS COMPARED TO EμMYC NR4A1+/+ UNDER LPS STIMULATION..... 27
FIGURE 13 EμMYC NR4A1 -/- MOUSE WITH A BIG CERVICAL TUMOUR, AN ENLARGED SPLEEN AND INFILTRATED PERIPHERAL LYMPH NODES. 30
FIGURE 14 ILLUSTRATION OF THE PRACTICAL USE OF THE RIN VALUE - ADAPTED FROM "RNA INTEGRITY NUMBER (RIN) - STANDARDIZATION OF RNA QUALITY CONTROL", ODILO MUELLER, SAMAR LIGHTFOOT, ANDREAS SCHROEDER, 2004 (82) 32
FIGURE 15 REPRESENTATIVE RESULTS OF GENOTYPING - TG (DENOTES TRANSGENE) SHOWS THAT ALL MICE TESTED CONTAIN THE EμMYC TRANSGENE. SAMPLES 0112, 0186, 0195 WERE COMPARED TO THE CONTROL SAMPLE (C, WHICH WAS AN EμMYC MOUSE) EμMYC NR4A1+/+ MICE. SAMPLES 0092, 0150 AND 0170 WERE DETECTED AS EμMYC NR4A1-/- MICE. THE FIRST LANE REPRESENTS THE 100 BP GENE RULER. THE MUTANT IS SHOWN ON 350 BP, THE WILDTYPE ON 180 BP. 38
FIGURE 16 EXEMPLARY WESTERN BLOT OF AN OVEREXPRESSION OF P53 IN ONE EμMYC NR4A1+/+ MOUSE TUMOUR..... 39
FIGURE 17 REPRESENTATIVE WESTERN BLOT OF THE TUMOUR MICE..... 40
FIGURE 18 REPRESENTATIVE WESTERN BLOT OF THE TUMOUR MICE..... 41
FIGURE 19 REPRESENTATIVE WESTERN BLOT OF THE TUMOUR MICE..... 42
FIGURE 20 REPRESENTATIVE WESTERN BLOT OF THE TUMOUR MICE..... 43
FIGURE 21 FLOW CYTOMETRY OF ISOLATED B-CELLS FROM SPLEENS OF WILDTYPE (5095) AND NR4A1-/- (5096) MICE. ALL CELLS WERE GATED B220+/CD19+. 44
FIGURE 22 REPRESENTATIVE BLOT OF THE DETECTED P53 OVEREXPRESSION ON ONE NR4A1-/- MOUSE. 45
FIGURE 23 REPRESENTATIVE WESTERN BLOT OF THE ISOLATED SPLEENIC B-CELLS 46
FIGURE 24 REPRESENTATIVE WESTERN BLOT OF THE ISOLATED SPLEENIC B-CELLS 47
FIGURE 25 REPRESENTATIVE WESTERN BLOT OF THE ISOLATED SPLEENIC B-CELLS 48
FIGURE 26 REPRESENTATIVE WESTERN BLOT OF THE ISOLATED SPLEENIC B-CELLS 49
FIGURE 27 REPRESENTATIVE WESTERN BLOT OF THE TUMOUR MICE..... 51
FIGURE 28 REPRESENTATIVE WESTERN BLOT OF THE ISOLATED SPLEENIC B-CELLS 51
FIGURE 29 ILLUSTRATION OF THE RIN VALUE EVALUATION OF EμMYC NR4A1-/- AND EμMYC NR4A1+/+ - RNA WITH A RIN VALUE OF >7.5 WAS DETECTED AS "GOOD QUALITY" FOR RNA SEQUENCING ANALYSIS (82). 52
FIGURE 30 RELATIVE EXPRESSION OF EμMYC NR4A1+/+ TUMOUR CELLS. – NR4A1 EXPRESSION WAS 7-FOLD LOWER IN EμMYC NR4A1-/- TUMOUR MICE COMPARED TO THE EμMYC NR4A1+/+ MICE (P<0.04). NR4A1 IS 6-FOLD LOWER EXPRESSED IN

EμMyc Nr4a1 +/+ mouse tumours compared to non-neoplastic controls (p<0.05). Nr4a1 is 60-fold lower expressed in EμMyc Nr4a1-/- mouse tumours compared to the non-neoplastic control 53
Figure 31 Relative expression of Nr4a3 in the EμMyc Nr4a1 +/+ and EμMyc Nr4a1-/- mice tumours. Nr4a3 was highly expressed in immature B-cells and in EμMyc Nr4a1-/- mice, assumed due to the loss of Nr4a1 comparing to EμMyc Nr4a1+/+ mice, but not significantly. Additionally, an at least 4.6-fold higher expression in EμMyc Nr4a1-/- mouse tumours compared to non-neoplastic controls (p<0.05) was demonstrated. 54
Figure 32 Significantly enriched GO terms and pathways associated with the differentially regulated genes in EμMyc Nr4a1-/- versus EμMyc Nr4a1+/+ mice. Terms that are associated with the upregulated genes are coloured green, genes associated with downregulation are coloured red. The colour gradient shows the deregulated gene proportion associated with the term. The colour shade goes towards grey/white when the proportions are towards equal. 57
Figure 33 Representative blots from immunoblotting analysis of EμMyc Nr4a1+/+ tumours. Blots for Bcl-2, Bcl-xl-Bim, Mcl-1, Mdm2, p53, p19Arf and Parp protein expression. Beta actin was used as loading control on all blots. As antibody control a wildtype mouse spleen was used. 60
Figure 34 Relative density plots from tumours with or without Nr4a1. Status of protein levels of Bcl-2, Bcl-xl, Bim, Mcl-1 and cleaved Parp from tumours with or without Nr4a1 loss. Density was calculated using the ImageJ software and row data was normalized to the loading control Beta actin. The bars represent mean and standard deviation. *p<0.05 to EμMyc Nr4a1+/+ mice 61
Figure 35 Relative density plots from tumours with or without Nr4a1. Status of protein levels of Mdm2, p19Arf and p53 from tumours with or without Nr4a1 loss. Density was calculated using the ImageJ software and row data was normalized to the loading control Beta actin. The bars represent mean and standard deviation. *p<0.05 to EμMyc Nr4a1+/+ mice. 62
Figure 36 Immunoblotting analysis of spleenic B-cells.-Part 1- Representative blots for Bcl-2, Bcl-xl, Bim, Mcl-1, Mdm2, p19Arf, p53 and cleaved Parp protein expression. Beta actin was used as loading control on all blots. 63
Figure 37 Immunoblotting analysis of spleenic B-cells.-Part 2- Representative blots for Bcl-2, Bcl-xl, Bim, Mcl-1, Mdm2, p19Arf, p53 and cleaved Parp protein expression. Beta actin was used as loading control on all blots. 64
Figure 38 Relative density plots from spleenic cells with or without Nr4a1. Status of protein levels of Bcl-2, Bcl-xl, Bim, Mcl-1 and cleaved Parp from spleenic cells with or without Nr4a1 loss. Density was calculated using the ImageJ software and row data was normalized to the loading control Beta actin. The bars represent mean and standard deviation. *p<0.05 to Nr4a1+/+ mice 65
Figure 39 Relative density plots from spleenic B-cells with or without Nr4a1. Status of protein levels of Mdm2, p19Arf and p53 from the isolated spleenic B-cells with or without Nr4a1 loss. Density was calculated using the ImageJ software and row data was normalized to the loading control Beta actin. The bars represent mean and standard deviation. *p<0.05 to Nr4a1+/+ mice. 66

LIST OF ABBREVIATIONS

7AAD	7-aminoactinomycin D
ADP	Adenosine diphosphate
AID	activation-induced cytidine deaminase
AML	Acute myeloid leukemia
B-CLL	B-cell chronic lymphatic leukemia
BAD, Bad	BCL-2-associated death promoter (human/mouse)
BCL-2/-6, Bcl-2/-6	B-cell lymphoma-2, B-cell lymphoma 6 (human/mouse)
BCL-XL, Bcl-xl	B-cell lymphoma extra-large (human, mouse)
BCR	B-cell receptor
BER	base excision repair
BH-3, Bh-3	BCL-2-homology domain 3 (human/mouse)
BID, Bid	BH3- interacting domain death agonist (human/mouse)
BIM, Bim	BCL-2 interacting mediator (human/mouse)
BL	Burkitt's lymphoma
BM	bone marrow
BMF, Bmf	Bcl-2-modifying factor (human, mouse)
bp	base pair
BrdU-assay	Bromdesoxyuridin assay
BSA	Bovine serum albumin
C	Control
C-Myc	cellular myelocytomatosis oncogene
C-terminus	Carboxy-terminus
cDNA	complementary DNA
CHOP	cyclophosphamide, hydroxydaunomycine, vincristine, prednisolone
CSR	class-switch recombination
CVAD	Cyclophosphamide, Vincristine, Doxorubicin, Dexamethasone
DA-EPOCH-R	dose-adjusted etoposide, prednisone, vincristine, cyclophosphamide, doxorubicin plus Rituximab
DBD	DNA-binding domain
DLBCL	Diffuse Large B-cell lymphoma
DM	double minute chromosome

DNA	Deoxyribonucleic acid
eBL	endemic Burkitt's lymphoma
EBV	Ebbstein Barr Virus
EμMyc	c-Myc gene under control of Ig heavy chain enhancer
FDC	Follicular dendritic cell
FL	Follicular lymphoma
GAPDH	Glyerinaldehyd-3-phosphat-dehydrogenase
GC	germinal centre
GO	gene ontology
GR-1	myeloid differentiation antigen
HCV	Hepatitis C Virus
HHV-8	Human herpes Virus
HL	Hodgkin Lymphoma
HPRT	Hypoxanthine-guanine phosphoribosyl transferase
Ig	immunoglobulin chain
IgV	immunoglobulin variable region
IKKBeta	Inhibitor of nuclear factor Kappa-B-kinase
IRF4	Interferon regulatory factor 4
kDa	Kilo-Dalton
LBD	ligand binding domain
LPS	lipopolysaccharide
mAb	monoclonal antibody
MALT	mucosa associated lymphatic tissue
MCL-1, Mcl-1	induced myeloid leukemia cell differentiation protein (human/mouse)
MDM2, Mdm2	Mouse double minute 2 homolog (human, mouse)
MEF2B	Myocyte enhancer binding factor 2B
MIF	Macrophage migration inhibitory factor
MMR	mismatch repair
mRNA	messenger ribonucleic acid
MSH	mutS homologue
NAD	Nicotinamide adenine dinucleotide
NF-KappaB	Nuclear factor kappa-light chain enhancer of activated B-cells
NHL	non-Hodgkin's lymphoma

NLS	nuclear localization signals
NR4A, Nr4a	orphan nuclear receptor 4 A (human, mouse)
PARP, Parp	Poly ADP ribose polymerase (human, mouse)
PCR	polymerase chain reaction
PI3K	Phosphoinositide 3-kinase
POMP	6-Mercaptopurine, Vincristine, Methotrexate, Prednisone
PPIA	Peptidylprolyl isomerase A
PUMA, Puma	also BCL-2-binding component (human, mouse)
RAG 1, RAG 2	recombination activated gene ½
RIN	RNA integrity number
RIPA Puffer	radio immunoprecipitation assay buffer
RNA	ribonucleic acid
RT PCR	real-time polymerase chain reaction
SAGE-sequencing	Serial analysis of gene expression sequencing
sBL	sporadic Burkitt's lymphoma
SHM	somatic hypermutation
SPL	spleen
SRC	Non-Receptor Tyrosine kinase
SYK	Spleen Tyrosine Kinase
TBST	Tris-buffered saline and polysorbate
TCR	T-cell receptor
TG	transgene
TORC1	Transducer of regulated CREB activity 1
TRAIL	Tumour necrosis factor related apoptosis inducing ligand
U-G	Uracil-Guanine
UNG	uracil DNA glycosylase
US	United States of America
VDJ	variable diversity joining
WHO	World health organization
Wt	wildtype

- Doch Forschung strebt und ringt, ermüdend nie,
nach dem Gesetz, dem Grund, warum und wie. -

Johann Wolfgang von Goethe
deutscher Dichter und Naturwissenschaftler
(1749 – 1832)

ABSTRACT

The nuclear orphan receptors *Nr4a1* and *Nr4a3* have been demonstrated to be cooperating tumour suppressor genes leading to the rapid development of AML in double knock-out mice. Their expression is also reduced in leukemic blasts from human AML patients. My team has already published a comprehensive study on *NR4A* nuclear receptor expression levels in lymphoid neoplasms that revealed a marked reduction of both *NR4A1* and *NR4A3* in the majority of patients with B-cell chronic lymphocytic leukaemia, follicular lymphoma and diffuse large B-cell lymphoma. Interestingly, functional characterization demonstrated that *NR4A1* alone induces apoptosis of aggressive lymphoma cells *in vitro* and suppresses tumour growth in a xenograft model. Additionally, our recent data demonstrate that a loss of *Nr4a1* accelerates *Myc*-induced lymphomagenesis in mice. Taken all together, our data indicate a tumour suppressive function of *Nr4a1* in the development of aggressive lymphomas.

The aim of this work is to investigate the underlying mechanisms of *Nr4a1*-mediated tumour suppression in the development of aggressive lymphomas *in vivo*. In detail, I characterized the effect of *Nr4a1*-loss on pro- (*Bim* and *p19-Mdm2-p53* axis) and anti-apoptotic genes (*Bcl-2, Mcl-1* and *Bcl-xl*), which have to be inactivated or overexpressed for malignant transformation, in Myc-driven lymphomagenesis by using the EμMyc mouse model. Furthermore, expression analysis was performed to determine *Nr4a1* and *Nr4a3* expression in EμMyc Nr4a1-/- and EμMyc Nr4a1+/+ derived tumours and I investigated genetic programs which might be regulated by *Nr4a1* in aggressive B-cell lymphomas.

By Western blot analysis I demonstrated that Mdm2 and Bim were significantly overexpressed in the EμMyc Nr4a1-/- mouse tumours compared to EμMyc Nr4a1+/+ mice. Additionally, I observed a reduced cleavage of Parp as an apoptotic marker in the EμMyc Nr4a1-/- mouse tumours. It was shown, that EμMyc Nr4a1+/+ mouse tumours expressed *Nr4a1* 7-fold higher compared to the EμMyc Nr4a1-/- mouse tumours on mRNA levels. Comparing the EμMyc Nr4a1+/+ mouse tumours to the non-neoplastic control a 6-fold higher *Nr4a1* mRNA-expression could be demonstrated. EμMyc Nr4a1-/- derived mouse tumours were shown to have a 60-fold lower *Nr4a1*-expression compared to a non-neoplastic control. EμMyc Nr4a1-/- mouse tumours were revealed to have a 4.6-fold higher expression of Nr4a3 compared to the EμMyc Nr4a1+/+ mice

Thus, this project provides new insights into the molecular mechanisms by which *Nr4a1* impacts the development of malignant lymphomas and normal B-cells.

ZUSAMMENFASSUNG

Es wurde bereits demonstriert, dass *Nr4a1* und *Nr4a3* bei der Entstehung von AML bei Doppel-Knockout-Mäusen als Tumorsuppressor Gene wirken. Auch im menschlichen Organismus wurde bereits gezeigt, dass die Expression der beiden Gene in leukämischen Blasten von AML Patienten vermindert vorkommen. Meine Arbeitsgruppe hatte bereits eine Studie über *NR4A*-Rezeptor Expressionslevels in lymphatischen Neoplasmen publiziert, wonach in der Mehrheit von B-CLL-, FL- und DLBCL-Patienten eine reduzierte Expression von *NR4A1* und *NR4A3* aufgefunden werden konnte. Überraschenderweise konnte bewiesen werden, dass bereits *NR4A1* alleine ausreicht, um in aggressiven Lymphomen *in vitro* das Tumorwachstum zu inhibieren bzw. um Apoptose auszulösen. Dazu zeigen uns unsere neuen Daten, dass der Verlust von *Nr4a1* in EμMyc Nr4a1-/- Mäusen eine Akzeleration der *Myc*-getriggerten Lymphomentstehung zur Folge hat. Dementsprechend schließen wir aus unseren Daten, dass *Nr4a1* eine tumorsuppressive Funktion hinsichtlich der Entwicklung von aggressiven Lymphomen unterhält.

Das Ziel dieser Arbeit ist es herauszufinden, auf welche Weise die *Nr4a1*-mediierte Tumorsuppression im Hinblick auf die Entstehung von aggressiven Lymphomen *in vivo* abläuft. Ich charakterisierte den Effekt eines *Nr4a1*-Verlustes auf pro- (*Bim* und *p19-Mdm2-p53* Achse) und anti-apoptotische Gene (*Bcl-2, Mcl-1* und *Bcl-xl*), welche für eine maligne Transformation inaktiviert oder überexpremiert sein müssen, in der *Myc*-getriggerten Lymphomentstehung. Dazu verwendete ich das EμMyc Lymphom Mausmodel. Zusätzlich führte ich eine Expressionsanalyse durch, um das Expressionsmuster von *Nr4a1* und *Nr4a3* in EμMyc-Nr4a1-/- und EμMyc Nr4a1+/+ getriggerten Tumoren zu ermitteln und um genetische Abläufe, welche durch *Nr4a1* in aggressiven B-Zell-Lymphomen reguliert sein könnten, besser zu verstehen.

Mittels Western Blot Analyse konnte ich veranschaulichen, dass in den EμMyc Nr4a1-/- Maus-Tumoren im Vergleich zu den EμMyc Nr4a1+/+ Mäusen Mdm2 und Bim signifikant überexprimiert werden. Zusätzlich zeigten meine Ergebnisse eine verminderte Spaltung der *Parp*-Banden in den EμMyc Nr4a1-/- Maus-Tumoren, somit zeigen diese Tumore im Vergleich zu den EμMyc Nr4a1+/+ Maus-Tumoren eine verminderte Apoptose.

Die EμMyc Nr4a1+/+ Maus-Tumore zeigten eine 7-fach erhöhte Expression von *Nr4a1* im Vergleich zu EμMyc Nr4a1-/- Mäusen. Weiters konnte gezeigt werden, dass EμMyc Nr4a1+/+ Maus-Tumore im Vergleich zu den nicht-neoplastischen Kontrollen *Nr4a1* 6-fach höher exprimierten. Die EμMyc Nr4a1-/- Maus-Tumore zeigten sogar eine 60-fach erniedrigte *Nr4a1*-Expression im Vergleich zu den nicht-neoplastischen Kontrollen. Die Expression von *Nr4a3* ist in den EμMyc Nr4a1-/- Maus-Tumoren im Vergleich zu den EμMyc Nr4a1+/+ Mäusen 4.6-fach erhöht.

Dieses Projekt lieferte neue Einblicke in die molekularen Mechanismen, welche *Nr4a1* auf die Entstehung von malignen Lymphomen und normalen B-Zellen unterhält.

1 INTRODUCTION/BACKGROUND

1.1 Lymphomas

1.1.1 Lymphomas – so many different types

Nowadays, a lymphoma, per definition of the WHO, is a neoplasm of the hematopoietic and lymphoid tissue. This definition has been used since the year 2001 in studies and clinical trials to provide a basis for further investigations under the genetic and molecular aspect (1).

Lymphomas are divided into Hodgkin and Non-Hodgkin lymphomas. Non-Hodgkin lymphomas can be subdivided into B- and T-cell types. There are more than 30 different B-cell lymphomas (2) and regarding all subtypes more than 50 types in total (Table 1), referring to the publication of the WHO in 2008 (1). These subtypes can be distinguished either by using clinical and pathological approaches or by gene expression analysis. Each type of lymphoma evolves from one particular differentiation grade (2,3). The differentiation stage of various lymphomas normally takes place in a particular histological body structure and gives the possibility to graduate different types of lymphomas depending on the stage of differentiation they are in (Figure 1) (4).

It is a fact, that lymphomas represent a rising number of cancer cases. In the western world nowadays approximately 20 new cases out of 100,000 people are reported per year. Nearly 95 % of these cases are B-cell lymphomas so the further focus of this diploma thesis will be on them (4).

According to a statistical evaluation of STATISTIK AUSTRIA, taking data from the Austrian cancer registry (as at October 2, 2015), the Non Hodgkin lymphoma incidence of the Austrian population has risen steadily from 492 in the year 1983 up to 1,271 cases in 2011, slightly falling to 1,265 cases in 2012 (5). In 2012, 617 patients died from their disease, representing 3 % of cancer deaths reported in Austria. Age standardized mortality was 1.4 to 1.8 times higher for men than for women (6).

Lymphomas are malignancies of every age but are more likely in the population with increasing age. By the end of 2012, 5,431 men and 5,152 women were living with the

diagnosis Non-Hodgkin-lymphoma. The histological type of B-Cell-lymphomas represented 60 % of all Non-Hodgkin-lymphomas. About 10 % were T-cell-lymphomas. The relative 1- and 5-year survival rate increased from 73 % in the late nineties to 78 % in 2012 (6).

The Hodgkin lymphomas, by comparison, showed an incidence of 161 persons in 2012 in Austria (7).

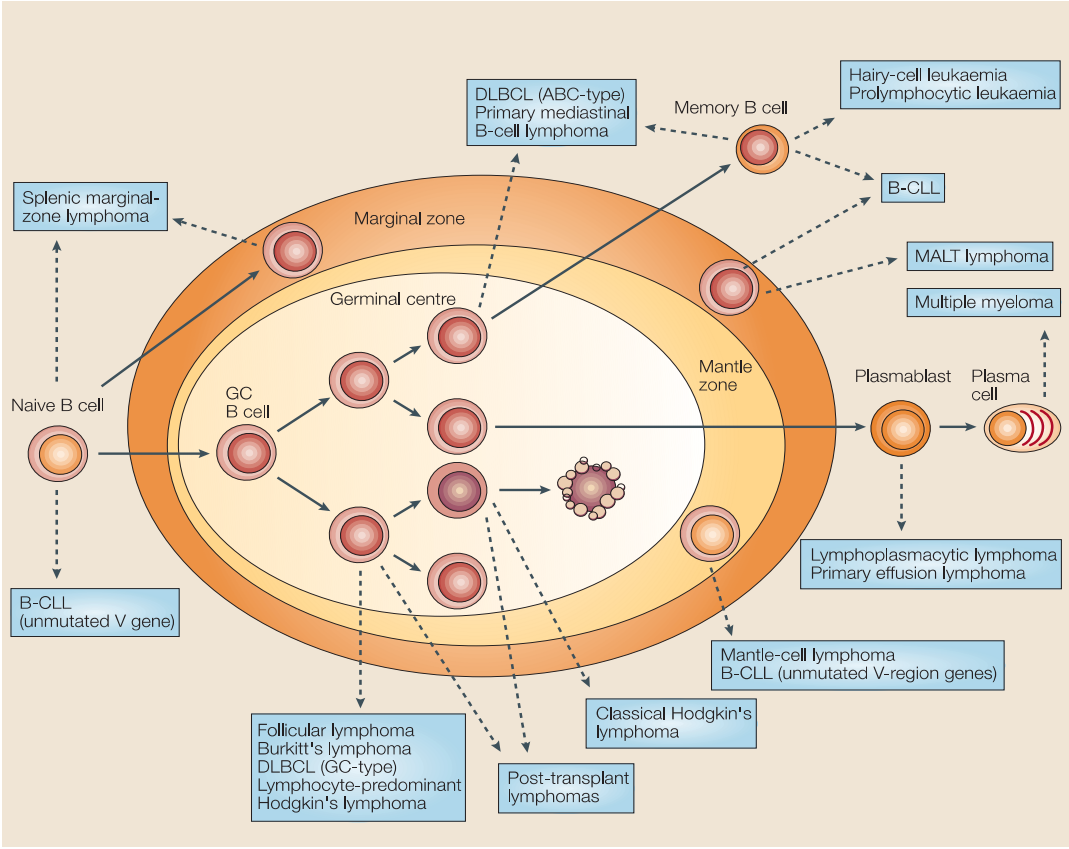

Figure 1 Illustration of the origin of various types of lymphomas - adapted from Küppers, R., et. al. (4)

Table 1 List of human mature B-cell lymphomas - adapted from Küppers, R., et. al. (4)

Lymphoma	Features	Frequency among lymphomas (in %)
B-cell chronic lymphocytic leukaemia	Leukaemia of small B-cells that express the CD5 antigen, involving peripheral-blood and bone-marrow cells. It is common in elderly patients.	7
Mantle-cell lymphoma	Arise from cells that populate the mantle zone of follicles, express CD5 and show an aberration in cyclin-D1 expression.	5
Follicular lymphoma	A nodal lymphoma with follicular growth pattern. Lymphoma cells morphologically and phenotypically resemble GC B-cells. Most cases are associated with BCL-2-IgH translocation.	20
Hairy-cell leukaemia	Chronic B-cell malignancy involving spleen and bone marrow. Very few circulating leukaemia cells.	<1
MALT lymphoma	Extranodal marginal-zone B-cell lymphoma. Develops mostly in acquired lymphoid structures.	7
Burkitt's lymphoma	Fast growing. Mostly extranodal. Characterized by a MYC-Ig translocation. Patients with eBL are EBV-positive in nearly all cases. Patients with sBL are EBV-positive in about 30 % of cases.	2
Diffuse large B-cell lymphoma	Heterogeneous group of lymphomas characterized by large B-cells. Several subtypes are recognized. Morphological variants include centroblasts and immunoblasts.	30-40
Multiple myeloma	Neoplastic proliferation of plasma cells in the bone marrow.	10
Classical Hodgkin's lymphoma	Characterized by bizarre, large tumour cells. Hodgkin and Reed-Sternberg cells account for less than 1 % of cells in the tumour and are mixed with various non-neoplastic cell-types.	10

1.1.2 B-Cell development

1.1.2.1 Development and differentiation of B-cells

The early B-cell development takes place in the bone marrow and is completed when a very early type of B-cells, a so called B-cell-precursor, is able to express Ig heavy- and light chain genes and holds a functioning surface antigen receptor. Only B-cells with a correct BCR are modified to so called mature naive B-cells and are now able to exit the bone marrow and if needed can be activated by antigens to allow an appropriate immune response of the body. The structure of the BCR is essential in the B-cell development and therefore plays a major role in all differentiation steps. The BCR consists of four Ig-chains, two identical heavy chains and two identical light chains that are linked via disulphide bridges. The BCR is essential for a B-cell, because only a constant expression of the BCR allows a B-cell to not undergo programmed cell death, so called apoptosis (4).

B-cell differentiation takes place in the germinal centres of the lymph follicles. The lymph follicles are formed of IgM+/IgD+ naive B-cells (Figure 2).

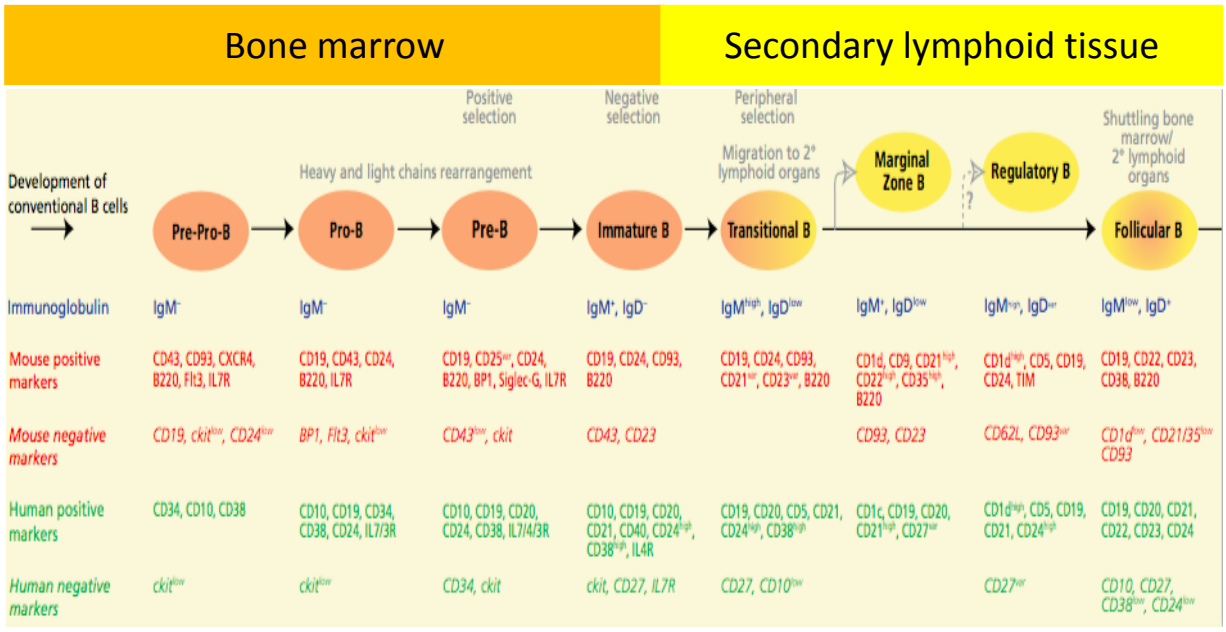

Figure 2 Illustration of the B-cell development - where it takes place and the immunophenotypic differences of the B-cells - adapted from https://www.bdbiosciences.com/documents/Bcell_Brochure.pdf

In between these follicles areas full of T-cells, so called T-cell zones, can be found, while in the centre of the follicles FDCs are located (Figure 3):

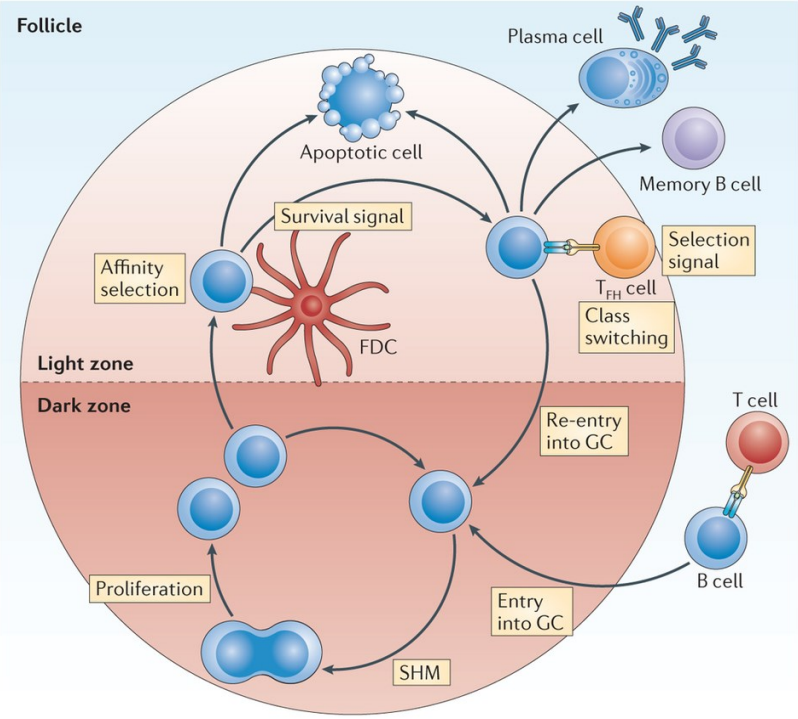

Figure 3 Illustration of the dark and the light zone of a lymph follicle - adapted from Balthasar, A., Heesters, et. al., 2014

By antigen contact naive B-cells become activated and start their way to the border of the T-cell zone to proliferate and bind with antigen-specific T-cells in the interfollicular region of the lymph node. Naive B-cells move to the centre of the follicle to form the so called early germinal centre. There, B-cells mature to so called B-cell blasts that grow rapidly and start interacting with the FDCs. At this point the B-cell blasts dislodge the IgM+ IgD+ B-cells causing the formation of the mantle zone in the secondary lymphoid tissue. Histologically, a dark and a light zone can be distinguished within the lymph follicles. The dark zone is packed fully with B-cells, the light zone contains less B-cells plus other cells like FDCs and macrophages. Germinal centre B-cells mature and multiply within the dark zone and undergo the somatic hypermutations, producing B-cell clones with high affinity to various antigens. B-cells with this high-affinity-antigen-receptors move through the light zone. This procedure is done several times and provides further selection. Plasma cells and memory B-cells that are able to identify and fight the pathogens are the results of this procedure (Figure 3) (8).

1.1.2.2 Important proteins of GC initiation

BCL-6 upregulated expression is essential for naive B-cells to enter the follicle (8). BCL-2 and BCL-6 show an inverse relationship concerning their expression in the normal secondary lymphoid follicle (9). MEF2B expression by antigen-activated B-cells leads to an upregulation of the expression of BCL-6, showing the initiating factor of MEF2B in precursor B-cells. IRF4 plays an important role in the late GC B-cell development. IRF4 also induces the expression of BCL-6. MYC is a protein, which is necessary in nearly all proliferating cells. In the step of the early GC MYC+/BCL-6+ blasts were detected, so MYC also plays a role in GC formation. In a mouse model, where MYC was deleted from activated B-cells, they do not form GCs. MCL-1 regulates the survival of B-cells during the GC building, BCL-XL in this case was nonessential (8), but had been taken under consideration during my Western blot evaluation as well.

1.1.3 The cellular origin of the B-cell lymphomas

A very high number of B-cell lymphomas evolve from GC B-cells. Due to genetic transformation B-cells can transform to malignant cells. The majority of the B-cell lymphomas origins directly from GC B-cells: FL, Burkitt's lymphoma, DLBCL, Hodgkin's lymphoma and post-transplant lymphoma. The cellular origin of the B-CLL are the naive B-cells. Mantle-cell lymphomas evolve from mantle zone B-cells, the MALT-lymphoma as well as a type of B-CLL origins from marginal zone cells, the hairy cell leukaemia from the memory B-cells and the multiple myeloma from plasma cells (Table 1) (4). These lymphomas also vary in their BCR-status, especially in 25 % of all Non-Hodgkin's lymphomas no BCR-expression is found (Table 2) (4).

Table 2 List of the BCR-status of various types of lymphomas - adapted from Küppers, R., et. al. (4)

Type of lymphoma	BCR-expression	No BCR-expression
Diffuse large B-cell lymphoma	✓	×
Hairy-cell leukaemia	✓	×
Burkitt's lymphoma	✓	×
Follicular lymphoma	✓ in some patient samples BCR is autoreactive	×
Gastric MALT lymphoma	✓ autoreactive BCR, especially with rheumatoid factors	×
B-CLL	✓ BCR often autoreactive	×
Classical Hodgkin's lymphoma	×	✓ in at least 25 % of all cases

1.1.4 Molecular Lymphomagenesis

1.1.4.1 VDJ, SHM and CSR

The molecular mechanisms of lymphomagenesis mainly involve the Ig gene locus and can be attributed to genetic alterations occurring during VDJ recombination, SHM and CSR (Figure 4):

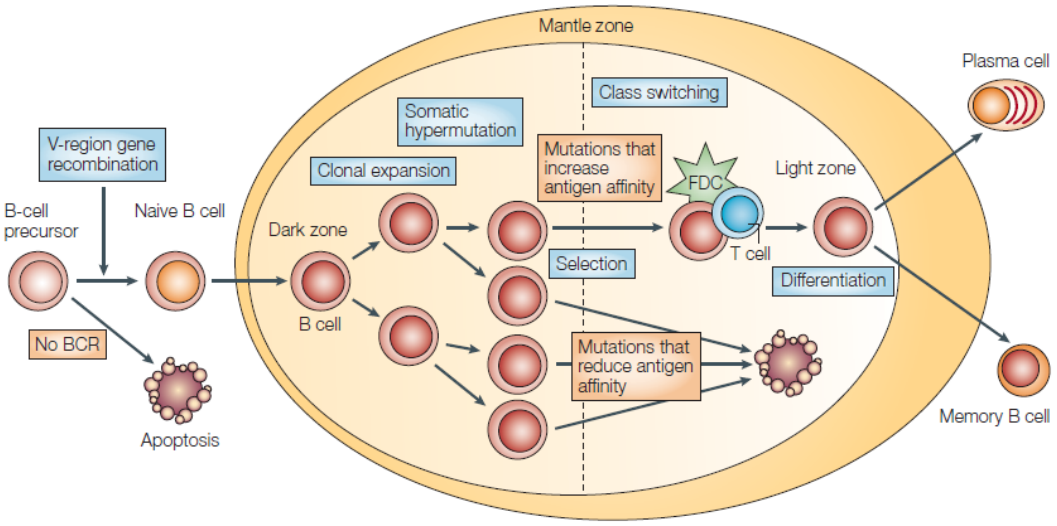

Figure 4 Illustration of the VDJ, the SHM and the CSR in the B-cell development - adapted from Küppers, R., et. al. (4)

During different stages of B-cell maturation, BCRs undergo high levels of genetic rearrangement in *V (variable), D (diversity)* and *J (joining)* segments of variable regions of *V* and *J segments* of *heavy* and *light chains* of i*mmunoglobulins* called *VDJ* recombination, in order to generate a rich repertoire of diverse antibodies providing a broad-spectrum cover against the majority of antigens (10,11). The *VDJ* recombination occurs at early B-cell development stages in the bone marrow. During this process three gene segments (*V, D* and *J*) of the *variable region* of the *heavy chains* and two (V and J) of the *variable region* of the *light chains* are assembled. The DNA located between the rearranging gene segments is deleted by two endonucleases –*RAG 1* and *2* - causing double strand breaks. The *heavy chain* assembly occurs in two steps. In the first step, a DH gene segment is rearranged to a JH segment, and in the second step a VH segment is rearranged to a DH joint (12,13).

When B-cells enter the dark zone of the GC, the variable regions of BCRs undergo somatic hypermutation to increase the diversity of immunoglobulins. Cells then migrate to

centrocytes of the GC light zone to undergo a process called class switching recombination in order to create different classes of *immunoglobulins* (*IgG, IgM, IgE and IgA*). The SHM introduces point mutation, deletion and duplication in the rearranged variable regions of heavy and light chains and their flanking sequences (11). In the CSR, the expressed heavy chain constant region (C_H) gene (usually Cμ and Cδ) is replaced by a downstream C_H gene. The recombination involves deletion of the DNA between repetitive regions (switch regions sμ, sγ and sα) upstream of the recombining C_H genes (14). The enzyme *activation-induced cytidine deaminase* is required for SHM and CSR. In the first phase of both molecular processes, *AID* deaminates cytidine to uracil to generate a U-G mismatch. U-G mismatches normally are corrected by base excision and mismatch repair pathways. In the second phase of SHM, U-G mismatch are repaired by error-prone *BER* and *MMR* pathways to generate mutations (15). BER and MMR are mediated by the action of *UNG* and *MSH2/MSH6*, respectively. CSR is initiated by *AID*-mediated cytidine deamination on the opposing DNA strands within the switch region. The action of *UNG* and apurinic/apyridimic *endonuclease 1* or *MSH2/MSH6* activity cause double strand breaks. Further processing and joining of broken switch region is facilitated by factors involved in classical and alternative nonhomologous end joining (16).

1.1.4.2 Genetic alterations

Not only the mechanisms described above but also mutations in so called tumour suppressor genes (e.g. *TP53*, coding for *p53*) and translocations that do not occur in *Ig* loci and viruses (e.g. EBV) are known to cause malignant B-cell development. Viruses are also associated with lymphomagenesis, like HHV-8. The EB virus is found in most Burkitt's lymphomas and in 40 % of all Hodgkin's lymphomas. Even bacteria, e.g. Helicobacter pylori can cause gastric MALT Lymphomas (4).

Although the number of B- and T-cells in the human body is approximately the same, the number of B-cell lymphomas is significantly higher than the T-cell types. This is caused by different special determinants that direct the lymphomagenesis. The origin of the different types of lymphomas is important as their heterogeneous clinical appearance and behaviour requires different treatment strategies. Furthermore, the class switching recombination and the somatic hypermutation processes do not occur in T-cells, so this could explain the higher number of B-cell than T-cell lymphomas (4).

1.1.4.3 Tumour suppressor genes

Tumour suppressor genes are genes, that code for proteins, protecting cells from unregulated cell growth. Proto-oncogenes or oncogenes code for proteins that, when overexpressed, lead to uncontrolled cell growth.

One of the most-discussed tumour suppressor genes is *TP53*, that codes for P53, the so called "Guardian of the genome" and is mutated in about 50 % of all human tumours (35,36). *MDM2* is the prime regulator of *p53*, binding on it and causing an ubiquitination and degradation (Figure 9). But *p53* also affects *MDM2* in an autoregulatory process by promoting its transcription (17).

P14ARF (in mice it is called *p19Arf*) binds to *MDM2* and leads to an activation of *p53* in the so called *p19ARF-MDM2-P53*-pathway (18).

1.1.4.4 Important cell cycle proteins

Translocations are the main chromosomal aberrations in haematological malignant transformation resulting in defect B-cell-development-genes, proliferation genes, cell proliferation determinants, and more. These gene defects and further misleading pathways can be seen as the driving force for lymphomagenesis (20).

BIM

The Bh3-only protein *Bim* is known as a major regulator of lymphoid and myeloid homeostasis and as a tumour suppressor gene by its role of being an antagonist of *Bcl-2*. It is expressed in many different cell types (21). Egle, A., *et al.* (2004) showed that a *Bim*-knockout does not necessarily lead to tumour growth proving that a *Myc* overexpression is needed. However, mice with *Bim*+/+ were shown to have a higher frequency of lymphomagenesis (21). One explanation for this could be, that some Bh3-only proteins like *Bim* and *Puma* bind very closely to pro-survival proteins, e.g. *Bcl-2* or *Bcl-xl* (22). However, the Bh3-only proteins might not always affect tumorigenesis. It is more likely that there is a variety of the proteins in different cancers (23).

It is assumed that other members of the Bh3-only protein group, e.g. *Bid*, *Bad*, *Bmf* might serve as tumour suppressor genes as well, giving the idea to maintain developing *Bh3*-mimetics in cancer therapy research (21).

BCL-2

Most of the follicular lymphomas contain a t(14;18) translocation that involve the human *BCL-2*. Reed, J. C., *et al*. (1988) performed a gene transfer to identify the oncogenic potential of *BCL*-2 (24). In the same year it was proved that *BCL*-2 is rearranged in a high number of *DLBCLs* (25). Nowadays it is known, that a higher expression of *BCL*-2 reduces apoptosis by inhibiting the mitochondrial cytochrome c triggered release of other apoptotic stimuli (26).

BCL-XL

BCL-XL is the long isoform of BCL-X and is also known to inhibit the cytochrome c triggered apoptosis and prolongs cell survival (26) either alone or in cooperation with *C-MYC* (29). The *Bcl-xl* of transgenic mice even shows resistance to apoptosis in *in vivo* experiments (26,27). *BCL*-XL overexpression is found in AML, HL, NHL, HIV-associated leukemia, myeloma and in murine B- and T-cell tumour lines (28).

MCL-1

MCL-1 is a member of the *BCL-2* family and thus an antiapoptotic gene (29,30). More than 80 % of EμMyc mice, that overexpressed *Mcl*-1 developed different types of B-cell lymphomas (31). Rassidakis, G. Z., *et al.* (2002) showed that *MCL*-1 was overexpressed in anaplastic large cell lymphomas as well as in DLBCLs (33).

P19-MDM2-P53

P53 plays the most important role in cell induced death and is mutated in about 50 % of all tumours (37,38). In combination with *p19ARF* and *MDM2* it forms an important cell signalling pathway in mice: *MDM2* essentially regulates *p53* by binding to it and thus promoting its degradation. *P19ARF* binds to *MDM2* and therefore inhibits its activity which leads to a stabilized and well working *P53*. This pathway is often non-functioning in *c-Myc*-driven overexpression hence malignant cells can evolve (36).

PARP

PARP is a protein, which is activated by endogenous cellular reactions or genotoxic agents that cause DNA strand breaks. When activated it transfers ADP-ribose units from NAD to nuclear proteins including PARP itself resulting in cellular dysfunction and cell death (39). Until today the function of PARP is still discussed controversially.

1.1.5 Aggressive B-cell lymphomas

Aggressive B-cell lymphomas are malignancies of the lymphatic tissue with a high proliferation rate and fast growing malignant cells that normally require instant treatment. The most common aggressive Non-Hodgkin lymphomas are the DLBCL, the follicular lymphoma grade 3 and the Burkitt's lymphoma (40).

1.1.5.1 DLBCL

The DLBCL is a very heterogeneous type of lymphoma with lots of different pathways being deregulated (20). Global gene expression profiling showed that all DLBCL cluster in three different subtypes based on similarity in expression patterns to their cellular origin: The GCB, the ABC DLBCL and the PMCL, evolving from thymic B-cells (20). Other variants of the DLBCL is the T-cell-rich/histiocyte-rich type with reactive T-cells and histiocytes, the anaplastic type with pleomorphic nuclei and CD30 expression and the plasmablastic DLBCLs that are often found in HIV-positive patients (41). The most prevalent genetic aberration in ABC-DLBCL is the 3q27 alteration causing a *BCL-6* overexpression (42). Amplifications of *BCL-2* on chromosome 18 and deletion of *INK4A-ARF* on chromosome 9 shows, that the inhibition of programmed cell death plays a role in ABC-DLBCL (43).

15 years ago the first positive outcomes of DLBCL treatment with the monoclonal antibody Rituximab were reported and R-CHOP is still the gold standard of therapy (44).

1.1.5.2 Burkitt's Lymphoma – a highly proliferative and aggressive type of lymphoma, mainly in children

The Burkitt's lymphoma is a highly proliferative type of lymphoma, which was primary described by Dennis Burkitt in 1958, when he studied children in equatorial Africa, where

this disease is known to account for 30-50 % of all childhood cancer but only 1-2 % in adults (20). Later on, first cases of BL were reported in Europe and the US as well. Burkitt's lymphomas can be divided into three different types: The African eBL, the sBL for tumours elsewhere diagnosed and the HIV-mediated immunodeficiency-related BL. EBV was shown to be present in all cases of eBL, but only in 10-20 % of sBL. All three types of BL have in common that *MYC* is translocated. In fact, this is the most common mutated gene in BL. The mutation of the proapoptotic *BCL-2*-family member *BIM* leads to higher proliferative and less apoptotic function of *MYC*. Mutations in *TP53* are frequently found in BL (35 % of all cases). BL cells still express BCR, but compared to other aggressive lymphomas it lacks expression of *NF-KappaB* target genes (45). Yustein and Dang, stated that the therapeutic approach to cure BL implicates the use of intensive chemotherapy thus BL is often curable, however, older individuals often do not endure the hard therapy (46).

1.1.6 Lymphoma therapy approaches

Nowadays chemotherapy, radiation and the anti-CD20 antibody Rituximab are the key factors of lymphoma therapy (47).

The positive outcome of a combined therapy compared to a single agent therapy was firstly described in the 1970s. CHOP became the first-line therapy by combining the chemotherapeutics cyclophosphamide, adriamycin, vincristine and prednisolone (47). In 1997 the human-mouse monoclonal anti-CD20 antibody Rituximab (R) was homologated by the US Food and Drug Administration for the treatment of lymphomas. This antibody shows specific anti-lymphoma activity (48). R-CHOP nowadays remains the first-line therapy in aggressive lymphomas. The R-CHOP therapy consists of 14- or 21-day cycles. Each cycle starts with Rituximab on day 1, followed by cyclophosphamide, doxorubicin and vincristine on day 2, accompanied by prednisolone on days 1-5 (49).

It is recommended to use granulocyte stimulating factor to avoid neutropenia during the therapy (50). The role of radiation in DLBCL is not clear yet and needs further investigation and evaluation (51). For relapsed patients the therapy of choice is a high-dose chemotherapy followed by autologous stem cell transplantation. Only patients with a

response of at least one year to the inductive R-CHOP therapy are expected to have a good outcome (52). Allogenic transplantation has to be considered in these patients with a bad response to induction chemotherapy (53).
However, Burkitt's lymphoma can often be cured by using intensive chemotherapy (45).

Moreover, it was hypothesized that the drug clearance of the patients impacts the drug concentration-response significantly when receiving prolonged infusion therapy over a period of time. This was the basis for the dose-adjusted (DA) EPOCH therapy schedule where doxorubicin, vincristine and etoposide are infused over 96 hours plus cyclophosphamide and prednisone are given as a bolus. Depending on the number of neutrophil granulocytes, doxorubicin, etoposide and cyclophosphamide are dose-adjusted (90, 91, 92, 93). It was approved by a clinical trial that an addition of Rituximab elevates the overall survival rate in the therapy of this type of lymphoma, resulting in avoidable radiotherapy. Dunleavy *et. al.* 2013 demonstrated that patients suffering from primary mediastinal B-cell lymphoma (sort of a DLBCL) had a 97 % overall survival rate after undergoing a treatment of DA-EPOCH-R (DA-EPOCH combined with Rituximab) (94).

1.2 The Nuclear Orphan Receptor *NR4A*

1.2.1 Background of *NR4A*

Figure 5 Illustration of the NR4A1 gene locus in human DNA adapted from the USCS Genome Browser – NR4A1 is located at the long (q-) arm of chromosome 12 and consists of 8,105 bp.

In the 1980s many nuclear receptors were discovered (54), which all have a characteristic structure in common (Figure 6A): A variable N-terminal region, the so called amino-terminal region, a central DBD and a variable linker region that connects the DBD with the region E/F at the C-terminus including the LBD (54,55).

The nuclear orphan receptors (Figure 6B) of the Nur77-family, belong to the steroid nuclear hormone receptor superfamily and consist of *NR4A1* (Figure 5) (*Nur77*), *NR4A2* (Nurr1) and *NR4A3* (*NOR*-1) (56). Their genetic structure is very similar giving the hint of a common gene "ancestor" (57). All three are normally located in the nucleus due to their NLS. NR4A1 has a *BCL-2*-binding domain and upon translocation from the nucleus to the cytoplasm is able to bind to mitochondria on a hydrophobic groove. This procedure results in a change of the *BCL-2* phenotype transforming it from cytoprotective into cytodestructive, by inducing cytochrome c release from mitochondria and consequently leading to apoptotic cell death (56). *NR4A3* seems to have an analogue transcriptional regulation as *NR4A1* (58).

NR4As function as transcription factors. The name "orphan" is used due to a lacking proof of a physiological ligand. *NR4A1*, *NR4A2* and *NR4A3* are nuclear receptors that seem to be regulated by external stimuli and that are expressed in many different tissues: heart tissue, kidney tissue, liver tissue, brain tissue, skeletal muscle tissue, fat tissue and T-cells (56).

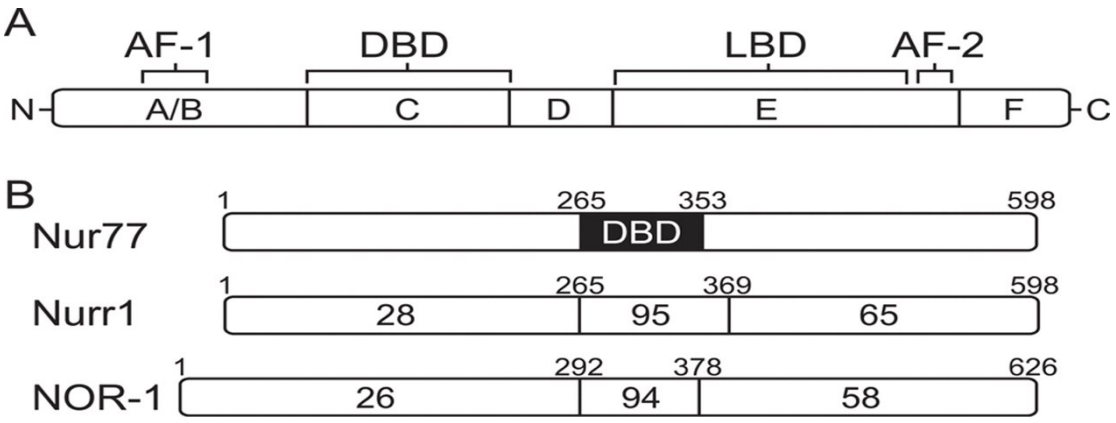

Figure 6 Illustration of the NR4A-family and its members NR4A1 (Nur77), NR4A2 (Nurr1) and NR4A3 (NOR-1) - adapted from José Martinez-González, Lina Badimon, et. al., 2005

A) Characteristic structure of NR4A-family members: A variable N-terminal region, the so called amino-terminal region, a central DNA-binding domain (DBD) and a variable linker region that connects the DNA-binding domain with the region E/F at the C-terminus including the ligand binding domain (LBD).

B) Each family member of NR4A (54,55).

NR4As are so called immediate-response genes, which means that they are stimulated by several factors like prostaglandins, growth factors, fatty acids and neurotransmitters (59). The activation of *NR4As* results in an activation of target genes that are important for cell cycle regulation, apoptosis, inflammatory processes, atherogenesis, metabolic processes, DNA-repair and tumorigenesis (60), and thus they play an important role in metabolic, cardiovascular, neuronal, articular, inflammatory and malignant diseases (61).

NR4A1 and *NR4A3* are known to contribute to the negative selection of the T-lymphocytes and the IgM-mediated as well as the viral-induced B-cell apoptosis (56). Hence a dysregulated NR4A-receptor may lead to malfunctioning apoptosis and malignant transformation.

1.2.2 *NR4A*'s role in myeloid neoplasms and lymphoid malignancies

Nr4a1-/- and Nr4a3-/- mice rapidly develop AML and die within four weeks. Human AML patients showed downregulated *NR4A1* and *NR4A3* as a specialty of leukemic blasts in comparison to healthy CD34+ progenitor cells of the bone marrow (62). *Nr4a1* and *Nr4a3* resulted in an upregulation of *MYC*. This is confirmed by the finding that *NR4A1* and *NR4A3* seem to be able to occupy *MYC's* promoter region and perform a suppressive function on it (63).

Deutsch *et al.,* 2014 showed that *NR4A1* and *NR4A3* were significantly downregulated in B-CLL, FLs and DLBCLs compared to normal controls. Furthermore, low *NR4A1* expression was associated with poor cancer-specific survival. Overexpression of *NR4A1* resulted in a higher number of apoptotic lymphoma cells accompanied with diminished apoptotic signals of *TRAIL*, *BIM* and *PUMA* (Figure 7) (65).

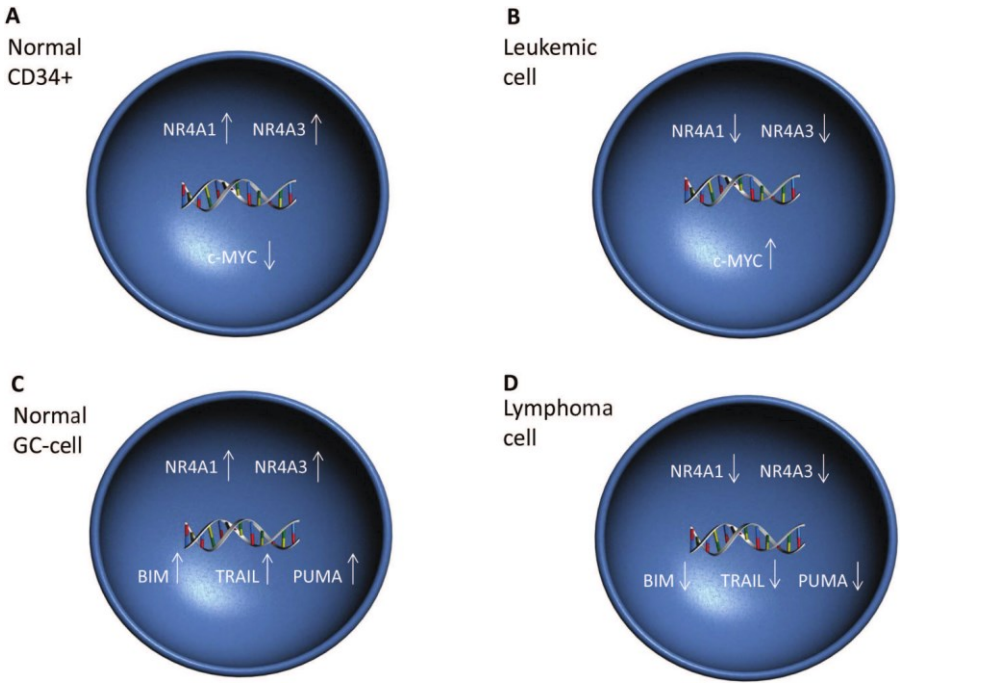

Figure 7 Schematic representation of the NR4A1 and NR4A3 functions in hematopoietic cells - adapted from Wenzl, K., et. al., 2015
A) NR4A1 and NR4A3 upregulation and C-MYC downregulation in normal CD34+ cells,
B) NR4A1 and NR4A3 downregulation and C-MYC upregulation in leukemic CD34+ cells,
C) NR4A1, NR4A3, BIM, TRAIL and PUMA upregulation in GC B-cells,
D) NR4A1, NR4A3, BIM, TRAIL and PUMA downregulation in lymphoma cells (64)

1.3 The EμMyc mouse

1.3.1 EμMyc transgenic mouse model

When creating a transgenic mouse model, a transgene is inserted in the mouse genome. (85). Alan W. Harris *et al*, 1988 tried to mimic this translocated *Myc* genes that were found in lymphoid tissue by introducing a DNA sequence into mice, that was isolated from a mouse plasmacytoma, where a functioning and normal *Myc*-gene had been coupled to the Ig heavy chain enhancer. The results were transgenic mice expressing the *EμMyc* transgene only in B-lymphoid cells resulting in an overstimulated proliferation (85).

EμMyc mice exhibit an initial preneoplastic phase characterized by the polyclonal expansion of pre B -cells even before birth. Within their first year of life, EμMyc mice develop malignant monoclonal lymphomas (mean latency of 12-16 weeks) (74,75,76).

1.3.2 *C-Myc* – the cellular myelocytomatosis oncogene

Figure 8 Illustration of the MYC gene locus in human DNA - adapted from the USCS Genome Browser
MYC is located at the long (q-) arm of chromosome 8 and consists of 5,336 bp.

MYC is one the best described proto-oncogenes and is deregulated in many types of cancers, and also is important in NHL-lymphomagenesis (66). It is a helix-loop-helix leucine zipper protein lying on chromosome 8 (Figure 8), that controls many cellular functions (67) and promotes and regulates ribosomal protein transcription (68) and ribosomal biogenesis (69). Normally a balance between apoptosis (induced by the *p19ARF-MDM2-P53*-pathway) and antiapoptotic factors e.g. *BCL-2, BCL*-XL sensitizes a cell to apoptotic stimuli.
This leads to the assumption that there has to be a second mutation, a so called "second hit" to break this balance: *C-Myc*-driven tumours are known to have an inactivation of this important pathway resulting in uncontrolled cell proliferation and was formerly detected in Burkitt's lymphoma (18). Tumours of EμMyc mice showed either a deranged *p19Arf-Mdm2-p53*-pathway or overexpressed antiapoptotic proteins Bcl-2 or Bcl-xl. *Bim* was proofed to be a suppressor of *EμMyc* induced lymphomagenesis (19).

MYC interacts with other cell cycle proteins e.g. p53, p19ARF, MDM2 (70). Several other genes are described to have an effect on MYC. It suppresses *Nfkb2*, a member of the Rel/NF-KappaB family, and is shown to result in lymphomagenesis proofed *in vitro* in primary mouse fibroblasts and B-cells and *in vivo* in the *EμMyc* transgenic mouse model of human BL (71). Deregulated *MYC* is also found in 5-10 % of all DLBCLs (66).

It was detected that during the B-cell lymphomagenesis in mice there was an increase of the total RNA and mRNA copies per cell. *Myc* is assumed to not act as a global

transcription factor but is shown to be able to activate and repress some genes resulting in global RNA production (72).

1.3.3 The second hit model of the *EμMyc* mouse: Inactivation of pro-apoptotic genes and/or overexpression of anti-apoptotic genes are needed for malignant transformation

C-Myc is known to activate apoptotic- and to suppress anti-apoptotic pathways, which are supposed to safeguard against *c-Myc*-induced transformation. In this scenario, *p53* accumulates as a result of *p19Arf* induction, which relieves an *Mdm2*-dependent feedback mechanism and triggers apoptosis. Alternatively, high levels of *c-Myc* suppress the expression of the anti-apoptotic genes *Bcl-2, Mcl-1 and Bcl-xl*. Thus, efficient transformation by *c-Myc* requires concomitant hits to counterbalance apoptosis (Figure 9) (73,74).

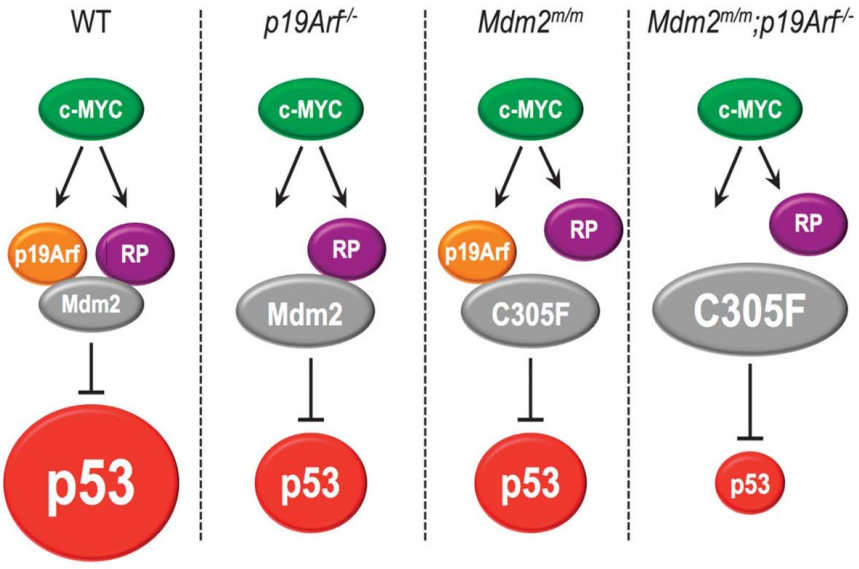

Figure 9 Illustration of effects from c-Myc on tumour suppressor genes - adapted from Meng, X., et. al. (38)
In wildtype mice p19Arf and Rp both inhibit Mdm2 resulting in maximum p53 stabilization (first panel). In cells with p19Arf mutation (second panel) or Mdm2-mutation (third panel) c-Myc signals are still functioning on one of the remaining pathways, but p53 induction is lower. In cells suffering a p19Arf- and Mdm2-mutation a c-Myc overexpression is not able to activate p53 (fourth panel) (38).

1.3.4 Loss of *Nr4a1* accelerated *Myc*-driven lymphomagenesis

To explore whether *Nr4a1* suppresses tumour formation in oncogene-driven B-cell lymphoma development, mice, lacking the Nr4a1 protein, were crossed with the *EμMyc* transgenic mice, which develop malignant monoclonal lymphomas with a mean latency of 12-16 weeks (75,76,77). For comparison, my group generated a cohort of EμMyc mice with (EμMyc Nr4a1+/+, n=75) and without *Nr4a1* (EμMyc Nr4a1-/-, n=46) and monitored them until onset of overt disease. EμMyc Nr4a1-/- mice developed visible tumours significantly faster compared to EμMyc Nr4a1+/+ mice (median = 44 days for EμMyc Nr4a1-/- vs. 107 days for EμMyc Nr4a1+/+; p<0.001; Figure 10). Additionally, EμMyc Nr4a1-/- mice had a significantly shorter life span (median survival = 77 days) compared to EμMyc Nr4a1+/+ mice (median survival = 156 days; p<0.001, Figure 10). Taken together, these findings demonstrate that *Nr4a1* possesses tumour suppressive properties in a *Myc*-driven system.

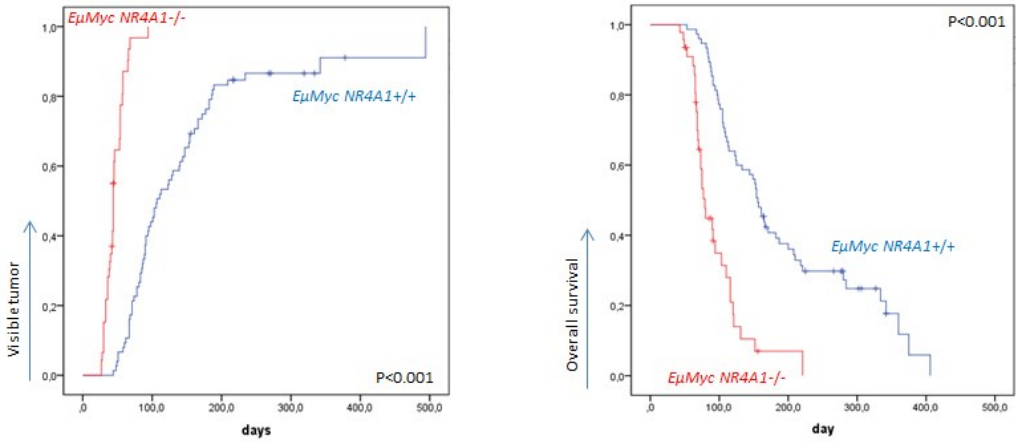

Figure 10 Development of lymphomas and survival of EμMyc Nr4a1+/+ and EμMyc Nr4a1-/- mice - adapted from Wenzl, K., et. al., 2015

Tumours developing in *EμMyc* mice normally have an immature B-cell lymphoma immunophenotype (Pro B-cell-, Pre B-cell- or an immature B-cell lymphoma phenotype) (75,76,77). Therefore, we isolated tumour cells developed in the EμMyc Nr4a1+/+ mice (n=17) and EμMyc Nr4a1-/- mice (n=19) and phenotypically analysed them by flow cytometry (using antibodies against B-cell-, T-cell and myeloid cell markers).

Furthermore, flow cytometry analysis of bone marrow (BM) and spleen (SPL) cells from EμMyc Nr4a1-/- (n=18), EμMyc Nr4a1+/+ (n=17) and wild type (n=4) mice was performed. In BM the ratio of Gr-1+ cells to B220+ cells was lower in the group of the

EμMyc Nr4a1-/- mice compared to EμMyc Nr4a1+/+ (p=0.025) and wildtype mice (p=0.009) (Figure 11). Additionally, in SPL cells, the ratio of B220+ cells to TCR+ cells was higher in EμMyc Nr4a1-/-, compared to EμMyc Nr4a1+/+ (p=0.006) and wildtype mice (p<0.007), and the ratio of Gr-+ cells to B220+ cells was lower in EμMyc Nr4a1-/- (0.025) and EμMyc Nr4a1+/+ (p=0.089) mice compared to wt mice (Figure 11). About 95% of the B220+ cells isolated from BM and SPL of EμMyc Nr4a1-/- and EμMyc Nr4a1+/+ mice exhibited the same immunophenotype as the lymphoma. By combining all of these findings, our data suggest that in the EμMyc Nr4a1-/- and EμMyc Nr4a1+/+ mice, the lymphoma cells infiltrate the BM and SPL, and the amount of infiltration in the EμMyc Nr4a1-/- mice is even more pronounced. These data suggest that loss of *Nr4a1* increases the dissemination potential of *EμMyc* lymphoma cells.

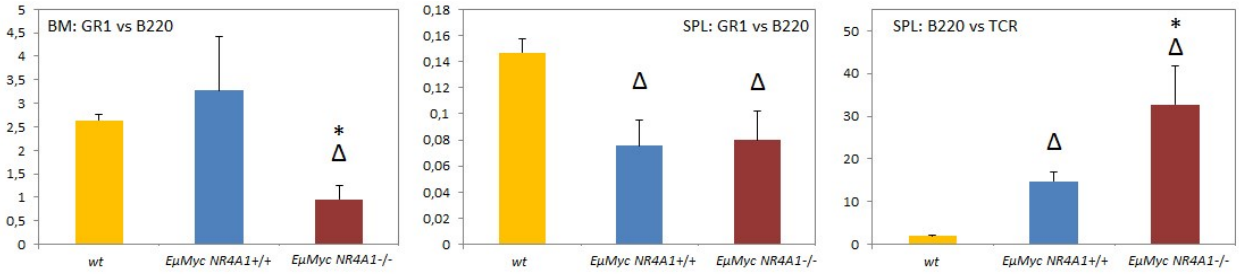

Figure 11 Comparison of the ration of Gr-1+ cells to B220+ cells in bone marrow (BM) and spleen (SPL) and the ratio of B220+ cells to TCR+ cells in SPL of EμMyc Nr4a1-/- and EμMyc Nr4a1+/+ mice. – adapted from Wenzl, K., et. al., 2015 The triangle denotes p<0.05 compared to wildtype mice (wt) and the asterisk denotes p<0.05 compared to EμMyc Nr4a1+/+ mice.

To further investigate the impact of *Nr4a1* loss on the oncogenic potential of *EμMyc* lymphoma cells, we isolated viable tumour cells (B220+ and 7AAD-) from EμMyc Nr4a1-/- (n=5) and EμMyc Nr4a1+/+ (n=8) mice, cultured them for 72h with or without LPS stimulation and determined the number of viable cells and the viability (B220 and 7AAD-staining by flow cytometry analysis) each day. As expected, a high proportion of B220+ lymphoma cells isolated from EμMyc Nr4a1+/+ and EμMyc Nr4a1-/- mouse tumours stained positive for 7AAD after 24h, 48h and 72h with and without LPS-stimulation (Figure 12). Interestingly, the number of viable EμMyc Nr4a1-/- cells increased over time and was significantly higher in Nr4a1-/- cells after 72h compared to cultured B220+ tumour cells isolated from EμMyc Nr4a1+/+ mouse tumours (2.05*106/ml vs 1.5*105/ml, p=0.052; Figure 12). Moreover, a BrdU assay was performed to gain insight into proliferation rates of the B220+ tumour cells isolated either from EμMyc Nr4a1-/- or EμMyc Nr4a1+/+ mouse tumours after 72h of culturing time. B220+ tumour cells isolated from EμMyc Nr4a1-/- mouse tumours exhibited a significantly higher percentage of

BrdU+ cells compared to EμMyc Nr4a1+/+ (19.28% vs 4.28%, p=0.038; Figure 12). Furthermore, the number of viable cells was significantly higher after culturing B220+ isolated from EμMyc Nr4a1-/- mouse tumours compared to EμMyc Nr4a1+/+ mice (4.18*106/ml vs 9.4*105/ml, p=0.056; Figure 12). These data indicate that loss of *Nr4a1* accelerates the proliferation of tumour cells in vitro (unpublished data generated by the research group of Alexander Deutsch).

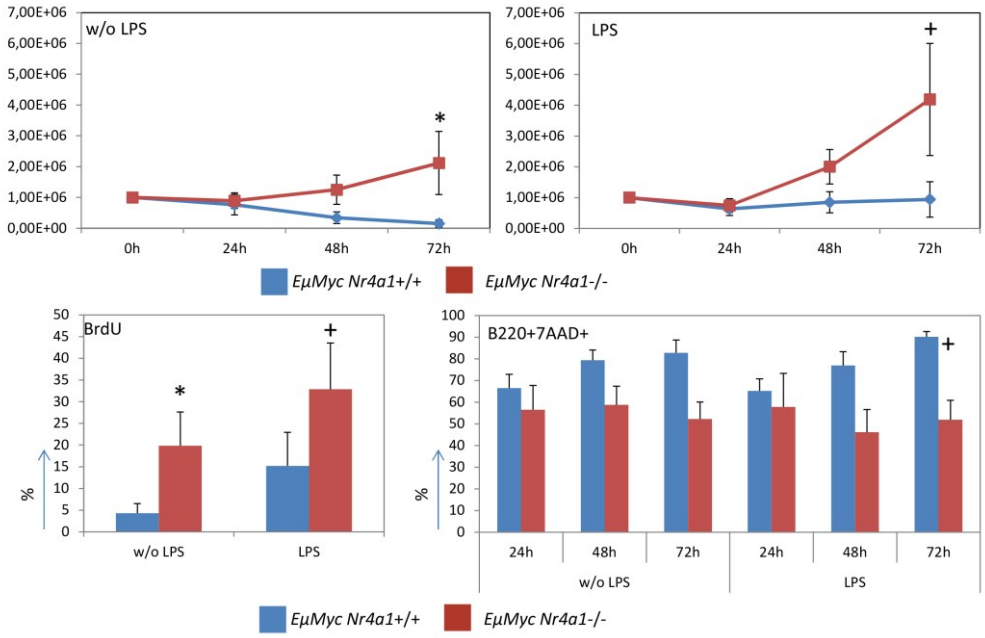

*Figure 12 In vitro growth and proliferation behaviour of B220+ tumour cells either isolated from EμMyc Nr4a -/- or EμMyc Nr4a1+/+ mouse tumours determined by estimation of cell number, BrdU-assay and B220/7AAD staining. – adapted from Wenzl, K., et. al., 2015 *denotes p<0.01 comparing B220+ cells isolated from EμMyc Nr4a -/- tumours compared to EμMyc Nr4a1+/+. + denotes p<0.01 comparing B220+ cells isolated from EμMyc Nr4a1-/- tumours compared to EμMyc Nr4a1+/+ under LPS stimulation.*

1.4 Aim

The aim of this work was to investigate the role of *Nr4a1* in the *c-Myc*-triggered lymphomagenesis. In detail, EμMyc Nr4a1-/- mice were compared to EμMyc Nr4a1+/+ mice and wildtype mice to clarify whether a disruption of the *p19Arf-Mdm2-p53* pathway and/or overexpression of *Bcl-2, Bcl-xl* and *Mcl-1* is needed as a second hit for a malignant transformation in the EμMyc Nr4a1-/- mouse model. Furthermore, I explored which genes or genetic programs are regulated by *Nr4a1* in the *Myc*-driven lymphomas by mRNA-sequencing. Additionally, semi-quantitative RT-PCR analysis for *Nr4a1* and *Nr4a3* expression levels in the EμMyc Nr4a1-/- and EμMyc Nr4a1+/+ mice derived tumours was performed. We tried to uncover significant differences at gene expression levels in EμMyc Nr4a1-/- mice versus EμMyc Nr4a1+/+ mice regarding important cell cycle proteins, in order to identify new molecular mechanisms of *NR4A1* in lymphomagenesis.

2 MATERIALS AND METHODS

2.1. The mice

2.1.1 Mouse models

Mice were generated on a C57bl/6 background. The *EμMyc* transgenic mice and Nr4a1-/- mice were purchased from the Jackson Laboratories. *EμMyc* transgenic mice and Nr4a1-/- mice were recrossed to generate a cohort of EμMyc Nr4a1+/+ and EμMyc Nr4a1-/- mice for phenotypical analysis. The well-being, health status and signs of potential lymphoma developement were controlled 3 times a week. The moribund EμMyc Nr4a1+/+ and EμMyc Nr4a1-/- were sacrificed and an autopsy (Figure 13) for general visual inspection was performed.

Nr4a1-/- mouse

The Nr4a1-/- mouse, also called knockout mouse, was generated by homologous recombination using a targeting vector that contains a Neomycin resistance gene insertion in the region encoding the amino-terminal domain of *Nr4a1*. Mice homozygous for this targeted mutation are viable and fertile, with no gross anatomical or behavioural abnormalities (78,79).

***EμMyc* transgenic mouse**

Eμ-Myc mice exhibit an initial preneoplastic phase characterized by the polyclonal expansion of pre B-cells even before birth. Within their first year of life, these mice develop malignant monoclonal lymphomas (mean latency of 12-16 weeks) (74,75,76).

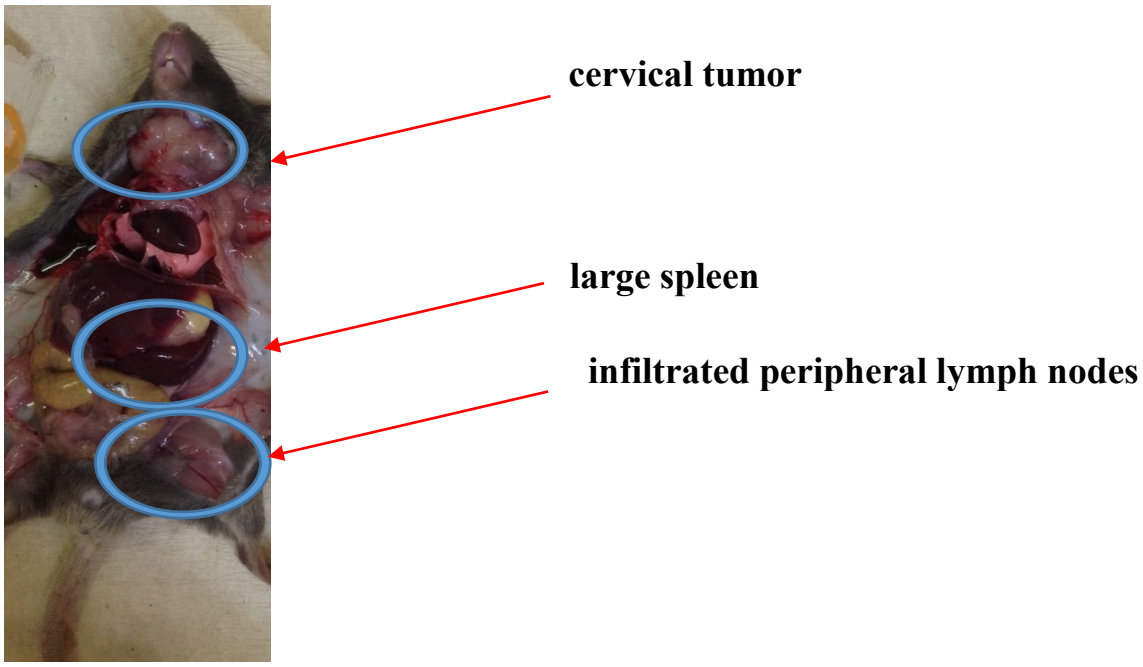

Figure 13 EμMyc Nr4a1 -/- mouse with a big cervical tumour, an enlarged spleen and infiltrated peripheral lymph nodes.

The neck tumours of the sacrificed mice were removed weighed and tissue sections were produced by using a cryomicrotome and then were snap frozen at -80°C for DNA, RNA and protein extraction. Additionally, wildtype mice were euthanized humanly and spleens were removed to be used as a wildtype control especially for Western blot analyses. All the experimental work on the mice was approved by the Austrian Federal Ministry of Science, Research and Economy.

2.2 DNA-isolation and Genotyping

2.2.1 DNeasy Mini Kit (Quiagen, Hilden, Germany)

The DNA-Extraction Kit Dneasy Mini Kit (Quiagen, Hilden, Germany) was used to isolate DNA from the mouse spleen and tumour tissue and for genotyping DNA isolated from mice tail tips. The quantity of the DNA was measured by a photometer and DNA was stored at +4°C.

2.2.2 Genotyping

The KAPA2G Fast Hot Start Kit (Peqlab, Erlangen, Germany) was used to perform a PCR and DNA-products were applied on a 3-%-Agarose (Biozym Scientific GmbH, Oldendorf, Germany) gel for the genotyping of the cells.

2.3 RNA-isolation and further processing

2.3.1 RNA-isolation using the RNeasy Mini Kit (Quiagen GmbH, Hilden, Germany)

The RNA was isolated with the RNeasy Mini Kit (Quiagen GmbH, Hilden, Germany) according to the manufacturer's protocol. RNA was frozen and stored at -80°C

2.3.2 cDNA Kit

The Kapa Probe Fast reaction mix (Peqlab, Erlangen, Germany) was used for creating cDNA. The TaqManR mix was applied to the samples for running a semi quantitative RT-PCR especially looking on *Nr4a1 and Nr4a3*. (Applied Biosystems, Invitrogen, Carlsbad, CA). This was performed by making triplicates using an ABI Prism 7900 detection system (Applied Biosystems, Carlsbad, CA, USA). *GAPDH, PPIA and HPRT* served as housekeeping genes. Control samples, to prove the absence of any contaminations of the RNA-samples were used.

2.3.3 mRNA sequencing

To find out whether the isolated RNA is intact it was analysed by using the Agilent 2100 Bioanalyzer. Therefore, the RNA 6000 Nano and Pico LabChip kits has evolved as a standard in the RNA quality assessment (80,81). The RIN gives information on the concentration, the ribosomal ratios and enables a visual inspection of the RNA integrity (82).

2.3.3.1 Use of RIN values

RIN values can be very useful in RNA integrity measurement. Figure 14 shows how RIN is used in practice (82). We isolated RNA from our tissue and performed a RT-PCR to validate the RIN values. A RIN threshold of 7.5 was detected and was used for the standard RNA- Quality control procedure (Figure 14, B). All samples with a RIN higher than the threshold successfully passed the quality control test (82).

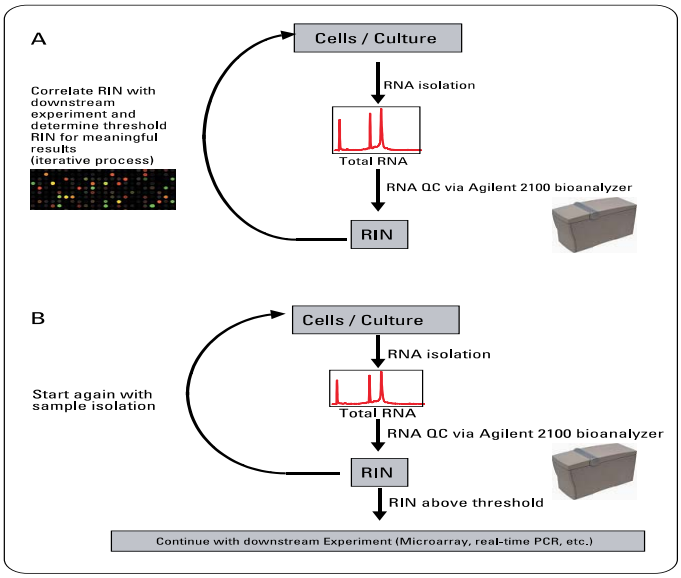

Figure 14 Illustration of the practical use of the RIN value - adapted from "RNA integrity Number (RIN) - standardization of RNA quality control", Odilo Mueller, Samar Lightfoot, Andreas Schroeder, 2004 (82)

2.3.3.2 mRNA sequencing procedure

5 EμMyc Nr4a1+/+, 5 EμMyc Nr4A1-/- mice and 5 wildtype mice samples (Table 3) were sent to an external laboratory in Innsbruck, Austria for SAGE-sequencing on the Ion Proton with Hi-Q chemistry. Three comparisons of the samples were made in order to investigate differentially expressed genes in:

- B220+ cells isolated from wildtype spleens (n=5)
- EμMyc Nr4a1-/- versus EμMyc Nr4a1+/+ (n=5)
- EμMyc Nr4a+/+ versus wildtype spleens (n=5)

The results were corrected for further testing by using their incorporated Benjamini-Hochberg-method. Analysis was performed for us by Mirjana Efremova.

Table 3 List of mice samples used for mRNA sequencing analysis

Sample number	Genotype
5095-0089	EμMyc Nr4a1+/+
5095-0112	EμMyc Nr4a1+/+
5095-0119	EμMyc Nr4a1+/+
5095-0195	EμMyc Nr4a1+/+
5095-0231	EμMyc Nr4a1+/+
5100-0072	EμMyc Nr4a1-/-
5100-0117	EμMyc Nr4a1-/-
5100-0150	EμMyc Nr4a1-/-
5100-0170	EμMyc Nr4a1-/-
5100-0174	EμMyc Nr4a1-/-
324_2	wildtype
324_3	wildtype
318_2	wildtype
318_3	wildtype
291_1	wildtype

2.4 Protein extraction

The frozen tumour tissue fragments from the EμMyc Nr4a1+/+ and the EμMyc Nr4a1-/- mice were lysed in RIPA buffer (Therma Scientific, Waltham, MA) by additionally adding a protease and phosphatase inhibitor cocktail (Therma Scientific, Waltham, MA). The proteins then were frozen and thawed 3 times in liquid nitrogen and centrifugated and a measurement of the protein concentration by performing the Lowry protein measurement method on the Bio-Rad protein assay (Bio-Rad Laboratories, Hercules, USA) was performed.

For Western blot Immuno Assay a 2-chamber Mini Trans Blot® Cell system was used. The protein lysates were appropriately diluted in a Laemmli-buffer (Bio-Rad, Hercules, CA, USA) and Beta-Mercapto-Ethanol mix (450 microliters + 50 microliters) and then heated up to 95°C for protein denaturation.

The protein lysates were resolved by SDS-PAGE using the Mini-PROTEAN® TGX™ gels (Bio-Rad Laboratories, Hercules, USA) and semi-dry transferred to a Midi-PVDF-membrane (Bio-Rad Laboratories, Hercules, USA). The size of the protein of interest was detected in the provider's antibody protocol and the membranes were cut to avoid any unintentional signal of other proteins (Table 4).

Table 4 kDa size of the antibodies and membrane allocation

Antibody	Size in kDa	Membrane number
p19Arf	19	Membrane number 3
BIM	20	Membrane number 2
BCL-XL	25	Membrane number 4
BCL-2	26	Membrane number 1
MCL-1	40	Membrane number 2
p53	53	Membrane number 3
MDM2	90	Membrane number 3
PARP	116 and 89	Membrane number 4
Beta Actin	43	On all membranes

Antibodies were used as described in Table 5 according to the manufacturer's instructions. Secondary antibodies were rabbit, mouse and rat (Santa Cruz, USA) conjugated to Horseradish Peroxidase (Table 6).

For the washing procedure a TBST washing buffer was used. This TBST buffer was also used to dilute the antibodies in either non-fat dry milk powder (Bio-Rad, Hercules, CA, USA) or in BSA Fraction 5 (GE Healthcare, Little Chalfont, UK).

The peroxidase activity was detected by using the WesternBright Chemiluminescence detection (Advansta, USA). The chemilumenescence effect was brought on CL-XPosure™

films (Thermo Fisher Scientific, Waltham, MA, USA) by the Agfa Curix 60 (Agfa, Mortsel, Belgium).

The protein band intensity was quantitatively and optically analysed. The quantification of the band intensity was performed on Image J (National Institutes of Health, Bethesda, MD) by using digital image densitometry analysis.

11 EμMyc Nr4a1+/+ and 13 EμMyc Nr4a1-/- mouse tumours were used for the Western blot analysis to detect varieties in gene expression. As control wildtype mice spleen was used.

Table 5 Parameters for the use of the first antibodies

Name of 1st antibody	Dilution	Incubation time	Second antibody
Beta Actin (13E5) Cell signaling	1:1000	2 hours	Anti-rabbit
p53 (1C12) Cell signaling	1:1000	2 hours	Anti-mouse
p19Arf (5-C3-1) Santa Cruz	1:500	2 hours	Anti-rat
BIM (C34C5) Cell signaling	1:1000	2 hours	Anti-rabbit
BCL-XL (54H6) Cell signaling	1:1000	over night	Anti-rabbit
BCL-2 (50E3) Cell signaling	1:1000	over night	Anti-rabbit
MDM2 (SMP14) Santa Cruz	1:500	over night	Anti-mouse
MCL-1 (Polyclonal) Rockford	1:10000	over night	Anti-rabbit
PARP (9542S) Cell signaling	1:1000	over night	Anti-rabbit

Table 6 Parameters for the use of the second antibodies

Name of 2nd antibody	Dilution	Incubation time
Anti-rabbit IgG HRP-linked Antibody 7074S from Cell signaling	1:3000	1 hour
Anti-mouse IgG HRP-linked Antibody 7076 s from Cell singaling	1:3000	1 hour
Anti-rat Pierce Rabbit Anti-Rat IgG HRP linked Antibody PA1-28573 from Thermo Fisher Scientific	1:5000	1 hour

2.5 B-cell isolation

Spleens of Nr4a1-/- (n=6) and Nr4a1+/+ (n=5) mice were removed and B-cells were isolated from the lymphoid tissue by using the IMag™ (BD Biosciences, Heidelberg, Germany).

2.5.1 B-Cell isolation and Flow cytometry

The removed spleen cells from the Nr4a1-/- mice and the Nr4a1+/+ mice were passed through a 70-µm nylon cell strainer using HBSS (Thermo Fisher Scientific, Waltham, MA, USA).

The B220+ CD19+ gated cell lysates were detected on their purity by FACS analysis. This was performed on a LSRII and data analysis was done with FlowJo Software.

The Flow cytometry-Mastermix contained following markers:

- Ter119
- CD43
- IgM
- B220
- CD19

2.6 Statistical methods

The statistical analysis of the Western blot analysis was performed by using the Statistical Package for Social Sciences version 17.0 (SPSS Inc., USA).

The representative plots and the protocols used for the genotyping, RNA-Extraction, cDNA Extraction, Protein-Isolation, Western blot analysis and B-cell isolation can be found in the Supplementary part.

3. RESULTS

3.1 Second hit analysis

3.1.1 Genotyping

Genotyping of all investigated mouse tumours was performed to guarantee the right phenotype of the mice for generating reliable and good quality results of the analyses.

Representative Figure 15 depicts that all mice tested contained the *EμMyc* transgene. Samples 0112, 0186, 0195 were compared to the control-sample (denoted as "C", an EμMyc mouse) EμMyc Nr4a1+/+ mice. Samples 0092, 0150 and 0170 were detected as EμMyc Nr4a1-/- mice. Only tumours with the right genotype were further processed for the Western blot and the gene expression analysis.

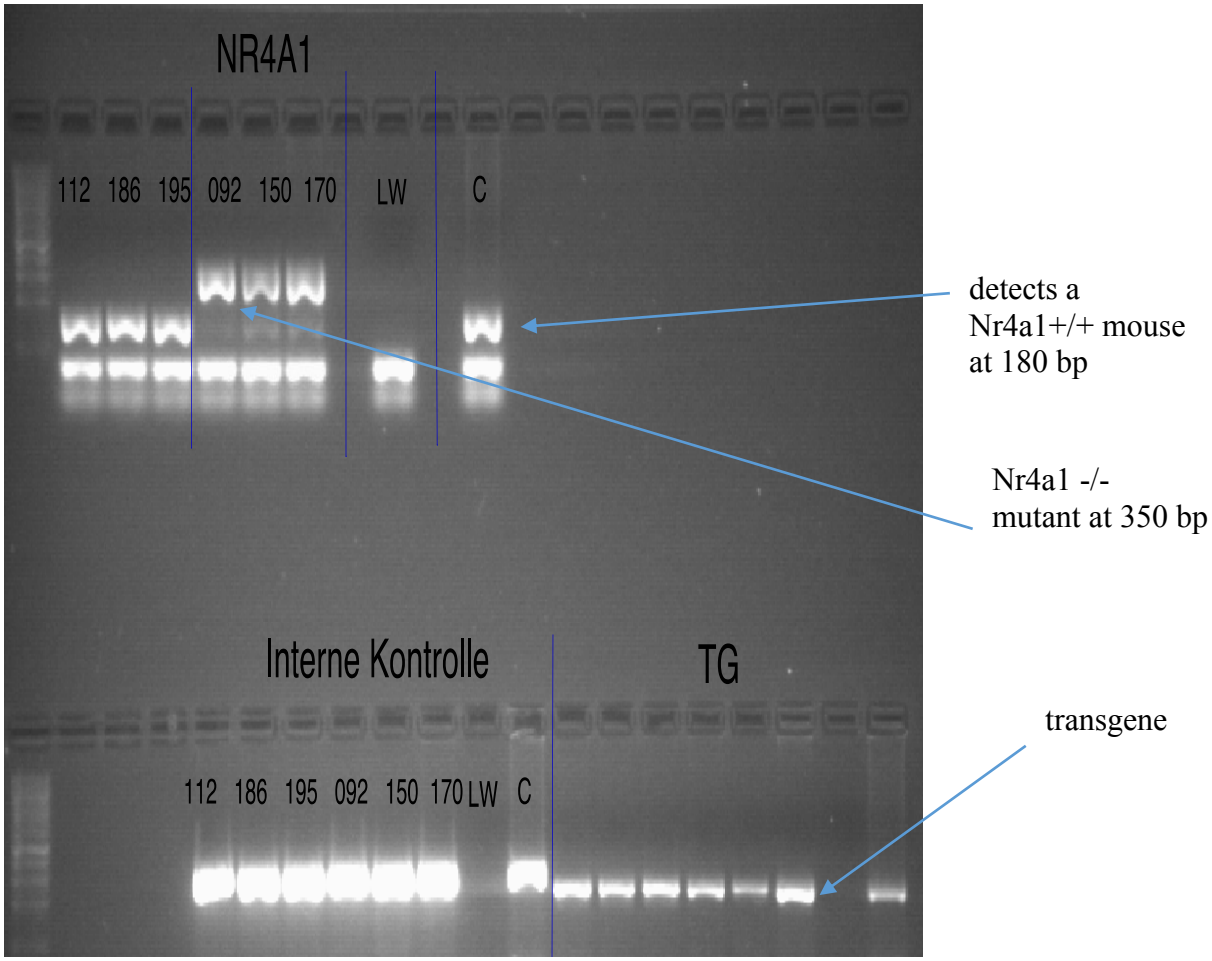

Figure 15 Representative results of genotyping - TG (denotes transgene) shows that all mice tested contain the EμMyc transgene. Samples 0112, 0186, 0195 were compared to the control sample (C, which was an EμMyc mouse) EμMyc Nr4a1+/+ mice. Samples 0092, 0150 and 0170 were detected as EμMyc Nr4a1-/- mice. The first lane represents the 100 bp gene ruler. The mutant is shown on 350 bp, the wildtype on 180 bp.

Genotyping revealed that 18 out of 34 mice were EμMyc Nr4a1-/- and 16 out of 34 mice were EμMyc Nr4a1+/+.

3.1.2 Western blot analysis of the tumours derived from the EμMyc Nr4a1+/+ and EμMyc Nr4a1-/- mice

To clarify whether a deregulated *p19Arf-Mdm2-p53* pathway or overexpressed *Bcl-2*, *Bcl-xl*, or deregulated *Mcl-1* or *Bim* are needed for deregulated expression in the EμMyc Nr4a1-/- mice for malignant transformation, I estimated the expression levels of *Bcl-2, Bcl-xl*, *Bim*, *Mcl-1, Mdm2*, *p19Arf* and *p53* by Western blot analysis on 13 EμMyc Nr4a1-/- and 11 EμMyc Nr4a1+/+ mice derived tumours.

Although we expected a different expression level, I detected a trend of higher *Bim* expression (1.6-fold higher, p=0.09) in EμMyc Nr4a1-/- mice derived tumours compared to EμMyc Nr4a1+/+ mice. Additionally, *Mdm2* in EμMyc Nr4a1-/- mouse tumours compared to the EμMyc Nr4a1+/+ mice was overexpressed significantly (4.9-fold, p=0.01). There were no significant changes in the *Bcl-2, Bcl-xl, Mcl-1, p19* and *p53* expression (Figure 17-20).

A chi-square test on the visual bands of *p53* expression profile in EμMyc Nr4a1-/- mice compared to the EμMyc Nr4a1+/+ mice revealed no statistically significant differences, as only one single overexpression of *p53* in an EμMyc Nr4a1+/+ mouse tumour was detected (Figure 16).

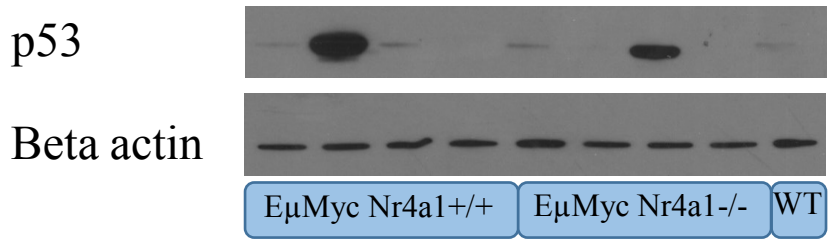

Figure 16 Exemplary Western blot of an overexpression of p53 in one EμMyc Nr4a1+/+ mouse tumour.

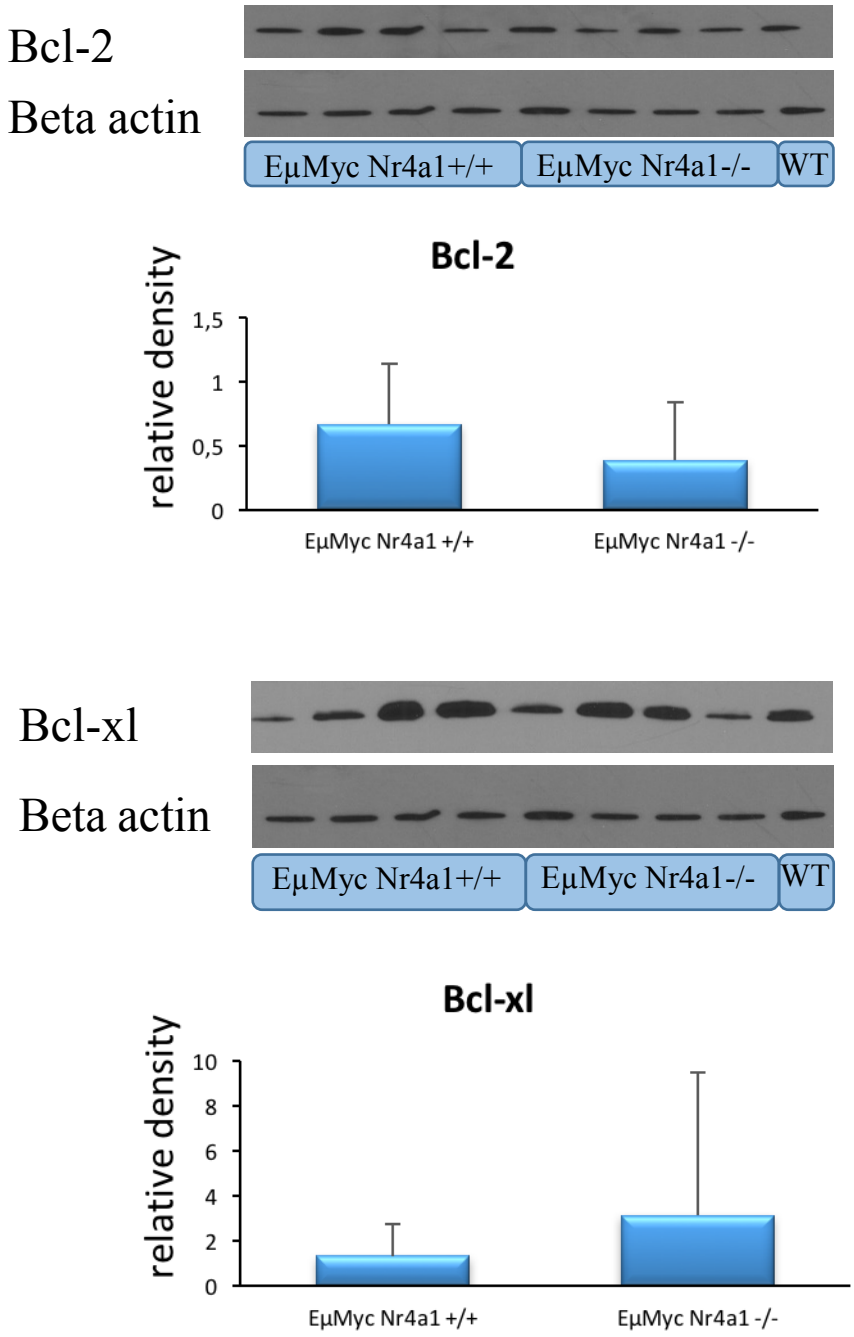

Figure 17 Representative Western blot of the tumour mice

EμMyc Nr4a1+/+ mice were compared to EμMyc Nr4a1-/- mice. The last band represents the wildtype control. For the relative density plots the density was calculated using ImageJ software, raw data was normalized to the loading control Beta actin. The bars represent the mean and standard deviation. We could demonstrate no significant changes in Bcl-2 and Bcl-xl expression comparing the EμMyc Nr4a1+/+ to the EμMyc Nr4a1-/- mice.

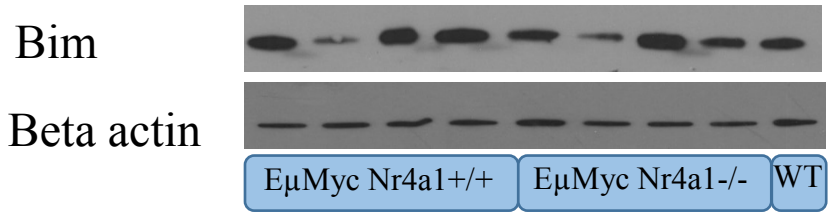

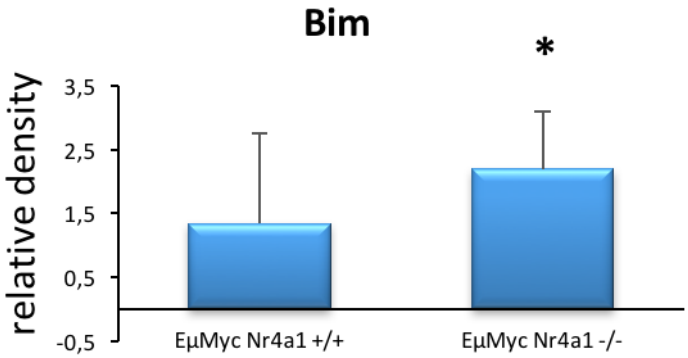

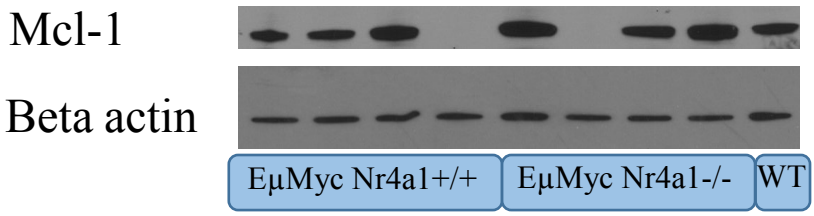

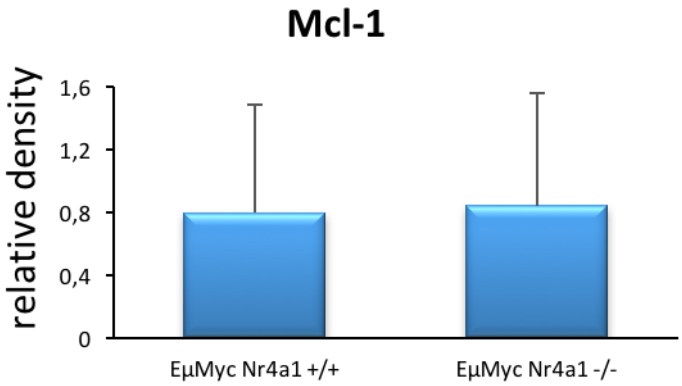

Figure 18 Representative Western blot of the tumour mice

*EμMyc Nr4a1+/+ mice were compared to EμMyc Nr4a1-/- mice. The last band represents the wildtype control. For the relative density plots the density was calculated using ImageJ software, raw data was normalized to the loading control Beta actin. The bars represent the mean and standard deviation. We could demonstrate no significant change in Mcl-1 expression comparing the EμMyc Nr4a1+/+ to the EμMyc Nr4a1-/- mice. Bim was surprisingly significantly overexpressed in the EμMyc Nr4a1-/- mice. *p<0.05 to EμMyc Nr4a1+/+ mice.*

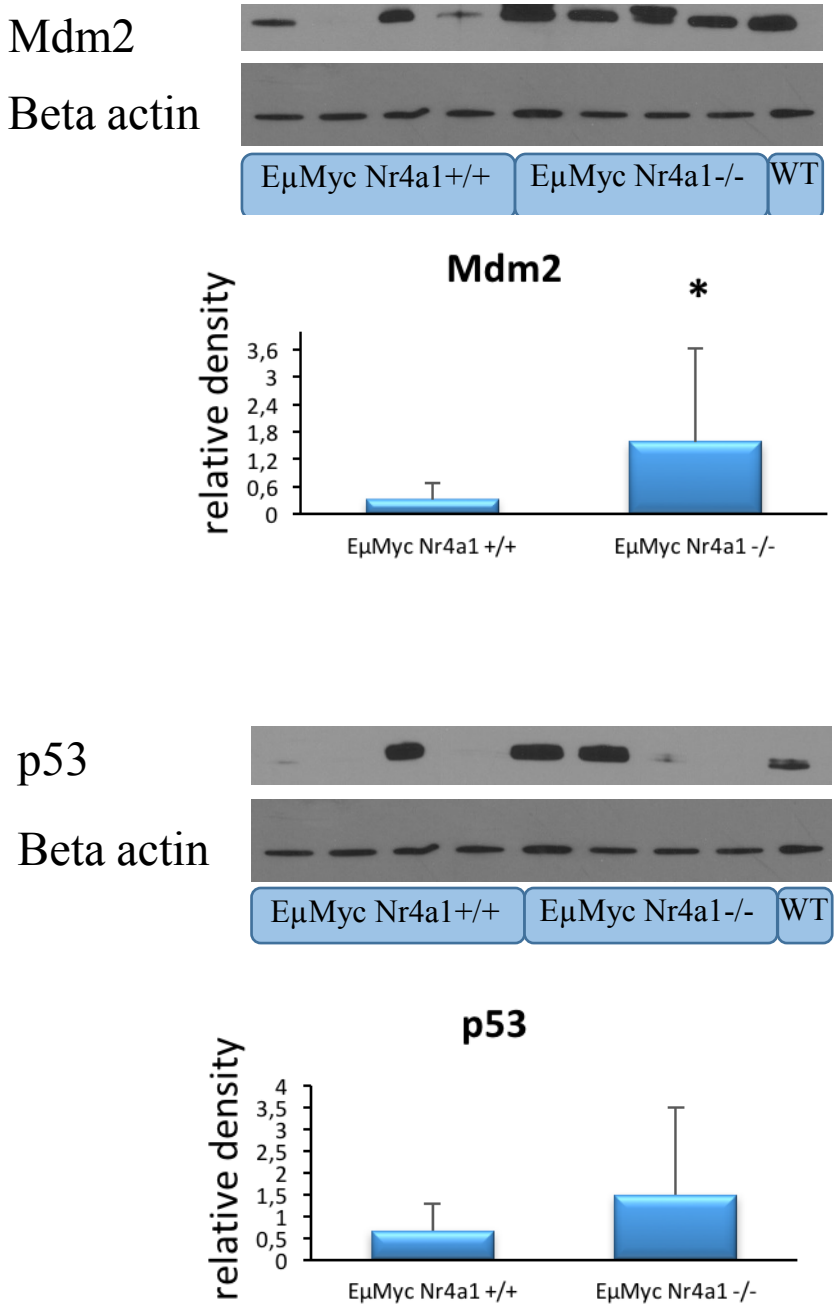

Figure 19 Representative Western blot of the tumour mice

*EμMyc Nr4a1+/+ mice were compared to EμMyc Nr4a1-/- mice. The last band represents the wildtype control. For the relative density plots the density was calculated using ImageJ software, raw data was normalized to the loading control Beta actin. The bars represent the mean and standard deviation We could demonstrate no significant change in p53 expression comparing the EμMyc Nr4a1+/+ to the EμMyc Nr4a1-/- mice. Mdm2 was significantly overexpressed in the EμMyc Nr4a1-/- mice. *p<0.05 to EμMyc Nr4a1+/+ mice.*

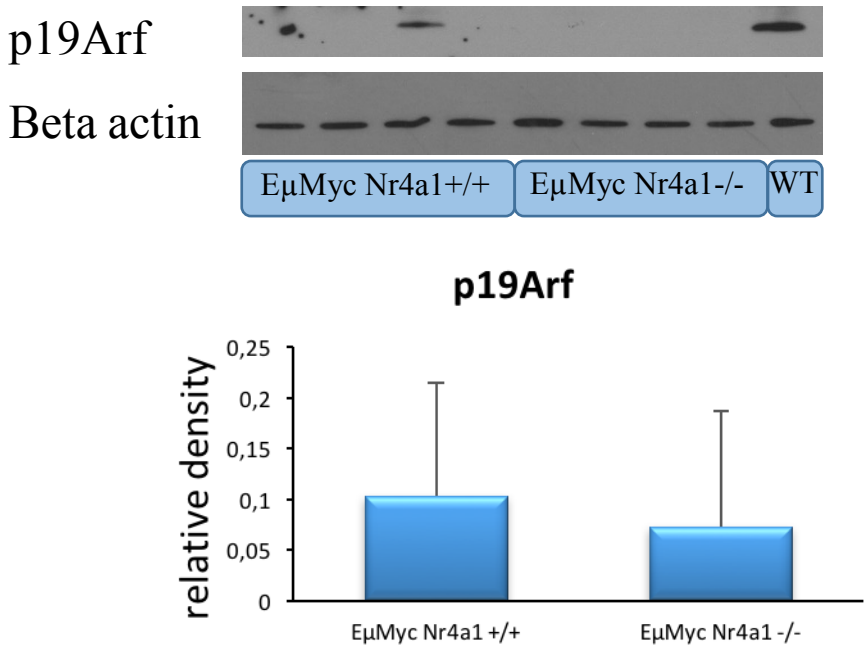

Figure 20 Representative Western blot of the tumour mice

EμMyc Nr4a1+/+ mice were compared to EμMyc Nr4a1-/- mice. The last band represents the wildtype control. For the relative density plots the density was calculated using ImageJ software, raw data was normalized to the loading control Beta actin. The bars represent the mean and standard deviation We could demonstrate no significant change in p19 expression comparing the EμMyc Nr4a1+/+ to the EμMyc Nr4a1-/- mice.

3.2 Analysis of spleenic B-cells of non-malignant Nr4a1+/+ and Nr4a1-/- mice

3.2.1 Purity of the isolated cells

To determine expression of *p19Arf, Mdm2, p53, Bcl-2, Bcl-xl, Mcl-1, Bim* and *Parp* in non-malignant B-cells, I isolated B220+ cells (B-cells) from mice spleens derived from Nr4a1-/- (n=6) and Nr4a1+/+ mice (n=5). B220+ cells were isolated by using the IMag™ (BD Biosciences, Heidelberg, Germany). B220+ cells with an at least 68% purity were processed for further Western blot analysis (Figure 21).

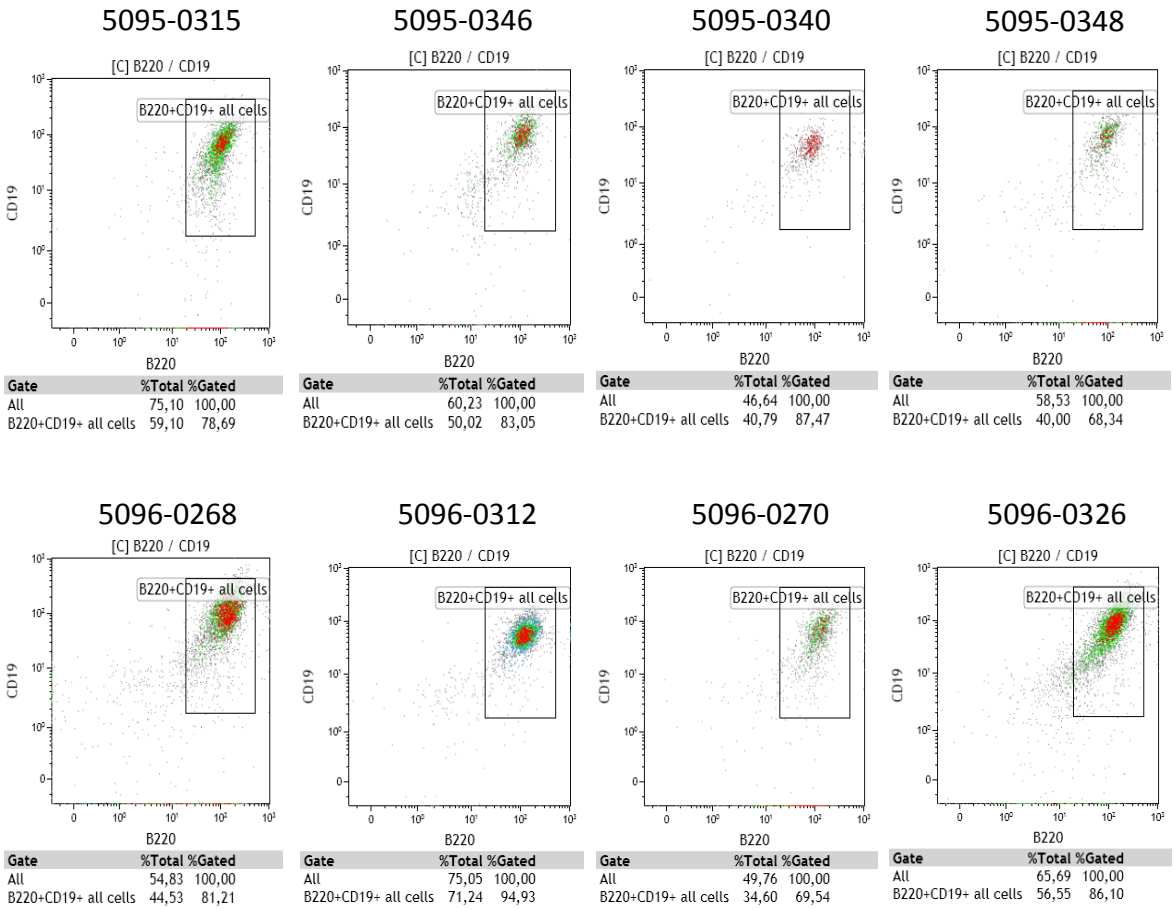

Figure 21 Flow cytometry of isolated B-cells from spleens of wildtype (5095) and Nr4a1-/- (5096) mice. All cells were gated B220+/CD19+.

3.2.2 Western blot results of the spleenic B-cells

The protein expression levels of the isolated spleenic B-cells of the Nr4a1-/- (n=6) and the Nr4a1+/+ mice (n=5) were analysed for detecting significant changes in the expression levels of *Bcl-2, Bcl-xl, Bim, Mcl-1, Mdm2, p19Arf* and *p53* (Figure 23-26).

The Western blot analysis of the extracted B-cells from the spleen tissue did not reveal any significant differences in the expression of *Bcl-2, Bcl-xl, Bim, Mcl-1, Mdm2, p19Arf* and *p53*. However, *p53* overexpression was detected in two B-cell specimens isolated from a Nr4a1-/- mouse.

A chi-square test on the visual amount of bands of p53 of the Nr4a1+/+ and the Nr4a1-/- did not reveal any significant result, although one band showed an overexpression (Figure 22).

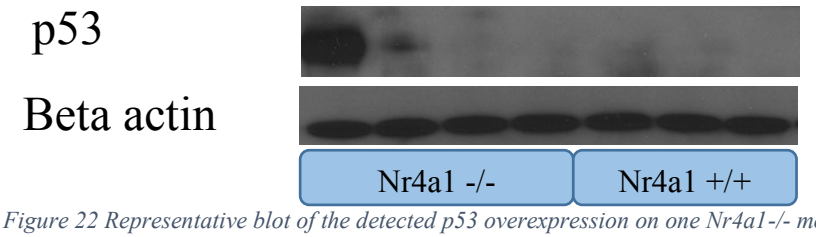

Figure 22 Representative blot of the detected p53 overexpression on one Nr4a1-/- mouse.

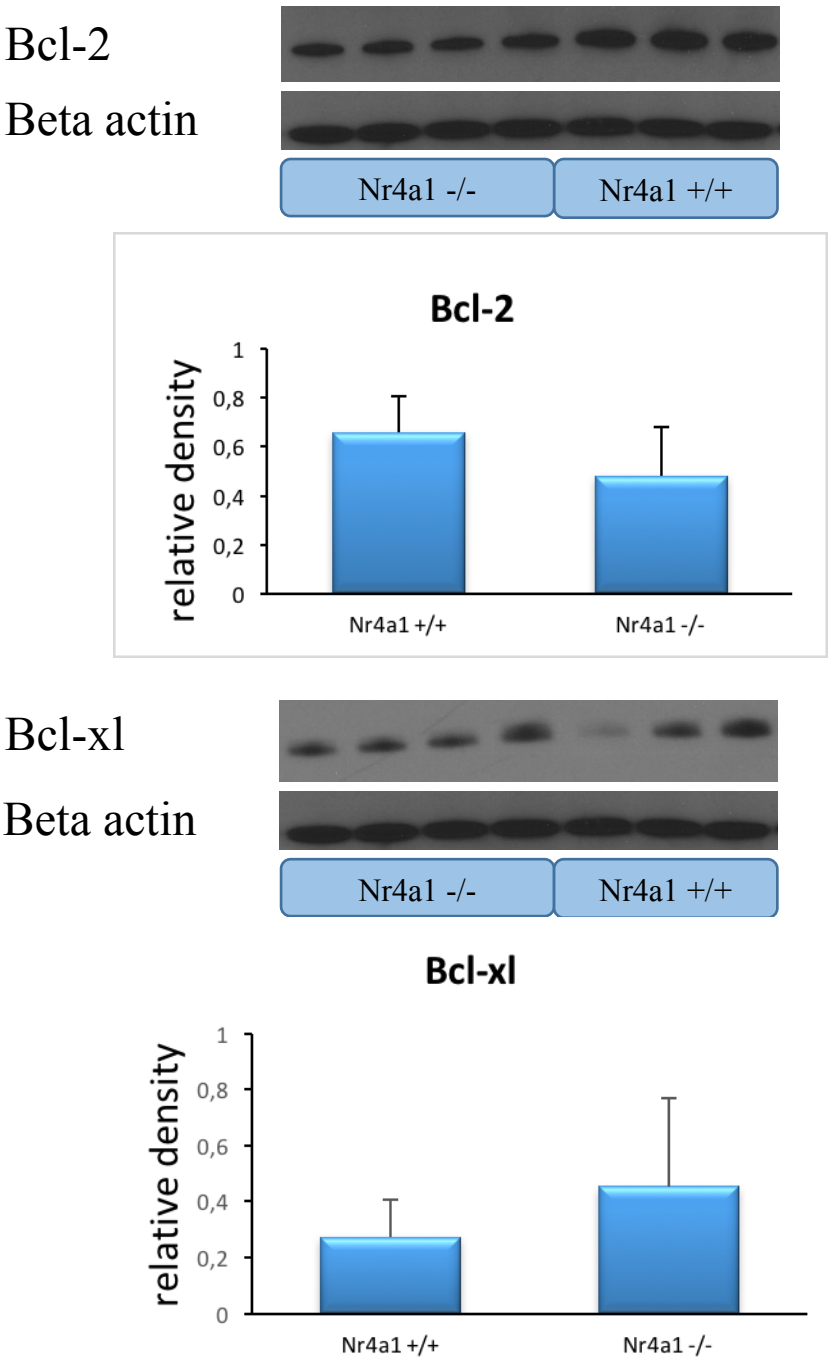

Figure 23 Representative Western blot of the isolated spleenic B-cells

Nr4a1+/+ mice were compared to Nr4a1-/- mice. For the relative density plots the density was calculated using ImageJ software, raw data was normalized to the loading control Beta actin. The bars represent the mean and standard deviation. We could demonstrate no significant changes in Bcl-2 and Bcl-xl expression comparing the Nr4a1+/+ to the Nr4a1-/- mice.

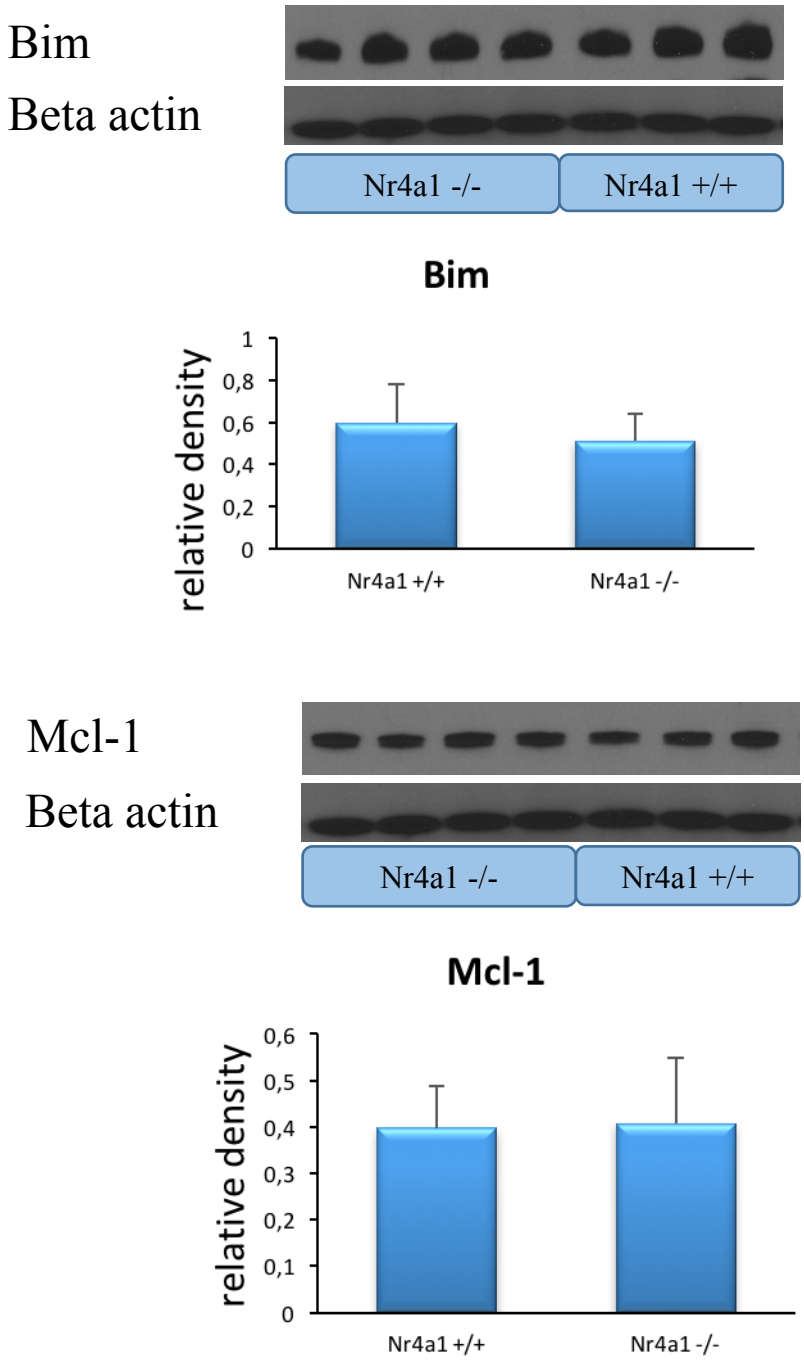

Figure 24 Representative Western blot of the isolated spleenic B-cells

Nr4a1+/+ mice were compared to Nr4a1-/- mice. For the relative density plots the density was calculated using ImageJ software, raw data was normalized to the loading control Beta actin. The bars represent the mean and standard deviation. We could demonstrate no significant changes in Bim and Mcl-1 expression comparing the Nr4a1+/+ to the Nr4a1-/- mice.

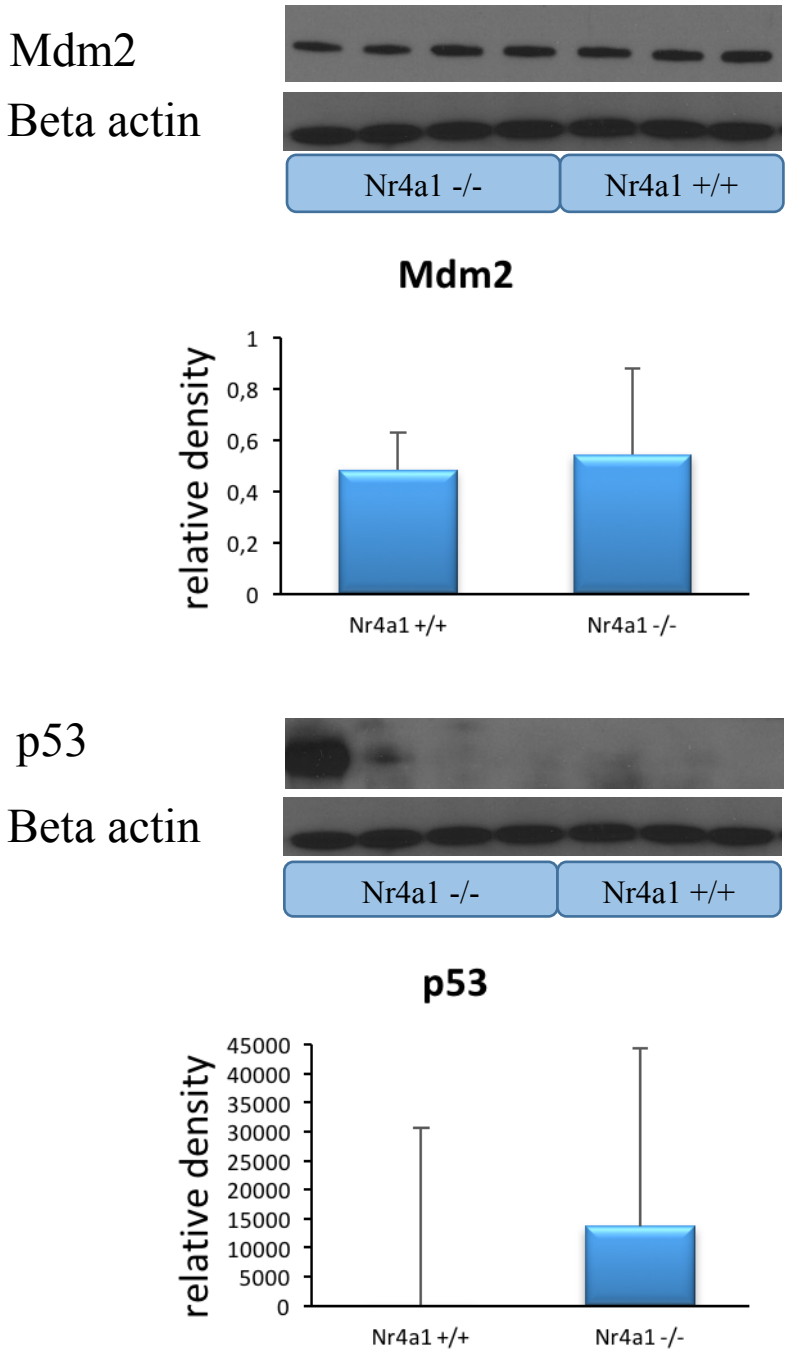

Figure 25 Representative Western blot of the isolated spleenic B-cells

Nr4a1+/+ mice were compared to Nr4a1-/- mice. For the relative density plots the density was calculated using ImageJ software, raw data was normalized to the loading control Beta actin. The bars represent the mean and standard deviation. We could demonstrate no significant changes in Mdm2 and p53 expression comparing the Nr4a1+/+ to the Nr4a1-/- mice, p53 seems to be overexpressed in Nr4a1-/- mice due to functional inactivation (83).

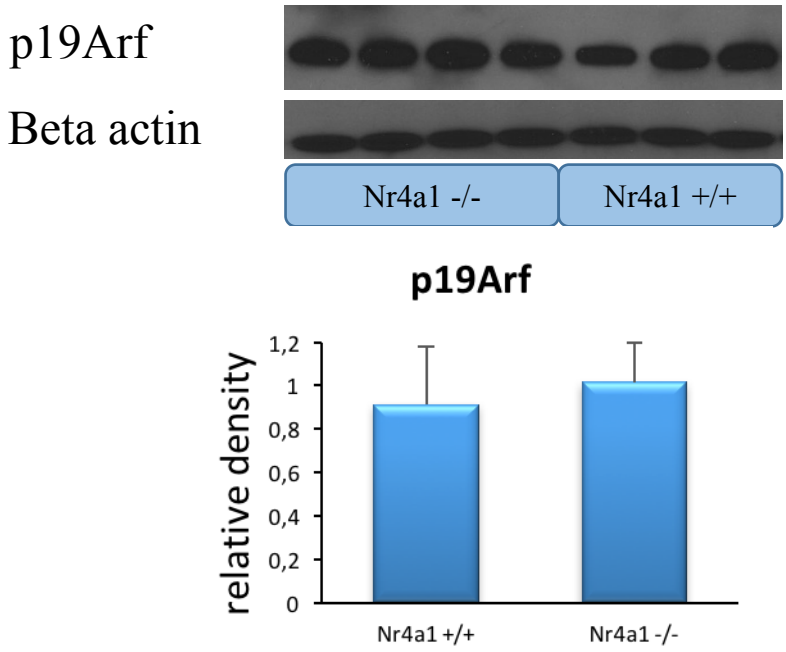

Figure 26 Representative Western blot of the isolated spleenic B-cells

Nr4a1+/+ mice were compared to Nr4a1-/- mice. For the relative density plots the density was calculated using ImageJ software, raw data was normalized to the loading control Beta actin. The bars represent the mean and standard deviation. We could demonstrate no significant change in p19Arf expression comparing the Nr4a1+/+ to the Nr4a1-/- mice.

3.2.3 Parp analysis comparing EμMyc tumours to wildtype spleenic B-cells

PARP is a protein, that is activated by endogenous cellular reactions or genotoxic agents that cause DNA strand breaks. When activated it transfers ADP-ribose units from NAD to nuclear proteins including PARP itself resulting in cellular dysfunction and cell death (39). Cleaved PARP is inactivated by caspase cleavage. Cleavage separates PARP into an 89 kDa and 116 kDa segment. The smaller moiety includes the zinc finger motif requisite in DNA binding. The 116 kDa fragment includes the auto-modification domain and catalytic domain. The putative mechanism of PCD activation via PARP inactivation relies on the separation of the DNA-binding region and the auto-modification domain. In this way, the DNA-binding domain will attach to a damaged site and be unable to affect repair, as it no longer has the catalytic domain. The DNA-binding domain prevents other, non-cleaved PARP from accessing the damaged site and initiating repairs, thus causing apoptosis (79).

To estimate the apoptotic activity in EμMyc Nr4a1+/+ versus EμMyc Nr4a1-/- mice tumors and wildtype mice versus Nr4a1-/- mice B cells, we performed a Western blot analysis of *Parp*. *Parp* cleavage was investigated in the tumour derived from EμMyc Nr4a1+/+ (n=8) and EμMyc Nr4a1-/- (n=8) mice tumors and in the isolated spleenic B-cells of the Nr4a1-/- (n=6) and the Nr4a1+/+ mice (n=5).

Parp cleavage is significantly downregulated in the EμMyc Nr4a1-/- mice (3-fold, p=0.02) compared to the EμMyc Nr4a1+/+ mice, indicating that apoptosis is down-regulated in the EμMyc Nr4a1-/- tumour cells (Figure 27). In the spleenic B-cells *Parp* cleavage does not show any differences between the Nr4a+/+ and Nr4a1-/- mice (Figure 28).

MOUSE TUMOUR CELLS

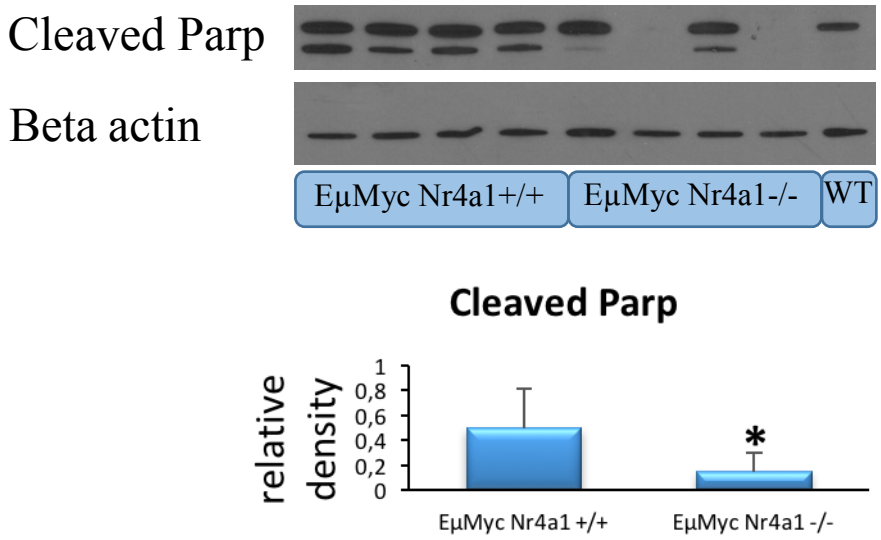

Figure 27 Representative Western blot of the tumour mice

*EμMyc Nr4a1+/+ mice were compared to EμMyc Nr4a1-/- mice. The last band represents the wildtype control. For the relative density plots the density was calculated using ImageJ software, raw data was normalized to the loading control Beta actin. The bars represent the mean and standard deviation. We could demonstrate a significant downregulation of cleaved Parp in EμMyc Nr4a1-/-. *p<0.05 to EμMyc Nr4a1+/+ mice.*

SPLEENIC B-CELLS

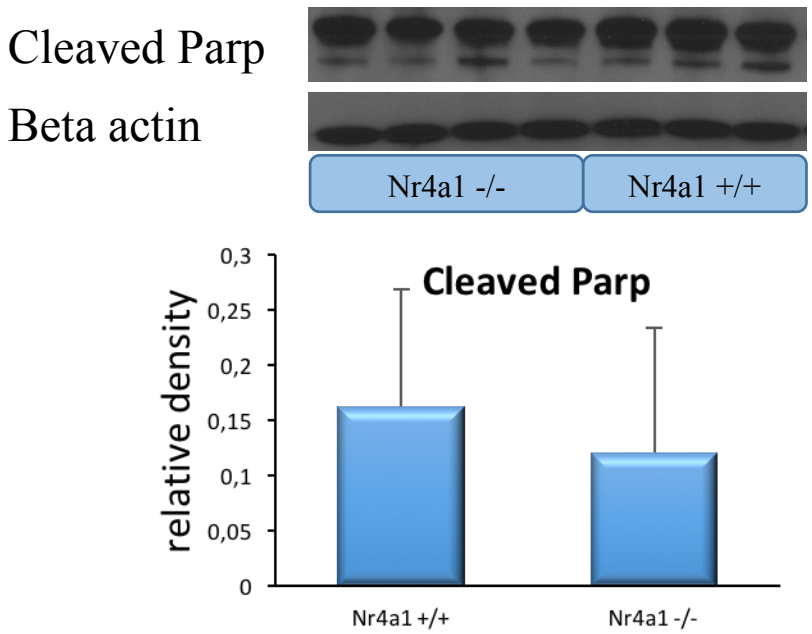

Figure 28 Representative Western blot of the isolated spleenic B-cells

Nr4a1+/+ mice were compared to Nr4a1-/- mice. For the relative density plots the density was calculated using ImageJ software, raw data was normalized to the loading control Beta actin. The bars represent the mean and standard deviation. We could demonstrate no significant changes in cleaved Parp expression comparing the Nr4a1+/+ to the Nr4a1-/- mice.

3.3 Gene expression analysis

3.3.1 Quality check via RIN-value

After RNA extraction I analysed the RNA of EμMyc Nr4a1-/- (n=5) and EμMyc Nr4a1+/+ mice (n=5) to further analyse the quality of the RNA by using the RIN value for further gene sequencing analysis (Figure 29). After RNA had been isolated it was analysed by the Bio-Analyzer. Figure 29 shows the results of the RNAs analysed. RIN-values > 7.5 were accepted as "good quality RNA". These analysed good quality RNAs were used for the further sequencing.

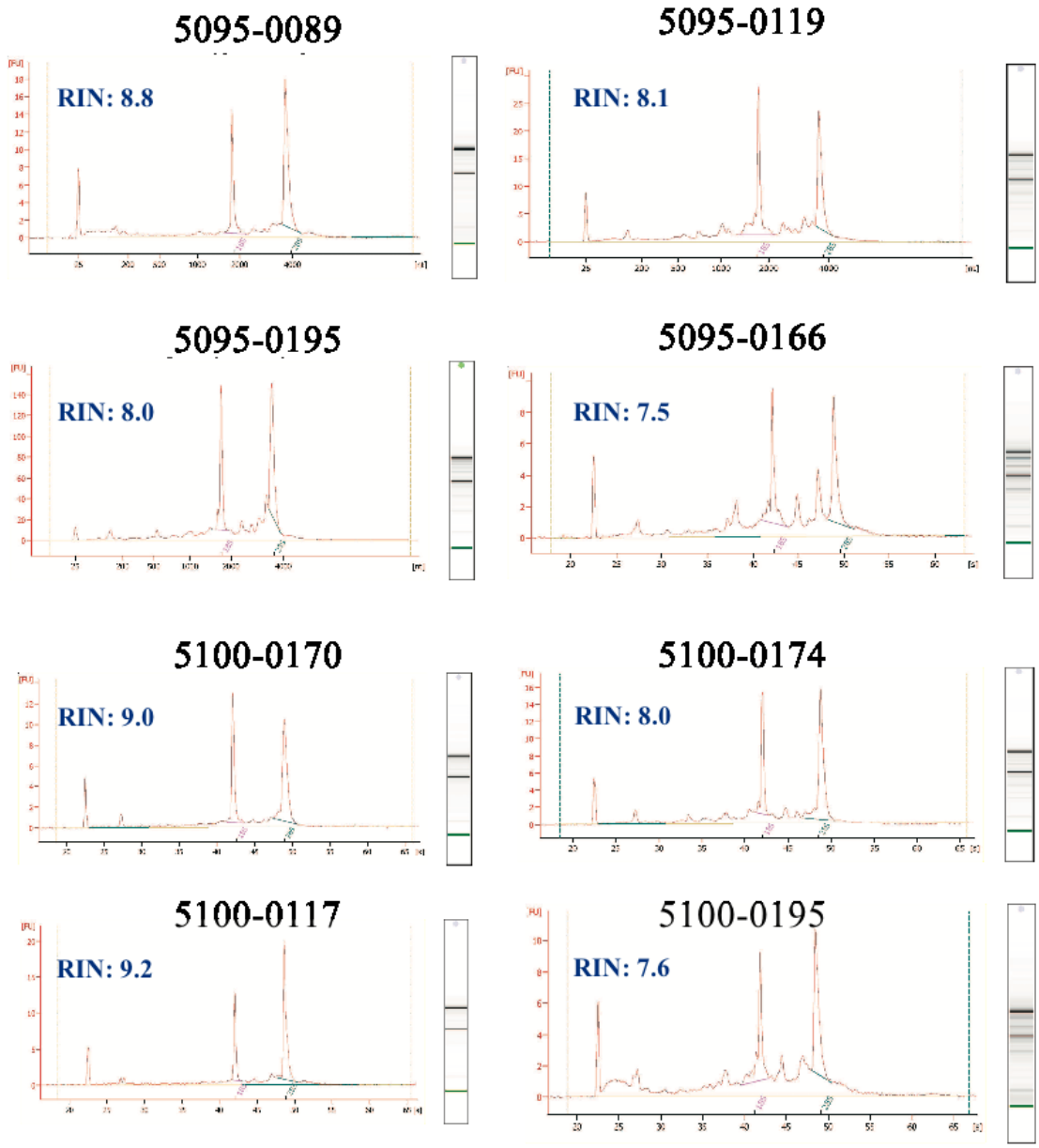

Figure 29 Illustration of the RIN value evaluation of EμMyc Nr4a1-/- and EμMyc Nr4a1+/+ - RNA with a RIN value of >7.5 was detected as "good quality" for RNA sequencing analysis (82).

3.3.2 mRNA expression of *Nr4a1* and *Nr4a3*

To determine the expression level of *Nr4a1* and *Nr4a3* in the EμMyc Nr4a1+/+ (n=14) and EμMyc Nr4a1-/- (n=12) mouse tumours and non-neoplastic controls, CD19+ IgM- CD43+ (pre-B-cells), CD19+ IgM- CD43- (pro-B-cells) and CD19+ IgM+ CD93+ (immature B-cells) –cells isolated from bone marrow and B220+ cells isolated from spleens of Nr4a1+/+ mice (n=5) were processed, cDNA was prepared and a semi quantitative RT-PCR was performed on the focus on *Nr4a1* and *Nr4a3*.

By comparing *Nr4a1* expression between EμMyc Nr4a1+/+ and EμMyc Nr4a1-/- mouse tumours we observed a 7-fold lower expression ($p<0.04$, Figure 30) in the knock out tumours. Additionally, *Nr4a1* is at least 6-fold lower expressed in EμMyc Nr4a1+/+ mouse tumours compared to non-neoplastic controls ($p<0.05$, Figure 30). By comparing EμMyc Nr4a1-/- mouse tumours to non-neoplastic control we observed an at least 60-fold lower expression of *Nr4a1* ($p<0.05$, Figure 30).

Nr4a3 is highly expressed in EμMyc Nr4a1-/- mouse tumours compared to non-neoplastic controls (4.6-fold, $p<0.05$) (Figure 31) indicating that a loss of *Nr4a1* might be compensated by a higher expression of *Nr4a3*.

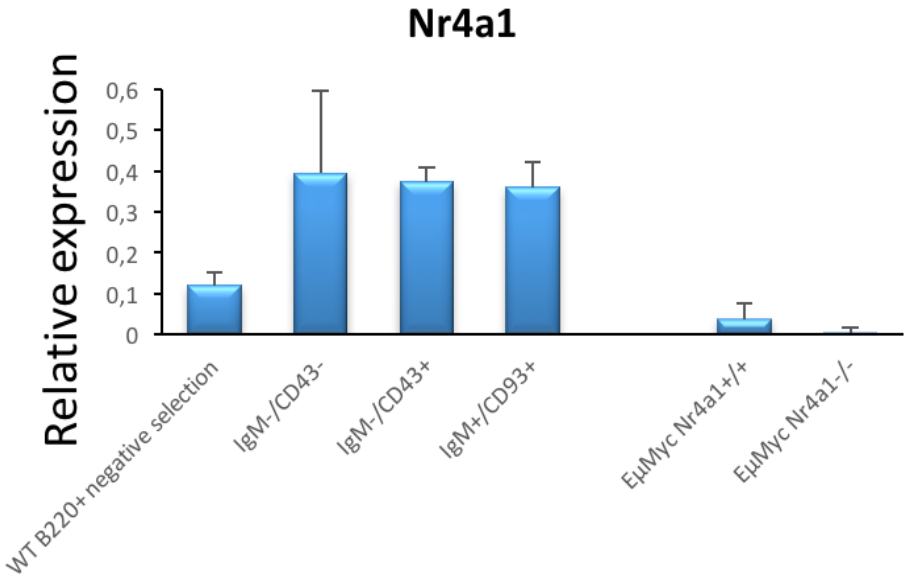

Figure 30 Relative expression of EμMyc Nr4a1+/+ tumour cells. – Nr4a1 expression was 7-fold lower in EμMyc Nr4a1-/- tumour mice compared to the EμMyc Nr4a1+/+ mice ($p<0.04$). Nr4a1 is 6-fold lower expressed in EμMyc Nr4a1 +/+ mouse tumours compared to non-neoplastic controls ($p<0.05$). Nr4a1 is 60-fold lower expressed in EμMyc Nr4a1-/- mouse tumours compared to the non-neoplastic control

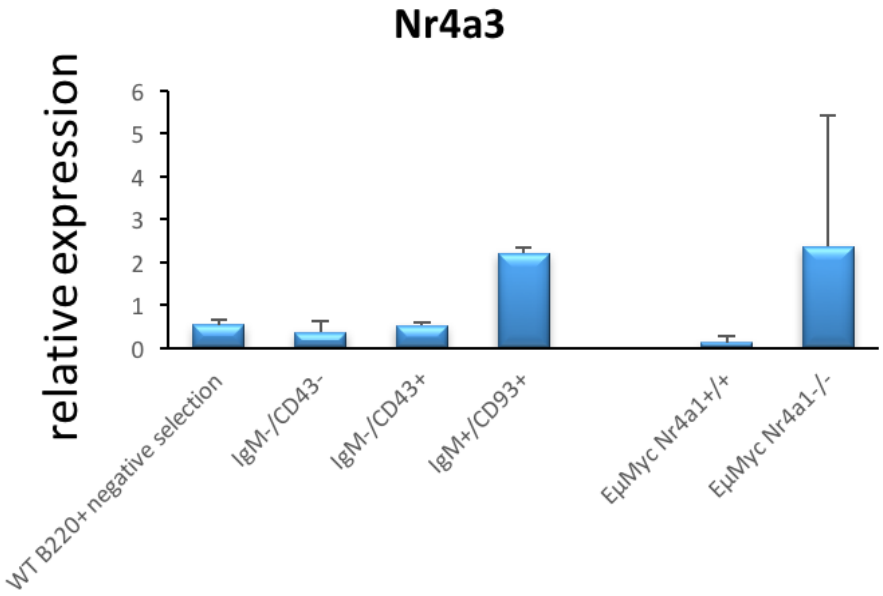

Figure 31 Relative expression of Nr4a3 in the EμMyc Nr4a1 +/+ and EμMyc Nr4a1-/- mice tumours. Nr4a3 was highly expressed in immature B-cells and in EμMyc Nr4a1-/- mice, assumed due to the loss of Nr4a1 comparing to EμMyc Nr4a1+/+ mice, but not significantly. Additionally, an at least 4.6-fold higher expression in EμMyc Nr4a1-/- mouse tumours compared to non-neoplastic controls ($p<0.05$) was demonstrated.

3.3.3 mRNA Sequencing

We wanted to find out which terms show an enrichment by deregulated genes in the EμMyc Nr4a1-/- (n=5) compared to EμMyc Nr4a1+/+ (n=5) mouse tumours.

The mRNA sequencing at the external laboratory in Innsbruck revealed that various GO terms and pathways of the immune-cell-system associated with the differentially regulated genes in EμMyc Nr4a1-/- versus EμMyc Nr4a1+/+ mice are significantly enriched (Table 7).

Table 7 shows the number of genes that showed significant changes either at the uncorrected and corrected significance threshold with log2 fold changes of greater than 1.50 and less than -1.50.

Table 7 Number of genes that showed significant changes in gene expression These changes are illustrated at the uncorrected and corrected significance threshold with log2 fold changes of greater than 1.50 and less than -1.50.

Comparison	Number of genes (FDR p-value < 0.10)	Number of genes (uncorrected p-value < 0.05)	Number of genes (FDR p-value < 0.10; logFC> 1.5 or logFC<-1,5)	Number of genes (uncorrected p-value < 0.05; logFC >1,5 or logFC< -1.5)
EμMyc Nr4a1 -/- vs. EμMyc Nr4a1 +/+	57 + 18	800 + 412	48 +9	410 + 128

The network of Figure 32 shows a network from ClueGO produced using the list of up- and downregulated genes for EμMyc Nr4a1-/- versus EμMyc Nr4a1+/+ mice. The size of the nodes reflects the enrichment significance of the terms. The functional groups are represented and visualized by their most significant term. The light grey nodes are the ones that did not group. For the analysis medium GO levels (3-8) were used.

Terms that are associated with the upregulated genes are coloured green, genes associated with downregulated are coloured red. The colour gradient shows the gene proportion of each type (either up- or downregulated) associated with the term. The colour shade goes towards grey/white when the proportions are towards equal which means that these terms are associated with both up- and downregulated genes.

Enrichment analysis of terms that are associated with upregulated genes:

- ⇑ Negative regulation of the T-cell-proliferation,
- ⇑ B-cell activation involved in immune response,
- ⇑ Regulation of cytokine biosynthetic process,
- ⇑ Regulation of leukocyte differentiation and
- ⇑ Positive regulation of homotypic cell-cell adhesion.

Enrichment analysis of terms that are associated with downregulated genes:

- ⇓ Negative regulation of immune response,
- ⇓ Regulation of response to biotic stimulus and
- ⇓ Immune response-activating cell surface receptor signalling pathway.

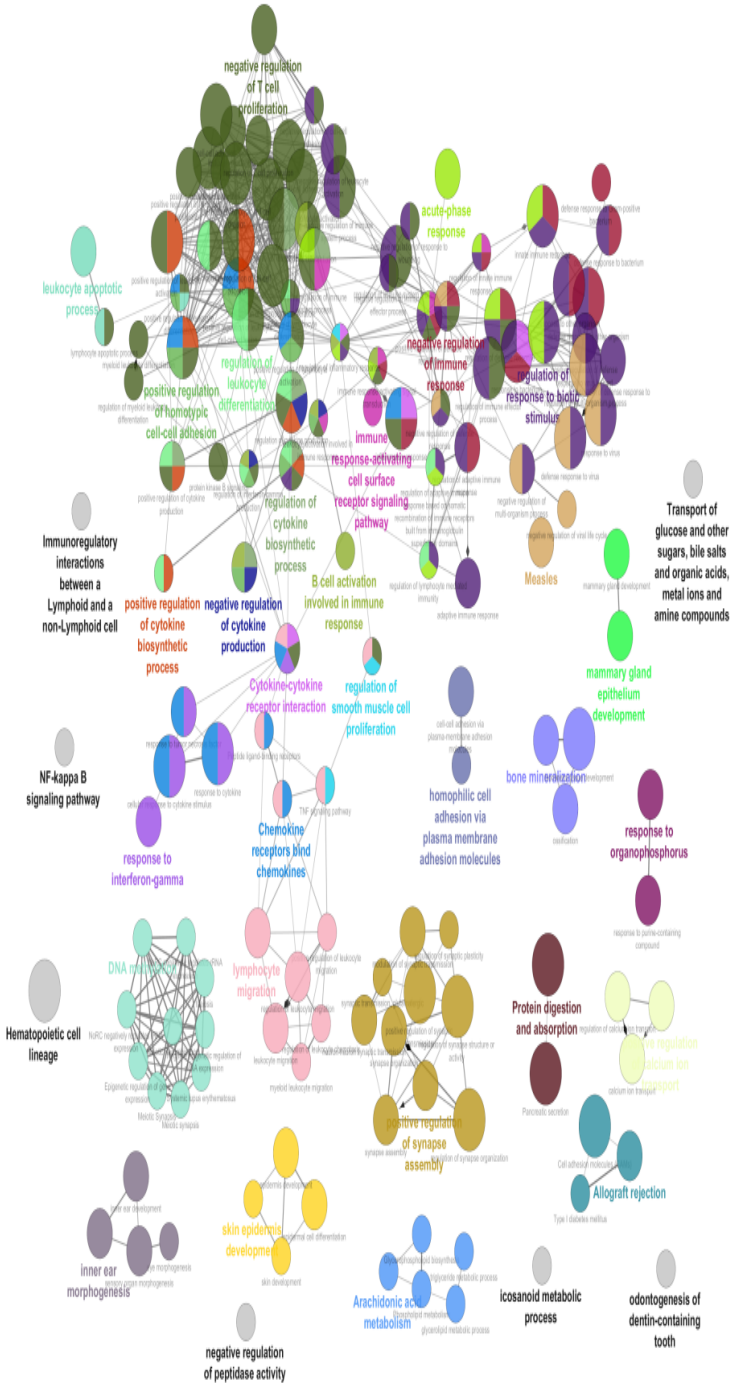

Figure 32 Significantly enriched GO terms and pathways associated with the differentially regulated genes in EμMyc Nr4a1-/- versus EμMyc Nr4a1+/+ mice. Terms that are associated with the upregulated genes are coloured green, genes associated with downregulation are coloured red. The colour gradient shows the deregulated gene proportion associated with the term. The colour shade goes towards grey/white when the proportions are towards equal.

4 DISCUSSION

My group demonstrated that *NR4A1* functions as a tumour suppressor in lymphomagenesis *in vivo* and in xenografts (65) and as previously described in Myc-driven lymphomagenesis (accepted abstract by ASH, Wenzl K. *et al*, 2015 Dec., Blood Journal). This study was designed to elucidate the molecular mechanism of the tumour suppressive function of Nr4a1 by investigating the effect of *NR4A1*-loss in combination with additional genetic aberrations *in vivo*, the so called second hit, and by performing a *Nr4a1* and *Nr4a3* expression analysis and global gene expression profiling by mRNA-sequencing.

Since, additional genetic alterations (second hit), either by a deregulated *p19Arf-Mdm2-p53* pathway or by overexpressed antiapoptotic *BCL2*-family members (73,74), is needed for malignant transformation in the *EμMyc* transgenic mouse model, we focused on the protein expression levels of: *Bcl-2, Bcl-xl*, *Bim*, *Mcl*-1, *p19Arf*, *Mdm2* and *p53*. We observed a 1.6-fold higher expression of Bim and a 4.6-fold higher expression of Mdm2 in tumours derived from the EμMyc Nr4a1-/- mice in comparison to EμMyc Nr4a1-/- mice. Bim belongs to the Bcl-2 family and has been shown to interact with the other family members, including BCL2, BCL2L1/BCL-XL and MCL-1 inducing apoptosis (86). Additionally, it has already been reported that Nr4a1 represses the expression of Mdm2 at both transcriptional and post-transcriptional level (87,88). Since p53 expression levels were equally in Myc-driven tumours with and without *Nr4a1* loss and the apoptosis was even reduced in Myc-induced lymphoma with *Nr4a1* loss as demonstrated by lower Parp cleavage it might be speculated that the Mdm2 significantly contributes to Myc-driven lymphomagenesis. The higher induction of Mdm2 might also suppress the apoptotic function of Bim in Myc-induced tumours with *Nr4a1*-loss and thereby significantly contributes to the accelerated lymphomagenesis.

P53 overexpression was observed in one B-cell specimen of the Nr4a1-/- mice, whereas in none of the analysed B-cell specimens a p53 overexpression could be detected. This overexpression might be explained by a functional inactivation of this gene (83). However, I speculate that Nr4a1-loss either enhanced the likelihood for DNA damage of this specific sample and thus induced p53 expression or, more likely due to its single detection, a false negative genotyping has occurred and the sample was mistaken for a premalignant EμMyc Nr4a1-/- mouse.

Nr4a1 and *Nr4a3* expression analysis revealed an at least 6-fold downregulation of *Nr4a1* in EμMyc Nr4a1-/- mouse tumours in comparison to non-neoplastic controls indicating that malignant transformation causes downregulation of *Nr4a1*. Furthermore, a higher expression of *Nr4a3* in EμMyc Nr4a1-/- mouse tumours was observed compared to EμMyc Nr4a1+/+ mouse tumours. It is clearly demonstrated that *NR4A1* and *NR4A3* possesses a functional redundancy in at least negative selection of the T-lymphocytes (56). However, based on our observation, it seems that in Myc-driven lymphomagenesis *Nr4a3* tries to insufficiently compensate the *Nr4a1* loss. Therefore, it might be hypothesized that Nr4a1 and Nr4a3 are not functional redundant in Myc-driven lymphomagenesis.

By mRNA sequencing we demonstrated that *Nr4a1* loss results in a significant induction of 58 genes and down-regulation of 18 genes in Myc-driven lymphomagenesis indicating that *Nr4a1* acts as a transcriptional repressor, which was at least described for c-Myc in AML (89). Furthermore, GO-term analysis revealed that upregulated genes were associated with the negative regulation of T-cell proliferation, B-cell activation, regulation of cytokine biosynthetic process, regulation of leukocyte differentiation and positive regulation of homotypic cell-cell-adhesion, whereas downregulated genes were associated with negative regulation of the immune response, regulation of response to biotic stimulus and immune-response-activation cell surface receptor signalling pathway. These results indicate that *Nr4a1* possesses immunoregulatory function in Myc-induced tumorigenesis and thereby significantly contributes to the accelerated lymphomagenesis. However, this issue will be further investigated by my research group by identifying direct target genes of Nr4a1 and additionally by determining the subtype and numbers of tumour infiltrating lymphocytes of EμMyc Nr4a1-/- and EμMyc Nr4a1+/+ tumours.

In conclusion, we could detect that the loss of *Nr4a1* accelerates the lymphoma development in the *Myc*-driven lymphomagenesis. A second hit in the way of an overexpression of *Mdm2* and *Bim* in the EμMyc Nr4a1-/- mouse tumours leads to the assumption that *Nr4a1* functions as a repressor of *Mdm2* and *Bim*, hence their overexpression in EμMyc mice with a *Nr4a1*-loss significantly accelerates the *Myc*-driven lymphomagenesis.

SUPPLEMENTARY

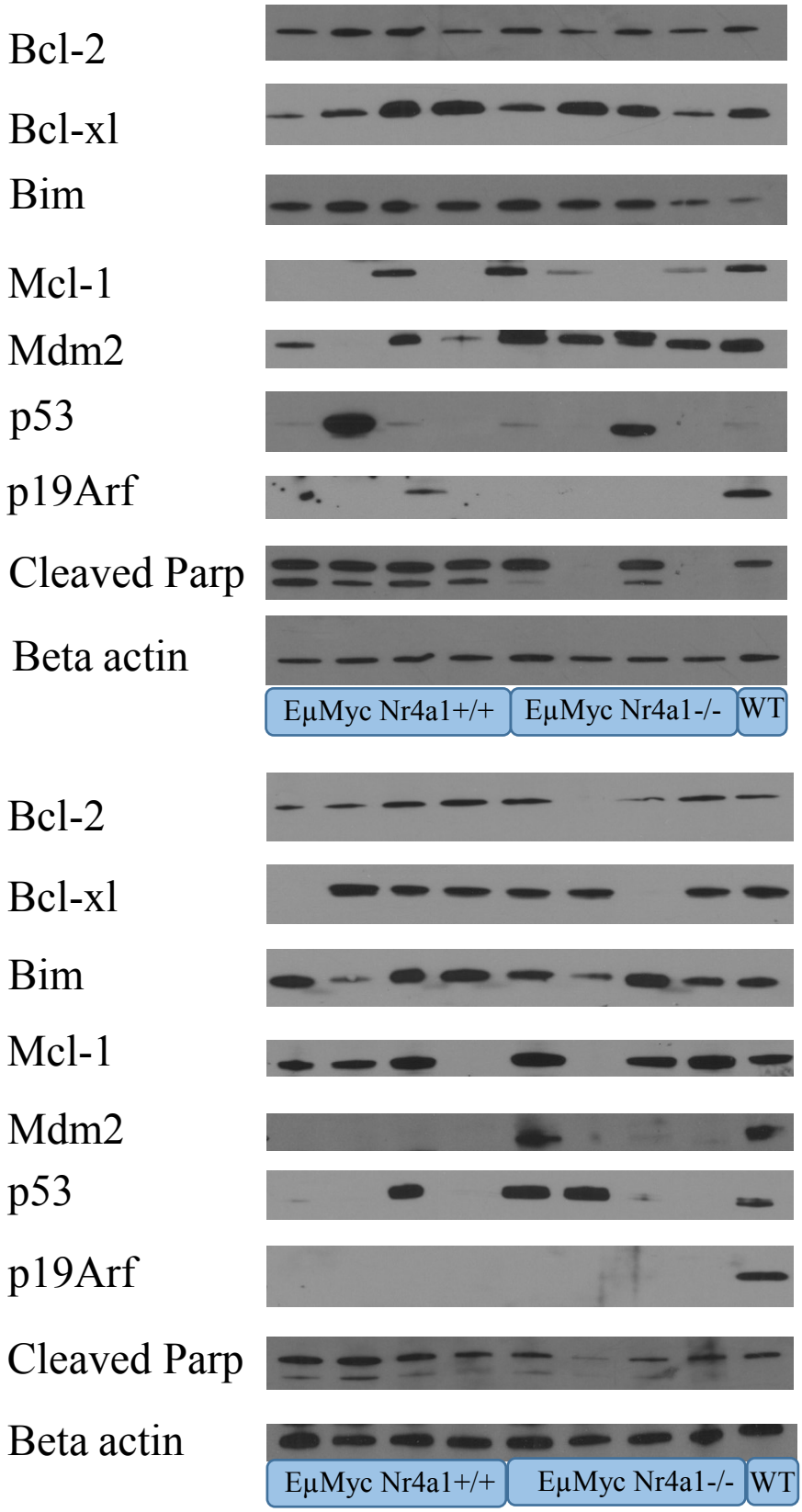

Figure 33 Representative blots from immunoblotting analysis of EμMyc Nr4a1+/+ tumours. Blots for Bcl-2, Bcl-xl-Bim, Mcl-1, Mdm2, p53, p19Arf and Parp protein expression. Beta actin was used as loading control on all blots. As antibody control a wildtype mouse spleen was used.

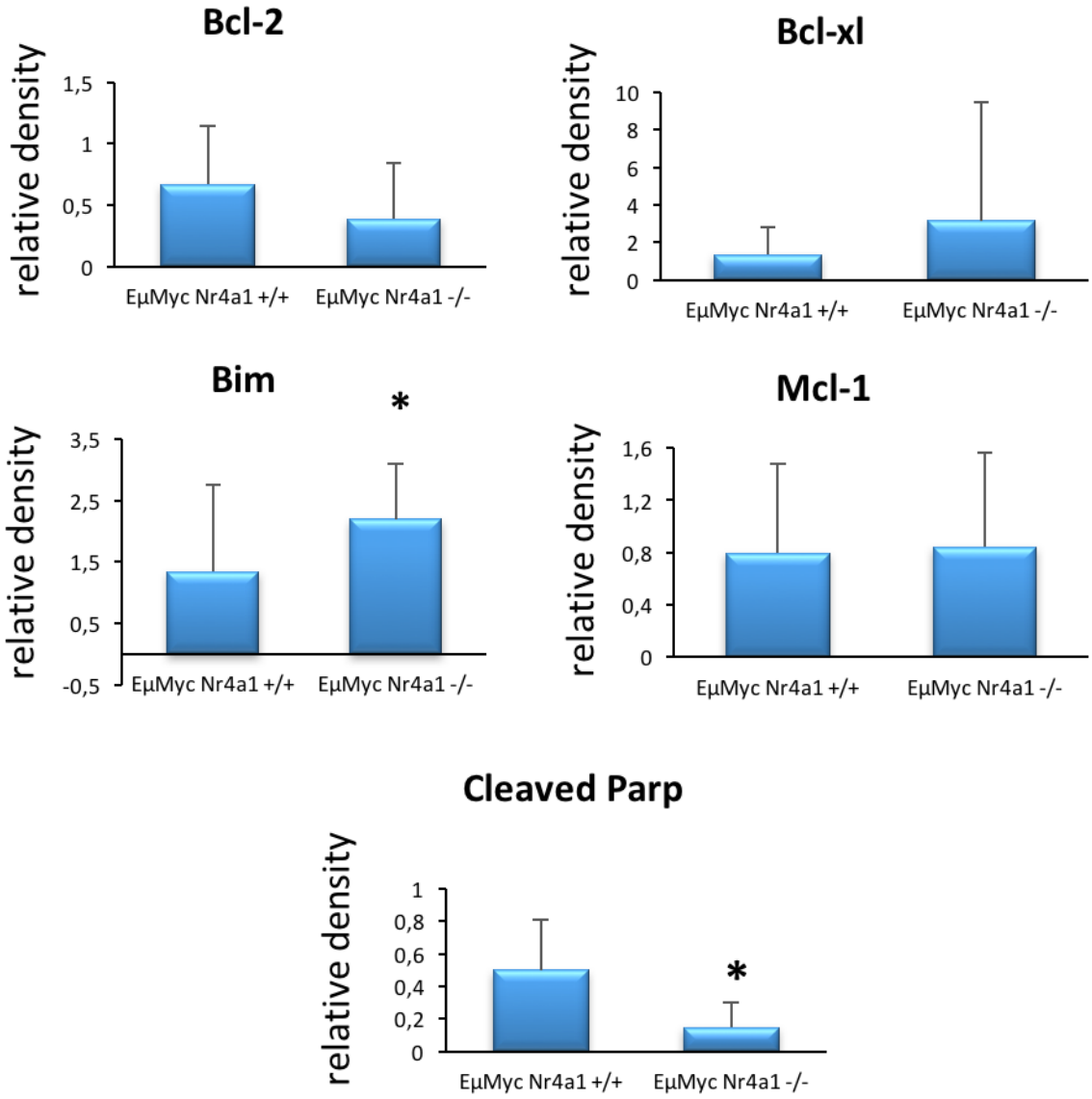

*Figure 34 Relative density plots from tumours with or without Nr4a1. Status of protein levels of Bcl-2, Bcl-xl, Bim, Mcl-1 and cleaved Parp from tumours with or without Nr4a1 loss. Density was calculated using the ImageJ software and row data was normalized to the loading control Beta actin. The bars represent mean and standard deviation. *p<0.05 to EμMyc Nr4a1+/+ mice.*

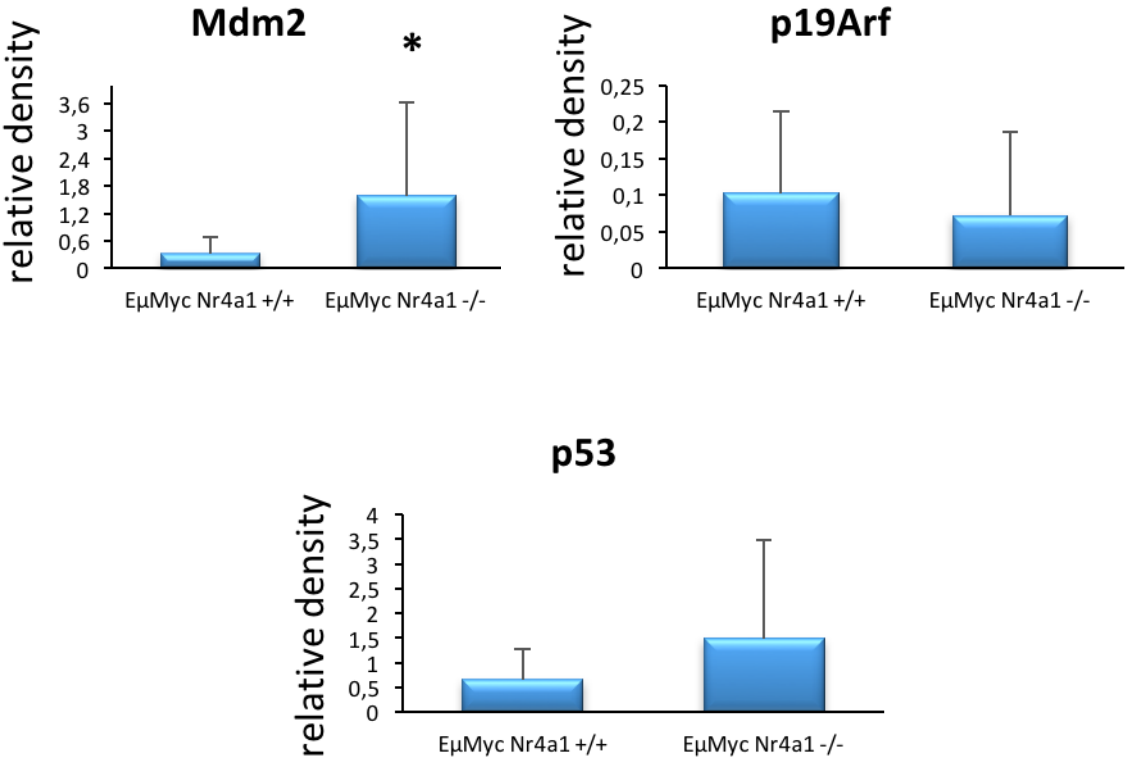

*Figure 35 Relative density plots from tumours with or without Nr4a1. Status of protein levels of Mdm2, p19Arf and p53 from tumours with or without Nr4a1 loss. Density was calculated using the ImageJ software and row data was normalized to the loading control Beta actin. The bars represent mean and standard deviation. *p<0.05 to EμMyc Nr4a1+/+ mice.*

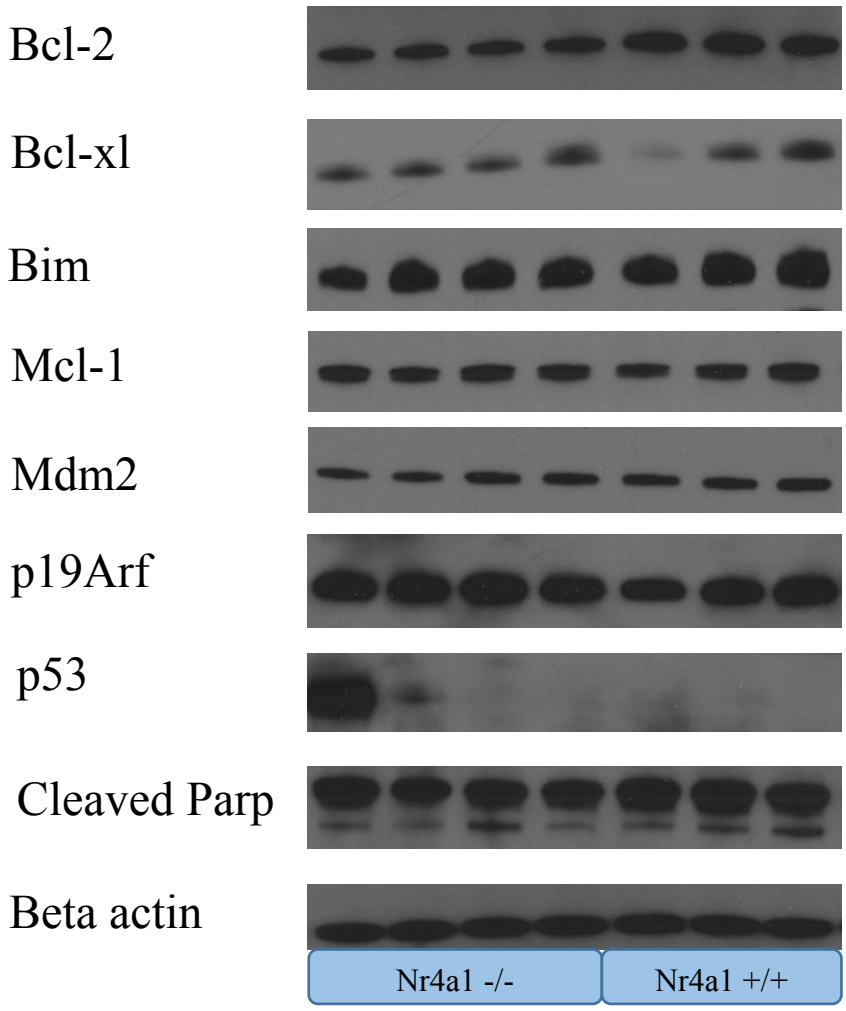

Figure 36 Immunoblotting analysis of spleenic B-cells.-Part 1- Representative blots for Bcl-2, Bcl-xl, Bim, Mcl-1, Mdm2, p19Arf, p53 and cleaved Parp protein expression. Beta actin was used as loading control on all blots.

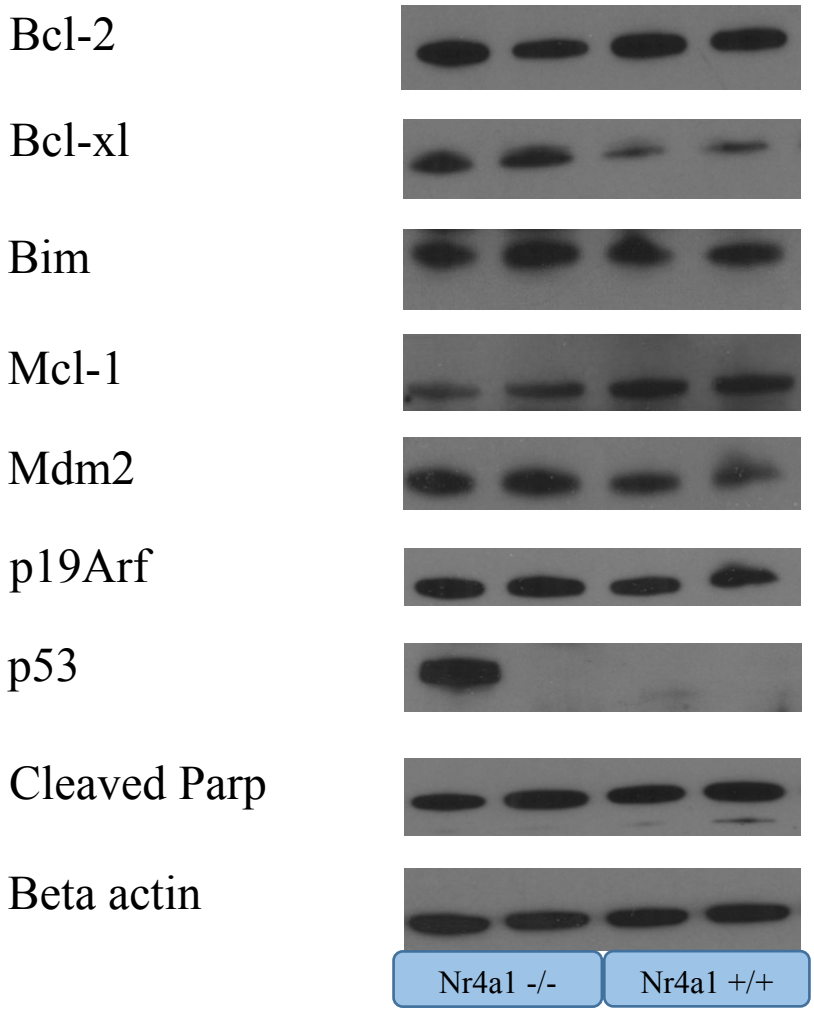

Figure 37 Immunoblotting analysis of spleenic B-cells.-Part 2- Representative blots for Bcl-2, Bcl-xl, Bim, Mcl-1, Mdm2, p19Arf, p53 and cleaved Parp protein expression. Beta actin was used as loading control on all blots.

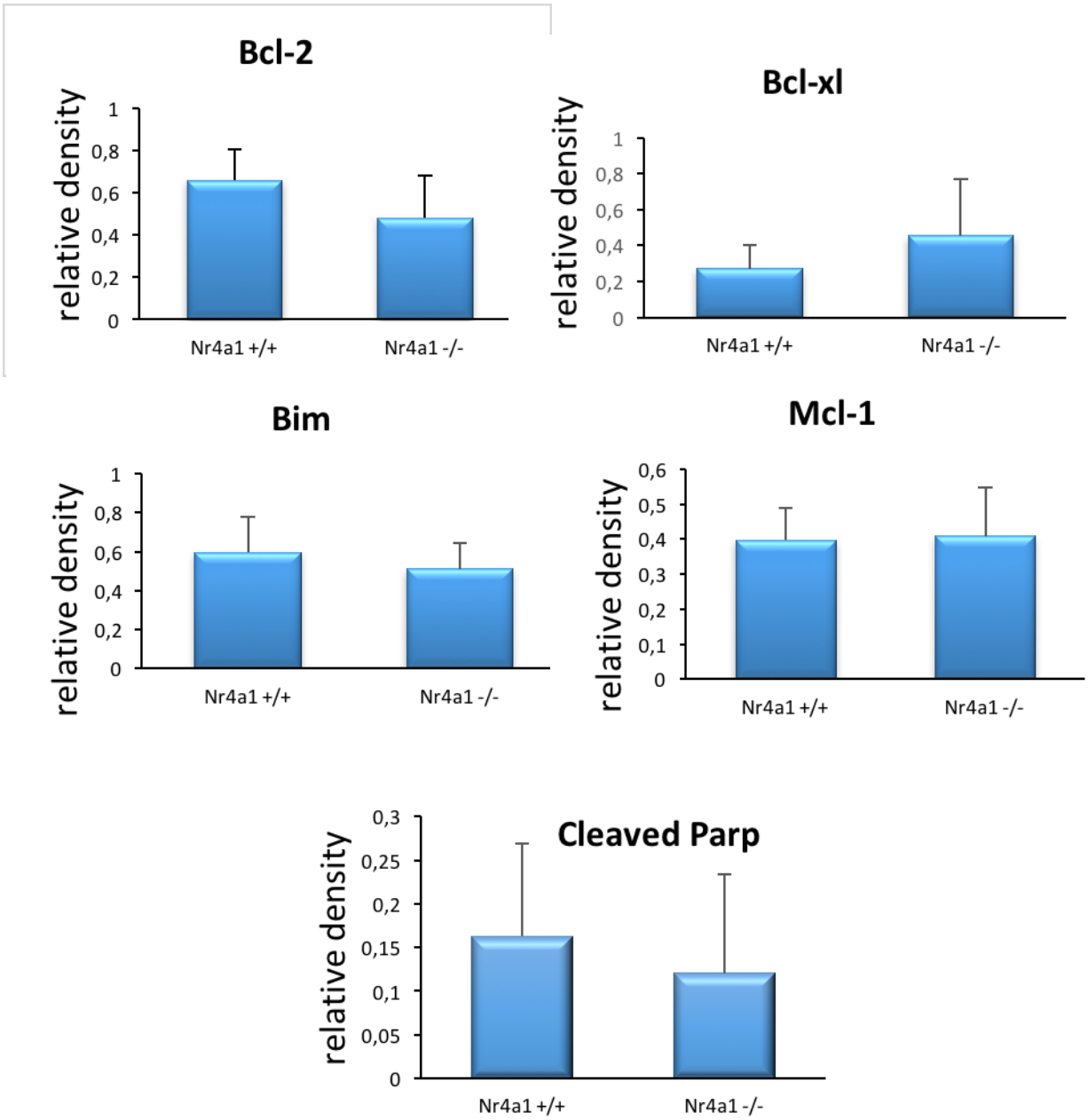

*Figure 38 Relative density plots from spleenic cells with or without Nr4a1. Status of protein levels of Bcl-2, Bcl-xl, Bim, Mcl-1 and cleaved Parp from spleenic cells with or without Nr4a1 loss. Density was calculated using the ImageJ software and row data was normalized to the loading control Beta actin. The bars represent mean and standard deviation. *p<0.05 to Nr4a1+/+ mice.*

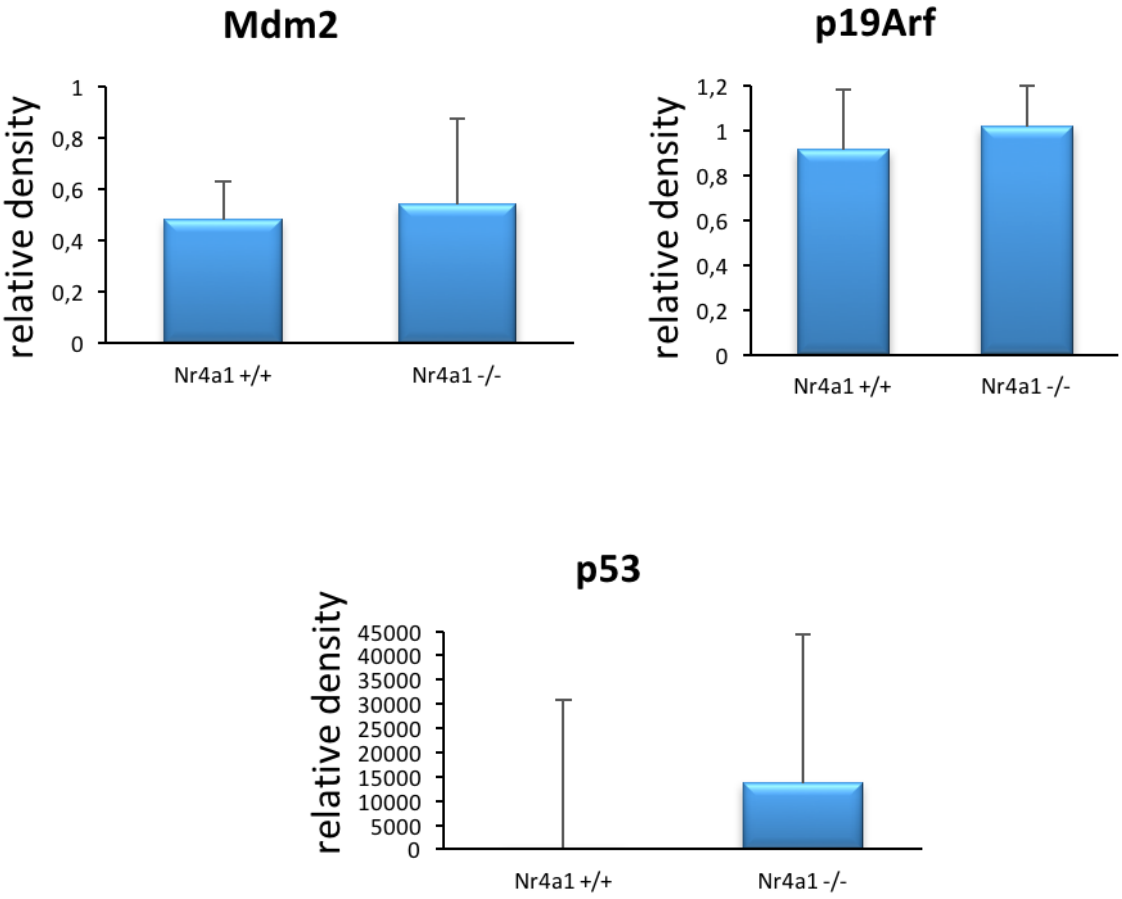

*Figure 39 Relative density plots from spleenic B-cells with or without Nr4a1. Status of protein levels of Mdm2, p19Arf and p53 from the isolated spleenic B-cells with or without Nr4a1 loss. Density was calculated using the ImageJ software and row data was normalized to the loading control Beta actin. The bars represent mean and standard deviation. *p<0.05 to Nr4a1+/+ mice.*

DNA extraction protocol with DNeasy Mini Kit (Quiagen, Hilden, Germany) followed by PCR for Genotyping

Preparation:

Heating plate is heated up to 56°C. Frozen Tissue fragments are ready for use.

A second heating plate was heated up to 70 °C.

Step 1

180 µl ATL-buffer are added to the frozen tissue fragments, then centrifugated (any time done in a HERAEUS PICO 17 Centrifuge, Thermo Scientific, Hilden, Germany).

Step2

Then 20 µl Proteinase K is added and then vortexed (by every time using the IKA Vortex 4 basic). The tubes were incubated at 56°C at the Eppendorf Thermomixer comfort for 1-3 hours. Tubes were mixed 2-3 times per hour. The tissue fragments needed to be solved entirely in the buffer. If not, some more Proteinase K can be added.

Once the tissue fragments were solved entirely the solution was vortexed.

Step 3

200 µl AL-buffer was added and the solution was pulse-vortexed for 15 seconds and then incubated at 70°C for 10 more minutes, then centrifugated again.

Step 4

200 µl Ethanol (96-100%) were added and the solution was pulse-vortexed again for 15 seconds and then centrifugated again.

Step 5

The solution was transferred into a Mini spin column which was placed into a 2 ml collection tube (both included in the DNeasy Mini Kit). The solution then was centrifugated for 1 minute at 8000 rpm. The mini spin column was placed into a new collection tube. The old collection tube with the flow-through was discarded.

Step 6

The mini spin column was opened carefully and 500 µl AW_1-buffer were added, then centrifugated for 1 minute at 8000 rpm. The collection tube was discarded ant the mini spin column was placed into a new one.

Step 7

500 µl AW_2-buffer were added and the solution was centrifugated again either at 13.300 rpm for 4 minutes or at full speed for 3 minutes. The flow-through collection tube was discarded and the mini spin column was placed into a new one and centrifugated for 1 minute at full speed again for higher clarity.

Step 8

For the last time the collection tube was discarded and the mini spin column was placed into a new one. Then 200 µl of AE-buffer were added and incubated for 1 minute at room temperature, then centrifugated at 8.000 rpm for 1 minute.

The DNA was solved in the AE-buffer in the collection tube and finally was transferred into a new Eppendorf tube. (Eppendorf, Hamburg, Germany)

Step 9

By using a photometer, the DNA-quantity was measured. For elution the AE-buffer was used, a blank was adjusted and 5 µl of the DNA per sample were placed on the photometer for quantitative measurement.

PCR

Mastermix was prepared in advance for the number of samples needed.

For each sample a 0,2ml Eppendorf PCR tube was used. (Eppendorf, Hamburg, Germany)

Mastermix for NR4A1

6µl KAPA2G Fast Hot Start Genotyping Mix (KAPA Bio systems Wilmington, MA, USA)

1,2µl oiMir 6602 (Eurofins, Austria)

1,8µl oiMir 6603 (Eurofins, Austria)

1,8µl oiMIr 2060 (Eurofins, Austria)

add 2µl DNA

Mastermix for Eμ-myc

Internal control

6µl KAPA2G Fast Hot Start Genotyping Mix (KAPA Bio systems, Wilmington, MA, USA)
0,6µl oiMir 7738 (Eurofins, Austria)
0,6µl oiMir 7739 (Eurofins, Austria)
2,8µl dest. H_2O (Eurofins, Austria

Transgene

6µl KAPA2G Fast Hot Start Genotyping Mix (KAPA Bio systems, Wilmington, MA, USA)
0,6µl 14377 (Eurofins, Austria)
0,6µl 14378 (Eurofins, Austria)
2,8µl dest. H_2O

PCR cycler program for Internal Control (2720 Thermal cycler, Thermo Fisher Scientific, Waltham, MA, USA)

1. 94°C: 10 min.

2. 94°C: 20 sec.
   65°C: 15 sec. repeat cycle 10 x
   68°C: 10 sec.

3. 94°C: 15 sec.
   60°C: 15 sec. repeat cycle 28 x
   72°C: 10 sec.

4. 72°C: 2 min.

5. Hold at 4°C

PCR cycler program for myc-TG (myc-tg) (2720 Thermal Cycler, Thermo Fisher Scientific, Waltham, MA, USA)

1. 94°C: 10 min.

2. 94°C: 15 sec.
   72°C: 15 sec. repeat step 2 -> 10 x
   72°C: 10 sec.

3. 94°C: 15 sec.
   65°C: 15 sec. repeat step 3 -> 28 x
   72°C: 10 sec.

4. 72°C: 1 min.

5. Hold at 4°C

PCR cycler program for NR4A1 (My Cycler Thermal cycler, Bio-Rad, Hercules, CA, USA)

1. 94°C for 10 min.

2. 94°C for 15sec.
   62°C for 15sec. repeat Step 2- > 35 x
   72°C for 15 sec.

3. 72°C for 2 min.

4. 4°C hold

RNA extraction with the RNeasy Mini Kit (Qiagen, Hilden, Germany)

Preparation when first user of the kit

- 10 µl Beta-Mercapto-Ethanol needs to be added per 1 ml RLT buffer
- 4 volumes of Ethanol (96-100 %) must be added to the RPE buffer
- DNAse needs to be prepared
- Crushed ice must be available

Step 1

Tissue fragments were taken on ice for further isolation procedures
350 µl RLT buffer were added and by using a needle the tissue was bruised, followed by centrifugation for 3 minutes.

Step 2

The supernant was transferred into a mini-spin column and centrifugated at 8.000 rpm for 15 seconds, then the flow-through was discarded and the mini spin column was placed into a new collection tube

Step 3

350 µl of 70 % Ethanol was added and the solution was mixed by pipetting up and down followed by centrifugation at 8.000 rpm for 15 seconds and discard of the flow-through. The mini spin column was placed into a new collection tube.

Step 4

350 µl RW_1-buffer was added, the liquid was centrifugated at 8.000 rpm for 15 seconds, the flow-through discarded and the collection tube reused.

Step 5

A DNase I Incubation Mix was prepared. For each sample 70 µl RDD and 10 µl DNase were added to the mini spin column followed by a 15-minute incubation time at room temperature.

Step 6

350 µl RW_1-buffer were added to the solution and centrifugated at 8.000 rpm for 15 seconds. The flow-through was discarded and the collection tube reused.

Step 7

500 µl RPE-buffer were added and the solution was centrifugated at 8.000 rpm for 15 seconds. The flow-through was discarded and the collection tube reused.

Step 8

500 µl RPE-buffer was added and the solution was centrifugated at 8.000 rpm for 2 minutes. The flow-through was discarded. Once again the tube was centrifugated for better clarity at full speed for 1 minute.

Step 9

The mini spin column was now placed in a new collection tube (containing a lid) and 40 µl RNAse free water were added, then centrifugated at 8.000 rpm for 1 minute. The RNA was collected in the collection tube and put on ice.

Step 10

Quantitative photometric analysis was performed, followed by freezing the RNA at -70°C. RNA samples were brought to the Bio analyzer and were there analysed properly concerning the potential for further sequencing procedures.

cDNA and RT-PCR

Step 1

cDNA was synthesized using the RevertAid™ H Minus First Strand cDNA Synthesis Kit (Fermentas, Waltham, MA, USA).

Step 2

The quantitative reverse transcriptase-polymerase chain reaction was performed by using KAPA Probe Fast reaction mix (Peqlab, Erlange, Germany) and TaqManR probes to

MYC, NR4A1 and NR4A3 (all from Applied Biosystems, Invitrogen, Carlsbad, CA, USA).

Step 3

RT-PCR reactions were performed using an ABI Prism 7900 detection system (Applied Biosystems, Invitrogen, Carlsbad, CA, USA). Housekeeping genes were GAPDH (Applied Biosystems, Invitrogen, Carlsbad, CA, USA), HPRT1 (Applied Biosystems, Invitrogen, Carlsbad, CA, USA) and PPIA (Applied Biosystems, Invitrogen, Carlsbad, CA, USA).

Step 4

Results were evaluated using the SDS 2.2.2 software. The results are shown as relatives units based on following calculation (see below), presenting the relative amount of target gene normalized to the endogenous control.

B-cell extraction from Spleen tissue using BD IMag™ (BD Biosciences, Heidelberg, Germany)

Step 1

Spleens were removed from the Nr4a1-/- and the wildtype mice and passed through a 70-µm nylon cell strainer using HBSS (Thermo Fisher Scientific, Waltham, MA, USA). The solution was centrifugated at 800 rpm for 5 minutes. The supernant was aspirated carefully.

Step 2

The IMag™ buffer (BD Biosciences, Heidelberg, Germany) was filled up to 50 ml with distilled water. 1000 µl of the buffer were added to each tube and were mixed.

Step 3

20 µl of a Mouse Fc Block™ purified CD16 mAb (BD Biosciences, Heidelberg, Germany) was added for blocking. (0,25 µl per 10^6 cells)

Step 4

Number of cells were counted. In each tube 50 µl of BD IMag™ anti-mouse CD45/B220 particles (BD Biosciences, Heidelberg, Germany) were added, mixed thoroughly and incubated at 4°C for 20 minutes.

Step 5

Cells were washed with the IMag™ buffer and centrifugated at 800 rpm for 5 minutes. The supernant was aspirated.

Step 6

1 ml of the buffer was added, and non-solved particles were gently smashed. The tubes were put on the IMagnet (BD Biosciences, Heidelberg, Germany) for 6-8 minutes at room temperature.

Step 7

The supernant was aspirated and again 1 ml of the buffer was added and placed on the IMagnet for 2-4 minutes again. Step 6 and 7 were repeated.

Step 8

Supernant was aspirated and 1 ml HBSS buffer was added.

Step 9

50 µl of the solution were used for the Flow cytometric procedures, the rest was centrifugated, the supernant was aspirated and the cell pellet was either frozen or followed by protein extraction.

Flow cytometry for Immunophenotyping

Step 1

The number of cells was counted and the Antibody Mastermix was added.
During antibody incubation cells were kept on ice and in the dark.
These were the antibodies therefore used: (all from BD Biosciences, Heidelberg, Germany)

- Ter119 (Dye BUV395)
- CD43 (Dye APC)
- IgM (Dye FITC)
- B220 (Dye APC-Cy7)
- CD19 (Dye PE)

Step 2

Cells were washed with HBSS, centrifugated, the supernant was aspirated and then refilled with 100 µl HBSS buffer.

Step 3

The Flow cytometry was performed on a LSRII and the data was analysed with the FlowJo Software.

Western blot Immuno Assay protocol

Step 1 - Production of protein Lysates

- Liquid nitrogen was prepared
- Frozen tissue fragments were taken out of the -80°C freezer
- Protease Inhibitor Cocktail 100x (Thermo Fisher Scientific, Waltham, MA, USA) were added to the buffer
    - E.g. in 1 ml 10 µl Protease was added.
- 100 µl (depending on the number of cells) of the RIPA buffer (Sigma-Aldrich, Germany) were added to the tissue/cells and it was pipetted up and down a several times.
- Freezing and thawing of the tissue in liquid nitrogen for 3 times
- The Lysate was centrifugated at full speed for 3-5 minutes at room temperature
- The supernatant was transferred into a new Eppendorf tube. (from now on tissue was handled on ice)

Step 2 - Protein concentration measurement via Lowry Protein Assay

- 1000 µl of DC™ Protein Assay Reagent A (Bio-Rad, Hercules, CA, USA) was mixed with 20 µl of DC™ Protein Assay Reagent S (Bio-Rad, Hercules, CA, USA)
- 6,0 mg/ml Protein Assay Standard (Bio-Rad, Hercules, CA, USA) (BSA diluted) was prepared and then by adding RIPA puffer 1:2 new Standards were created (6-3-1,5-0,75 mg/ml).
- 25 µl of Solution A+S were pipetted into each well to create triplets.
- 5 µl of each Sample were added including Blank and the Standards.
- After that 200 µl of DC™ Protein Assay Reagent B (Bio-Rad, Hercules, CA, USA) were added to each well
- It then took approx. 15 minutes to incubate at room temperature.
- By using the Spectramax device and the Omega Software the protein concentration can be measured.

Loading and Running

- Heating block was heated at 95°C.
- The Sample puffer was prepared by mixing 425 µl of 2x Laemmli sample buffer (Bio-Rad, Hercules, CA, USA) and 25 µl of Beta-Mercapto-Ethanol.
- Protein Lysates were taken on ice and thawed up.
- The amount of each Cell lysate needed was transferred into a new Eppendorf tube
    - E.g. Sample 5100-0055: 2,04180214 µl *2,5 for using it twice
    - I took 4,09 µl and added the same amount of my Sample Buffer.
- Protein Lysates including the Sample buffer were heated up to 95°C for 5 minutes.
- Meanwhile the Running Puffer was prepared: 900 ml Auqua dest. + 100 ml 10x TGS Tris/Glycine/SDS buffer (Bio-Rad, Hercules, CA, USA)
- The Western blot running-chamber Mini Trans Blot® Cell (Bio-Rad, Hercules, CA, USA) and the Mini-PROTEANR-TGX™ Gels (Bio-Rad, Hercules, CA, USA) were prepared, the running buffer was added.
- The prepared samples were centrifugated for 1 min. at full speed and then loaded onto the gel. The Precision Plus Protein Kaleidoscope protein standard (Bio-Rad, Hercules, CA, USA) was loaded onto the first line.
- The chambers were run with 80 Volt for approximately 1,5 hours.

Transfer

- As blocking solution nonfat dry milk powder (Bio-Rad, Hercules, CA, USA) was prepared
    - E.g.: 2,5g Milk powder solved in 50ml TBST puffer.
- The gels were placed into the running buffer and were divided from the plastic.
- Gels were placed on the prepared Trans-BlotR Turbo™ Midi Transfer Pack (Bio-Rad, Hercules, CA, USA)
- Transfer program was started on the Trans-BlotR Turbo™ Transfer System from Bio-Rad, Hercules, CA, USA. (The transfer program for 5-150kDa takes 5 minutes at 2,5 Ampère)
- Transfer membrane was blocked for 1 hour at room temperature on the shaker with the blocking solution.

- During the Blocking-process, the 1st and the 2nd Antibodies are prepared in either BSA Fraction 5- (GE Healthcare, Little Chalfont, UK)- or nonfat dry milk powder-TBST-solution.

TBST: 100ml of 10x TBS (Bio-Rad, Hercules, CA, USA) + 1000µl Tween 20® (Croda International PLC, Snaith, UK) - then filled up to 1 l with Aqua dest.

Table 8 Western blot overview of antibodies, incubation time, temperature and blocking solutions.

1st AB	Duration	Temp.	2nd AB	Duration	Temp.	Blocking solution
Beta-Actin (13E5) Cell signaling 1:1000 (in BSA)	2 hours	4°C	Anti rabbit	1 hour	Room temp.	Milkpowder
p53 (1C12) Cell signaling 1:1000 (in MP)	2 hours	4°C	Anti mouse	1 hour	Room temp.	Milkpowder
p19Arf (5-C3-1) Santa Cruz 1:500 (in MP)	2 hours	4°C	Anti rat	1 hour	Room temp.	Milkpowder
BIM (C34C5) Cell signaling 1:1000 (in BSA)	2 hours	4°C	Anti rabbit	1 hour	Room temp.	Milkpowder
BCL-XL (54H6) Cell signaling 1:1000 (in MP)	Over night	4°C	Anti rabbit	1 hour	Room temp.	Milkpowder
BCL-2 (50E3) Cell signaling 1:1000 (in BSA)	Over night	4°C	Anti rabbit	1 hour	Room temp.	Milkpowder
MDM2 (SMP14) Santa Cruz 1:500 (in MP)	Over night	4°C	Anti mouse	1 hour	Room temp.	Milkpowder
MCL-1 (Polyclonal) Rockland 1:10000 (in MP)	Over night	4°C	Anti rabbit	1 hour	Room temp.	Milkpowder
PARP (9542S) (Cell signaling) 1:1000 (in MP)	2 hours	4°C	Anti rabbit	1 hour	Room temp.	Milkpowder

Immunoblotting

- If needed (when Antibody is diluted in BSA solution), membrane is washed twice for 5 minutes with TBST washing buffer.
- Membrane was transferred to the 1st Antibody's tube (a 50 ml Falcon tube, Corning, USA) and is incubated either for 2 hours or overnight (Table 8). Antibody solution can be reused and therefore needs to be stored at -20°C.
- After this step the membrane was washed with TBST for 3 times, each 5 minutes (at least) and was incubated in the species appropriate 2nd Antibody for 1 hour at room temperature on a shaker (Table 8). Antibody solution can be reused and therefore needs to be stored at -20°C.
- After this step the membrane was washed again with TBST for 3 times for 5 minutes (at least).
- The Blot then was incubated with freshly prepared Western-Bright ECL (1 ml ECL + 1 ml Peroxide (Advansta Chemilumenescence) for 2 minutes. And placed into the Hypercassette™ (Amersham Bio Sciences UK Limited, UK)
- CL-XPosure™ Film, measuring 18 x 24 cm (Thermo Fisher Scientific, Waltham, MA, USA) were developed in the dark room by using the Curix 60 (Agfa, Mortsel, Belgium).

BIBLIOGRAPHY

1. WHO Classification of Tumours of Haematological and Lymphoid Tissues. Lyon: *IARC Press*: 2008.
2. Campo E, Swerdlow SH, Harris NL, Pileri S, Stein H, Jaffe ES. The 2008 WHO classification of lymphoid neoplasms and beyond: evolving concepts and practical applications. *Blood*. 2011;117(19):5019-32.
3. Shaffer, A. L., 3rd, *et al.* (2012). "Pathogenesis of human B cell lymphomas." *Annu Rev Immunol* 30: 565-610.
4. Küppers, R. (2005). "Mechanisms of B-cell lymphoma pathogenesis." *Nat Rev Cancer* 5(4): 251-262.
5. STATISTIK AUSTRIA, Austrian cancer registry (last update: 02/10/2015), malign invasive NHL cancer incidence
6. STATISTIK AUSTRIA, Austrian cancer registry (last update: 28/01/2016), NHL, cancer mortality
7. STATISTIK AUSTRIA, Austrian cancer registry (last update: 28/01/2016) Hodgkin Lymphoma incidence
8. De Silva, N. S. and U. Klein (2015). "Dynamics of B cells in germinal centres." *Nat Rev Immunol* 15(3): 137-148.
9. Skinnider BF, Horsman DE, Dupuis B, Gascoyne RD. Bcl-6 and Bcl-2 protein expression in diffuse large B-cell lymphoma and follicular lymphoma: correlation with 3q27 and 18q21 chromosomal abnormalities. *RD Hum Pathol*. 1999 Jul;30(7):803-8.
10. Alberts B. Molecular biology of the cell. 2002.
11. Kuppers R, Zhao M, Hansmann ML, Rajewsky K. Tracing B cell development in human germinal centres by molecular analysis of single cells picked from histological sections. *EMBO J*. 1993;12(13):4955-4967.
12. Xu Z, Fulop Z, Zhong Y, Evinger AJ, 3rd, Zan H, Casali P. DNA lesions and repair in immunoglobulin class switch recombination and somatic hypermutation. *Ann N Y Acad Sci.* 2005;1050:146-162.

13. Soulas-Sprauel P, Rivera-Munoz P, Malivert L, *et al.* V(D)J *and* immunoglobulin class switch recombinations: a paradigm to study the regulation of DNA end-joining. *Oncogene*. 2007;26(56):7780-7791.

14. Liu YJ, Malisan F, de Bouteiller O, et al. Within germinal centers, isotype switching of immunoglobulin genes occurs after the onset of somatic mutation. *Immunity*. 1996;4(3):241-250.

15. Stavnezer J. Complex regulation and function of activation-induced cytidine deaminase. *Trends Immunol*. 2011;32(5):194-201.

16. Bothmer A, Robbiani DF, Feldhahn N, Gazumyan A, Nussenzweig A, Nussenzweig MC. 53BP1 regulates DNA resection and the choice between classical and alternative end joining during class switch recombination. *J Exp Med*. 2010;207(4):855-865.

17. Wu X, Bayle JH, Olson D, Levine AJ. The p53-mdm-2 autoregulatory feedback loop. *Genes Dev*. 1993; 7:1126–1132.

18. Eischen CM, Weber JD, Roussel MF, Sherr CJ, Cleveland JL. Disruption of the ARF-Mdm2-p53 tumor suppressor pathway in Myc-induced lymphomagenesis. *Genes Dev*. 1999; 13:2658–2669.

19. Schuster, C., *et al.* (2011). "The cooperating mutation or "second hit" determines the immunologic visibility toward MYC-induced murine lymphomas." *Blood* 118(17): 4635-4645.

20. de Jong D, Balague Ponz O. The molecular background of aggressive B cell lymphomas as a basis for targeted therapy. *J Pathol*.223(2):274-82.

21. Egle, A., *et al.* (2004). "Bim is a suppressor of Myc-induced mouse B cell leukemia." *Proc Natl Acad* Sci U S A 101(16): 6164-6169.

22. Inoue, S., *et al*. (2007). "Apoptosis induced by histone deacetylase inhibitors in leukemic cells is mediated by Bim and Noxa." *Leukemia* 21(8): 1773-1782.

23. Delbridge, A. R., et al. (2015). "Functional antagonism between pro-apoptotic BIM and anti-apoptotic BCL-XL in MYC-induced lymphomagenesis." *Oncogene* 34(14): 1872-1876.

24. Reed, J. C., *et al.* (1988). "Oncogenic potential of bcl-2 demonstrated by gene transfer." *Nature* 336(6196): 259-261.

25. Aisenberg, A. C., *et al.* (1988). "The bcl-2 gene is rearranged in many diffuse B-cell lymphomas." *Blood* 71(4): 969-972.

26. Fang, W., D. L. Mueller, C. A. Pennell, J. J. Rivard, Y.-S. Li, R. R. Hardy, M. Schlissel, and T. W. Behrens. 1996. Frequent aberrant immunoglobulin gene rearrangements in pro-B cells revealed by a bcl-x$_L$ transgene. *Immunity* 4:291.

27. Grillot, D. A. M., R. Merino, J. C. Pena, W. C. Fanslow, F. D. Finkelman, C. B. Thompson, and G. Nunez. 1996. Bcl-x exhibits regulated expression during B cell development and activation and modulates lymphocyte survival in transgenic mice. *J. Exp. Med*. 183:381.

28. Swanson, P. J., *et al*. (2004). "Fatal acute lymphoblastic leukemia in mice transgenic for B cell-restricted bcl-xL and c-myc." *J Immu*nol 172(11): 6684-6691.

29. Linden, M., *et al*. (2004). "Targeted overexpression of Bcl-XL in B-lymphoid cells results in lymphoproliferative disease and plasma cell malignancies." *Blood* 103(7): 2779-2786.

30. Delsol G, Ralfkiaer E, Stein H, Wright D, Jaffe E: Anaplastic large cell lymphoma. Pathology and Genetics of Tumors of Haematopoietic and Lymphoid Tissues. *World Health Organization Classification of Tumours*. Edited by Jaffe E, Harris N, Stein H, Vardiman J. Lyon, France, *IARC Press*, 2001, pp 230–235

31. Duyster J, Bai RY, Morris SW: Translocations involving anaplastic lymphoma kinase (ALK). *Oncogene* 2001, 20:5623–5637

32. Zhou P, Levy NB, Xie H, Qian L, Lee CY, Gascoyne RD, Craig RW: MCL1 transgenic mice exhibit a high incidence of B cell lymphoma manifested as a spectrum of histologic subtypes. *Blood* 2001, 97: 3902–3909

33. Rassidakis, G. Z., *et al.* (2002). "Overexpression of Mcl-1 in anaplastic large cell lymphoma cell lines and tumors." *Am J Pathol* 160(6): 2309-2310.

34. Riley, M. F., *et al*. (2016). "Mdm2 overexpression and p73 loss exacerbate genomic instability and dampen apoptosis, resulting in B-cell lymphoma." *Oncogene* 35(3): 358-365.

35. Wade M, Li YC, Wahl GM. MDM2, MDMX and p53 in oncogenesis and cancer therapy. *Nat Rev Cancer* 2013; 13: 83–96.

36. Meng, X., *et al.* (2015). "Oncogenic c-Myc-induced lymphomagenesis is inhibited non-redundantly by the p19Arf-Mdm2-p53 and RP-Mdm2-p53 pathways." *Oncogene* 34(46): 5709-5717.

37. Lane DP. Cancer. p53, guardian of the genome. *Nature*. 1992; 358:15–16.

38. Meng X, Leslie P, Zhang Y, Dong J. Stem cells in a three-dimensional scaffold environment. *Springerplus*. 2014; 3:80.

39. D'Amours, D., Desnoyers, S., D'Silva, I., and Poirier, G. G. (1999) *Biochem. J.* 342, 249–268

40. Armitage JO, Weisenburger DD. New approach to classifying non-Hodgkin's lymphomas: clinical features of the major histologic subtypes. Non-Hodgkin's Lymphoma Classification Project. *Journal of Clinical Oncology*. 1998;16(8):2780-2795.

41. Friedberg JW. Diffuse Large B-Cell Lymphoma. *Hematology/oncology clinics of North America*. 2008;22(5):941-ix.

42. Spagnolo DV, Ellis DW, Juneja S*, et al*. The role of molecular studies in lymphoma diagnosis: a review. *Pathology* 2004 Feb;36(1):19–44. [PubMed: 14757555]

43. Lenz G, Wright GW, Emre NC, et al. Molecular subtypes of diffuse large B-cell lymphoma arise by distinct genetic pathways. *Proc Natl Acad Sci* USA 2008; 105: 13520–13525.

44. Sehn LH. Introduction to a clinical review series on aggressive B-cell lymphoma. *Blood.* 2015;125(1):1-2.

45. Schmitz R, Ceribelli M, Pittaluga S, Wright G, Staudt LM. Oncogenic mechanisms in Burkitt lymphoma. *Cold Spring Harbor perspectives in medicine*. 2014;4(2).

46. Yustein JT, Dang CV, "Biology and treatment of Burkitt's lymphoma", *Curr Opin Hematol*. 2007 Jul; 14(4): 375-81

47. McKelvey, E. M., Gottlieb, J. A., Wilson, H. E., Haut, A., Talley, R.W., Stephens, R., *et al.* (Oct. 1976). Hydroxyldaunomycin (Adriamycin) combination chemotherapy in malignant lymphoma. *Cancer*, 38(4), 1484-93.

48. Coiffier, B., Haioun, C., Ketterer, n., Engert, A., Tilly, H., Ma, D., *et al.* (Sep 1998). Rituximab (anti-CD20 monoclonal antibody) for the treatment of patients with relapsing or refractory aggressive lymphoma: a multicenter phase II study. *Blood*, 92(6), 1927-1932.

49. Coiffier, B., Thieblemont, C., Van Den Neste, E., Lepeu, G., Plantier, I., Castaigne, S., *et al*. (Sep 2010). Long-term outcome of patients in the lNH-98.5 trial, the first randomized study comparing rituximab-CHOP to standard CHOP chemotherapy in DLBCL patients: a study by the Group d'Etudes des Lymphomes de l'Adulte. *Blood*, 116(12), 2040-2045.

50. Récher, C., Coiffier, B., Haioun, C., Molina, T. J., Ferme, C., Casasnovas, O., *et al.* (Nov 2011). Intensified chemotherapy with ACVBP plus rituximab versus standard CHOP plus rituximab for the treatment of diffuse large B-cell lymphoma (LNH03-2B): an open-label randomized phase 3 trial. *Lancet*, 378(9806), 1858-1867.

51. Held, G., Murawski, N., Ziepert, M., Fleckenstein, J., Poschel, V., Zwick, C., *et al.* (Apr 2014). Role of radiotherapy to bulky disease in elderly patients with aggressive B-cell lymphoma. *J Clin Oncol*, 32(11), 1112-1118.

52. Gisselbrecht, C., Glass, B., Mounier, N., Singh Gill, D., Linch, D. C., Trneny, M., *et al. (*Sep 2010). Salvage regimens with autologous transplantation for relapsed large B-cell lymphoma in the rituximab era. *J. Clin Oncol*, 28(27), 4184-4190.

53. van Kampen, R. J., Canals, C., Schouten, H. C., Nagler, A., Thomson, K. J., Vernant, J.-P., *et al. (*Apr 2011). Allogenic stem-cell transplantation as a salvage therapy for patients with diffuse large B-cell non-Hodgkin's lymphoma relapsing after an autologous stem-cell transplantation: an analysis of the European Group for Blood and Marrow Transplantation Registry. *J. Clin Oncol*, 29(10), 1342-1348.

54. Mangelsdorf DJ, Thummel C, Beato M, Herrlich P, Schutz G, Umesono K, *et al.* The nuclear receptor superfamily: the second decade. *Cell* 1995;83:835 – 9.

55. Gigue`re V. Orphan nuclear receptors: from gene to function. *Endocr Rev* 1999;20:689 – 725.

56. Deutsch, A. J., *et al*. (2012). "The nuclear orphan receptors NR4A as therapeutic target in cancer therapy." *Anticancer Agents Med Chem* 12(9): 1001-1014.

57. Maruyama K, Tsukada T, Okhura N, Bandoh S, Hosono T, Yamaguchi K. The NGFI-B subfamily of the nuclear receptor superfamily. *Int J Oncol* 1998; 12:1237 - 43.

58. Tessem JS, Moss, LG, Chao LC, et al. Nkx6.1 regulates islet beta-cell proliferation via Nr4a1 and Nr4a3 nuclear receptors. *Proc Natl Acad Sci USA* 2014; 111: 5242 - 7.

59. Maxwell MA, Muscat GE. The NR4A subgroup: immediate early response genes with pleiotropic physiological roles. *Nucl Recept Signal* 2006;

60. Mohan, H. M., *et al.* (2012). "Molecular pathways: the role of NR4A orphan nuclear receptors in cancer." *Clin Cancer Res* 18(12): 3223-3228.

61. Safe, S., *et al*. (2016). "Nuclear receptor 4A (NR4A) family - orphans no more." *J Steroid Biochem Mol Biol* 157: 48-60.

62. Mullican, S. E., *et al.* (2007). "Abrogation of nuclear receptors Nr4a3 and Nr4a1 leads to development of acute myeloid leukemia." *Nat Med* 13(6): 730-735.

63. Boudreaux SP, Ramirez-Herrick am, Duren RP, Conneely OM. Genome-wide profiling reveals transcriptional repression of MYC as a core component of NR4A tumor suppression in acute myeloid leukemia. *Oncogenesis* 2012; 1: e19

64. Wenzl, K., *et al.* (2015). "The nuclear orphan receptor NR4A1 and NR4A3 as tumor suppressors in hematologic neoplasms." *Curr Drug Targets* 16(1): 38-46.

65. Deutsch, A. J., *et al.* (2014). "NR4A1-mediated apoptosis suppresses lymphomagenesis and is associated with a favorable cancer-specific survival in patients with aggressive B-cell lymphomas." *Blood* 123(15): 2367-2377.

66. Fog, C. K., *et al*. (2015). "Loss of PRDM11 promotes MYC-driven lymphomagenesis." *Blood* 125(8): 1272-1281.

67. Meyer N, Penn LZ. Reflecting on 25 years with MYC. Nat Rev Cancer. 2008; 8:976–990.

68. Menssen A, Hermeking H. Characterization of the c-MYC-regulated transcriptome by SAGE: identification and analysis of c-MYC target genes. *Proc Natl Acad Sci USA*. 2002; 99:6274–6279

69. Miliani de Marval PL, Zhang Y. The RP-Mdm2-p53 pathway and tumorigenesis. *Oncotarget*. 2011; 2:234–238.

70. Mateyak MK, Obaya AJ, Adachi S, Sedivy JM. Phenotypes of c-Myc-deficient rat fibroblasts isolated by targeted homologous recombination. *Cell Growth Differ*. 1997; 8:1039–1048.

71. Keller, U., *et al.* (2010). "Myc suppression of Nfkb2 accelerates lymphomagenesis." *BMC Cancer* 10: 348.

72. Sabo, A., *et al*. (2014). "Selective transcriptional regulation by Myc in cellular growth control and lymphomagenesis." *Nature* 511(7510): 488-492.

73. Chiarugi V, Ruggiero M. Role of three cancer "master genes" p53, bcl2 and c-myc on the apoptotic process. *Tumori*. 1996;82(3):205-209.

74. Greider C, Chattopadhyay A, Parkhurst C, Yang E. BCL-x(L) and BCL2 delay Myc-induced cell cycle entry through elevation of p27 and inhibition of G1 cyclin-dependent kinases. *Oncogene*. 2002;21(51):7765-7775

75. Adams JM, Harris AW, Pinkert CA, *et al.* The c-myc oncogene driven by immunoglobulin enhancers induces lymphoid malignancy in transgenic mice. *Nature*. 1985;318(6046):533-538.

76. Harris AW, Pinkert CA, Crawford M, Langdon WY, Brinster RL, Adams JM. The E mu-myc transgenic mouse. A model for high-incidence spontaneous lymphoma and leukemia of early B cells. *J Exp Med*. 1988;167(2):353-371.

77. Sidman CL, Denial TM, Marshall JD, Roths JB. Multiple mechanisms of tumorigenesis in E mu-myc transgenic mice. *Cancer Res*. 1993;53(7):1665-1669.

78. Lee SL, Tourtellotte LC, Wesselschmidt RL, Milbrandt J. Growth and differentiation proceeds normally in cells deficient in the immediate early gene NGFI-A. *J Biol Chem*. 1995;270(17):9971-9977.

79. Lee SL, Wesselschmidt RL, Linette GP, Kanagawa O, Russell JH, Milbrandt J. Unimpaired thymic and peripheral T cell death in mice lacking the nuclear receptor NGFI-B (Nur77). *Science*. 1995;269(5223):532-535.

80. "Quantitation comparison of total RNA using the Agilent 2100 bioana- lyzer, ribogreen analysis, and UV spectrometry", *Agilent Application Note*, Publication Number 5988- 7650EN, 2002.

81. “A microfluidic system for high- speed reproducible DNA sizing and quantitation”, *Electrophoresis*, 21(1), 128-34, 2000.

82. RNA Integrity Number (RIN) – Standardization of RNA Quality Control

    Odilo Mueller Samar Lightfoot Andreas Schroeder

83. Alain Lavigueur, Victor maltby, David Mock, Janet Rossant, Tony Pawson, Alan. High Incidence of Lung, Bone, and Lymphoid Tumors in Transgenic Mice Overexpressing Mutant Alleles of the p53. *Oncogene* ,12 June 1989

84. Adams, J. M., *et al*. (1985). "The c-myc oncogene driven by immunoglobulin enhancers induces lymphoid malignancy in transgenic mice." *Nature* 318(6046): 533-538.

85. Alan W. Harris, *et al.* (1988), “The Eμ-myc transgenic mouse – a model for high-incidence spontaneous lymphoma and leukemia of early B cells”. *J. Exp. Med*. 167: 353-371.

86. Dejean LM, Martinez-Caballero S, Manon S, Kinnally KW (February 2006). "Regulation of the mitochondrial apoptosis-induced channel, MAC, by BCL-2 family proteins". *Biochim. Biophys. Acta.* 1762 (2): 191–201.

87. Zhao B-x, Chen H-z, Lei N-z, Li G-d, Zhao W-x, Zhan Y-y, *et al.* “p53 mediates the negative regulation of MDM2 by orphan receptor TR3”. *The EMBO Journal*. 2006; 25(24): 5703-15.

88. Pawlak A, Strzadala L, Kalas W. Non-genomic effects of the NR4A1/Nur77/TR3/NGFIB orphan nuclear receptor. *Steroids*. 2015; 95: 1-6.

89. Boudreaux SP, Ramirez-Herrick AM, Duren RP, Conneely OM. Genome-wide profiling reveals transcriptional repression of MYC as a core component of NR4A tumor suppression in acute myeloid leukemia. Oncogenesis. 2012 Jul 2.

90. Wilson WH, Grossbard ML, Pittaluga S, Cole D, Pearson D, Drbohlav N*, et al.* Dose-adjusted EPOCH chemotherapy for untreated large B-cell lymphomas: a phar- macodynamic approach with high efficacy. *Blood.* 2002;99(8):2685-93.

91. Wilson WH, Grossbard ML, Pittaluga S, Cole D, Pearson D, Drbohlav N, *et al.* Dose-adjusted EPOCH chemotherapy for untreated large B-cell lymphomas: a phar- macodynamic approach with high efficacy. *Blood.* 2002;99(8):2685-93.

92. Wilson WH, Dunleavy K, Pittaluga S, Hegde U, Grant N, Steinberg SM, et al. Phase II study of dose-adjusted EPOCH and rituximab in untreated diffuse large B-cell lymphoma with analysis of germinal center and post-germinal center biomarkers. *J Clin Oncol*. 2008;26(16):2717-24.

93. Wilson WH, Bryant G, Bates S, Fojo A, Wittes RE, Steinberg SM, *et al.* EPOCH chemotherapy: toxicity and efficacy in relapsed and refractory non-Hodgkin's lymphoma. *J Clin Oncol.* 1993;11(8):1573- 82.

94. Kieron Dunleavy, M.D., Stefania Pittaluga, M.D., Ph.D., Lauren S. Maeda, M.D., Ranjana Advani, M.D., Clara C. Chen, M.D., *et al.* Dose adjusted EPOCH-Rituximab therapy in Primary Mediastinal B-cell lymphoma. *N Engl J Med.* 2013 April; 11; 368(15): 1408–1416.